Systematic Study of the Properties of Rotational Excited Levels in the Deformed Even-Even Nuclei in the Framework of Asymmetric Rotor Model

Biniyam Nigussie Edae

A Dissertation Submitted to Department of Physics

Presented in Fulfillment of the Requirements for the Degree of Doctor of Philosophy (Physics)

Addis Ababa University

Addis Ababa, Ethiopia

January 2019

Addis Ababa University
School of Graduate Studies

This is to certify that the thesis prepared by Biniyam Nigussie, entitled: *Systematic Study of the Properties of Rotational Excited Levels in the Deformed Even-Even Nuclei in the Framework of Asymmetric Rotor Model* and submitted In Fulfillment of the Requirements for the Degree of Doctor of Philosophy (Nuclear Physics) complies with the regulations of the university and meets the accepted standards with respect to originality and quality.

Signed by the Examining Committee:

Professor A. K. Jain Signature _____ Date _____
External Examiner

Dr. Tilahun Tesfaye Signature _____ Date _____
Internal Examiner

Professor A. K. Chaubey Signature _____ Date _____
Advisor

Dr. Teshome Senbeta Signature _____ Date _____
Chairperson of Department

DEDICATION

I would like to dedicate my work to my family, especially to

My lovely wife Helen Chikssa, and

My lovely daughters Yerusalem Biniyam and Bethlehem Biniyam

DECLARATION

I hereby declare that this thesis is my original work and has not been presented for a degree in any other University. All sources of material used for the thesis have been duly acknowledged.

Full Name: Biniyam Nigussie Edae

Signature: _____

Date: _____

This thesis has been submitted for examination with my approval as University advisor.

Supervisor: Prof. A. K. Chaubey

Signature: _____

Date: _____

Abstract

The measurement of B(E2) values, meanlives and energies of excited states in nuclei are most active areas of nuclear structure physics. In this work, the asymmetric rotor model of Davydov-Filippov (DF) has been employed to study the reduced transition probabilities, meanlives and energies of excited states in the rotational excited state band even-even nuclei of lanthanide and actinide series, which comprises of 57 nuclides. The E2-transitions ranging up to 12^+ spin states have been studied, in detail, in the spectra of nuclei whose mass number ranges as 150<=A<=190 and A>=228, and for those the first excited state 2^+ and the second excited state $2^{+'}$ gamma band energies are available. In data calculations, experimental and theoretical methods have been employed. The best input parameters for these approaches have also been determined. These input parameters comprise of energy involved in transitions, internal conversion coefficient, half-life, intrinsic quadrupole moment Q_o and nuclear asymmetric parameter γ. The reduced transition probability B(E2), meanlives and energies of excited states have been calculated by making use of the most recent available experimental data, for input parameters. Comparison of the calculated results of B(E2) values, meanlives and energies with the corresponding most recent experimental data shows a very good agreement, including high angular momentum states. Both the empirical and experimental B(E2) values usually increase with spin, for low-lying states, within a rotational ground state band. This work has determined, particularly, the B(E2) values for rotational nuclear excited states of which no work has been done so far. Moreover, this work has incorporated many nuclides and transitions for which neither experimental nor theoretical values are available.

Keywords: Nuclear Structure, Asymmetric Rotor Model, Reduced Transition Probabilities, Half-Life, Meanlives, Energy of Rotational Excited States, Asymmetric Parameter.

ADDIS ABABA UNIVERSITY

Author: Biniyam Nigussie Edae

Title:

Systematic Study of the Properties of Rotational Excited Levels in the Deformed Even-Even Nuclei in the Framework of Asymmetric Rotor Model

Department: Physics

Degree: Ph. D. **Year:** 2019

Permission is here with granted to Addis Ababa University to circulate and to have copied for non - commercial purpose, at its discretion, the above title up on the request of individuals or institutions.

_____

Signature of Author

Acknowledgements

Before all and above I am deeply thankful to Yahweh *(יהוה)* God, by the grace of whom the progress and success of this work was possible.

I would like to express my deepest gratitude to Prof. A. K. Chaubey, Professor of Nuclear Physics at Department of Physics, Addis Ababa University, for suggesting the present problem, supervising the research work, stimulating discussions, valuable comments, continuous encouragement and reading throughout the manuscript.

Special thanks to Dr. Tilahun Tesfaye for providing advice with technical issues, for his useful comments and illuminating constructive discussions in each step of my progress of the whole work.

I am grateful to Physics Department, Addis Ababa University, for providing the financial support in the form of research project. The library facilities and internet access provided by the university is also thankfully acknowledged. I am also thankful to Haramaya University for sponsoring this study.

Finally, I would like to express my cardiac gratitude and sincere appreciation to the staff members of Physics Department, Addis Ababa University, for their generous help and continuous encouragement throughout this work. They had done their best effort in guiding me to bring this work in the best shape.

Table of Contents

List of Figures

List of Tables

CHAPTER 1. Introduction

The work reported in this thesis presents the systematic study of the properties of rotational excited levels in the deformed even-even nuclei covering the heavy mass regions (150 <= A <= 190 and A >= 228) in the framework of Asymmetric Rotor Model (ARM) of Davydov and Filippov. There is an assumption that a rigid triaxial shapes with fixed shape parameters β and γ can be considered as an approximation to the actual nuclear wave functions, but this has been turned out to be very useful and is well supported by new data obtained from heavy ion experiments (Davydov & Filippov, 1958).

Our interest in this study is based on the expectation that it may provide a reasonable phenomenological description of a nucleus in some domain of angular momentum. The striking success of empirical relation over the other existing approaches in describing the B(E2) values of gamma-ray cascades has contradicted the axial symmetry in the nucleus at lower spins. There is a remarkable point here that till now there is no sound theoretical argument against the triaxial shape of the nucleus around $\gamma = 20°$ (Davydov & Filippov, 1958; Parveen & Harish, 2015).

A knowledge of approximate values of meanlives etc. is of great importance to the experimentalists (Rudigier, 2013). The study of B(E2) absolute values for the transitions depopulating 2^+ state of the gamma vibrational band had confirmed low lying levels as collective in nature, contradicting Zawischa et al. view point (Zawischa, Speth, & Pal, 1978). We have also employed the model dependent intrinsic quadrupole moment Q_0 in plotting our systematics which reflects the asymmetric spirit of the model in true sense.

Low-lying levels of the deformed even-even nuclei have been predicted by several phenomenological nuclear models. Davydov and Filippov, using ARM have derived the expressions for the reduced electric quadrupole transition probabilities, taking into account the interaction of rotation with gamma vibrations. Mc Gowan compared $B(E2)_{DF}$ values with experimental ones and found a good agreement (Davydov & Filippov, 1958).

It was suggested that (DeMille, Kavanagh, Moore, Weaver, & White, 1959) the agreement may be improved if the Bohr-Mottelson vibration-rotation interaction and a centrifugal stretching correction, analogous to the type used in molecular spectra are introduced. The Davydov-Filippov model seems to be particularly useful for nuclei in the transition region, between rotational and near harmonic modes of collective excitation.

A change of nuclear shape in excitations leads to some interaction of rotational motion with beta and gamma vibrations. Qualitatively (Demille et al., 1959; Varshney, 1982), the nuclei are deformed away from spherical shape because the nucleus is not rigid structure and the nucleons outside the closed shells can set up tensions in the closed shell core, thereby establishing polarization of the nucleus. If the forces between the external nucleons and the core are repulsive, there is a tendency to polarize the core by pushing the equatorial plane towards the center of the nucleus to form a prolate spheroid.

On the other hand, (Demille et al., 1959; Varshney, 1982), if the forces are attractive, the polarization is accomplished by pulling out the equatorial plane to form an oblate spheroid. Experimentally the resulting deformation is observed as a quadrupole moment. Other observed rotational bands, besides the ground state rotational bands, in even-even nuclei can be explained

by the hydrodynamic picture of the nucleus provided by the collective motion. These bands are formed from the coupling of the nuclear rotations to different vibrational oscillations.

The simplest such oscillations deform the nuclei away from spheroidal shapes ($\gamma = 0$). Such type of oscillations can be described as a temporary deviation from axial symmetry and are called gamma (γ) vibrations. The symmetry around z-axis is no longer maintained during such vibrations. For gamma vibrations K has a value 2. Rotational states are then added to this state to give a set of levels for which I = K, K+1, K+2 etc., where K is the projection of total angular momentum I, on the body fixed 3-axis.

Quadrupole vibrational motion can also take place in a plane parallel to z-axis. Such motion produces deformation (β) hence are called beta (β) vibrations. In this, there is no change of shape of a cross-sectional cut through the equatorial plane of the nucleus, only an expansion and contraction of the circularly shaped nuclear surface takes place. For this set of rotational states K = 0 and the nucleus has at all times the same basic shape as the ground state, but with an added time dependent oscillatory change in the magnitude of its deformation parameter (β). The rotational states thus formed have spins as the ground state band i.e., I = 0, 2, 4 etc. (Varshney, 1982).

The observable rotational motion is possible, if the nucleus is pictured to be a fluid drop or to have any form with a definite surface. This rotational effect can be either rigid in which case particles actually move in circles around the axis of rotation or wavelike in which case particles perform oscillatory motions and only the geometrical shape of the drop changes. Such wavelike rotations are observed only in deformed nuclei, because the apparent motion is solely a surface phenomenon.

The observed moments of inertia for deformed nuclei are smaller than those for rigid rotors. They are, however, larger than expected for purely wavelike surface motion (Varshney, 1982).

Thus the apparent rotational motion is intermediate between rigid rotation and wave like surface motion of constituent particles. According to the collective model (Davydov & Filippov, 1958; Varshney, 1982), moment of inertia of nuclei can be determined from the energies of their rotational states. Rotational energy levels of an axially symmetric nucleus can be described by the three constants of motion: I, the total angular momentum: K, the projection of I on the nuclear symmetry axis: and M, the projection of I on a space fixed axis. For a wavelike rotation, there can be no rotation about the symmetry axis. The quantum number K is, therefore, a constant for each set of rotational levels and represents an intrinsic angular momentum for that band.

Davydov and Filippov (Davydov & Filippov, 1958) assumed the nuclear deformation parameter β and the non-axiality parameter γ permanent to some degree which were dynamic in Bohr-Mottelson model. Furthermore, they assumed deformations in both the elongation parameter β and the asymmetry parameter γ. Excitation of the lower energy levels is caused from rotation of the whole structure, and the gamma-vibrations have been described as the states of anomalous rotational band of the non-axial rotor in the ARM.

The ARM is capable of making predictions for any nucleus for which the first and second 2^+ energy states are known (Davydov & Filippov, 1958). The level structure predicted by ARM for $\gamma = 0°$ or $60°$ is same as of the asymmetric rotor of Bohr-Mottelson model. Thus, ARM appears to provide a somewhat more general description of the nucleus than by other collective models.

In the present work, we have employed the most common method for the calculation of the non-axiality parameter γ using $E2^+$ values, and make use of most recent experimental data. The most important part of this work is the estimation of B(E2) values, meanlives and energies of rotational bands. The obtained results are compared with experimental data and an excellent agreement has been observed. The experimental data for input parameters are taken from the Table of Isotopes (Firestone, 1999) and, Atomic Data and Nuclear Data Tables (Raman, Nestor & Tikkanen, 2001).

The importance of this work lies in the estimation of B(E2) values, meanlives of rotational as well as gamma bands and the beta band head energies in respect of deformed even-even nuclei belonging to heavy mass regions, since the measurement of B(E2) values, meanlives and energies of excited states are one of the most active areas of nuclear structure physics. A knowledge of approximate values of meanlives predicted by us is also of great importance to the researchers (experimentalists).

Objectives

The General Objective is:

- To investigate and compute some properties of rotational nuclear excited levels of even-even nuclei using Asymmetric Rotor Model (ARM)

The Specific Objectives are:

- To estimate the electric transition probabilities B(E2) values,
- To predict meanlives of rotational excited nuclear states, and
- To calculate energies of rotational excited states of even-even nuclei

CHAPTER 2. Nuclear Structure Theory

Nuclear physics is the study of atomic nuclei. From deuteron to uranium, there are almost 1700 species that occur naturally on earth. In addition, large numbers of others are created in the laboratory and in the interior of stars. The main force responsible for nuclear properties comes from strong interaction (Samuel, 2004). However, both weak and electromagnetic interactions also play important roles. For these reasons, nuclear physics serves as an important platform where basic properties of subatomic matter can be examined and fundamental laws of physics can be studied.

However, nuclear physics lacks a coherent theoretical formulation (Krane, 1988) that would permit us to analyze and interpret all phenomena in a fundamental way. Much of what we know about nuclear structure comes from studying not the strong nuclear interaction of nuclei with their surroundings, but instead the much weaker electromagnetic interaction. That is, the strong nuclear interaction establishes the distribution and motion of nucleons in the nucleus, and we probe that distribution with the electromagnetic interaction. In doing so, we can use electromagnetic fields that have less effect on the motion of nucleons than the strong force of the nuclear environment; thus our measurements do not seriously distort the object we are trying to measure.

The atomic nucleus is not a single object but a collection of species ranging from hydrogen to the actinides (Casten, 1990), and displaying an unbelievably rich and fascinating variety of phenomena. The nucleus is extremely small, namely about 10^{-12} to 10^{-13} cm in diameter, and can contain up to a couple of hundred individual protons and neutrons that orbit relative to one another and interact primarily via the nuclear and Coulomb forces.

The structure of the nucleus determines the time-averaged distributions of charge and matter in the nucleus (Hodgson, Gadioli & Gadioli, 1997), and these strongly affect the way the nucleus interact with other particles. The charge distribution is mainly determined by the arrangement of the protons, and the matter distribution by that of the neutrons and protons combined. The charge and matter distributions can be measured by analyzing the way various particles are scattered by the nucleus.

The charge distribution is most conveniently studied by using a probe that interacts only with the charge (Krane, 1988), and in this respect the electron is ideal. The electromagnetic interaction is well understood, so studies of electron elastic scattering by nuclei have yielded accurate charge distributions. It is not so easy to determine the matter distribution. Neutrons are suitable in principle, as they interact with both the neutrons and the protons, but since they cannot be accelerated one must use secondary neutron beams which have low intensity and a rather poor energy resolution.

Any distribution of electric charges and currents produces electric and magnetic fields that vary with distance in a characteristic fashion (Krane, 1988). It is customary to assign to the charge and current distribution an electromagnetic multipole moment associated with each characteristic spatial dependence - the $1/r^2$ electric field arises from the net charge, which we can assign as the zeroth or monopole moment: the $1/r^3$ electric field arises from the first or dipole moment: the l/r^4 electric field arises from the second or quadrupole moment, and so on.

The magnetic multipole moments behave similarly, with the exception of the monopole moment: as far as we know; magnetic monopoles either do not exist or are exceedingly rare, and thus the

magnetic monopole field ($\propto 1/r^2$) does not contribute. Electromagnetic theory gives us a recipe for calculating the various electric and magnetic multipole moments, and the same recipe can be carried over into the nuclear regime using quantum mechanics, by treating the multipole moments in operator form and calculating their expectation values for various nuclear states. These expectation values can then be directly compared with the experimental values measured in the laboratory (Krane, 1988).

The simplest distributions of charges and currents give only the lowest order multipole fields. A spherical charge distribution gives only a monopole (Coulomb) field: the higher order fields all vanish. A circular current loop gives only a magnetic dipole field. Nature has not been arbitrary in the construction of nuclei, if a simple, symmetric structure (consistent with the nuclear interaction) is possible, then nuclei tend to acquire that structure. It is therefore usually necessary to measure or calculate only the lowest order multipole moment to characterize the electromagnetic properties of the nucleus (Krane, 1988).

Another restriction on the multipole moments comes about from the symmetry of the nucleus, and is directly related to the parity of the nuclear states. Each electromagnetic multipole moment has a parity, determined by the behavior of the multipole operator when $r \rightarrow - r$. The parity of electric moments is $(-1)^L$, where L is the order of the moment (L = 0 for monopole, L = 1 for dipole, L = 2 for quadrupole, etc.): for magnetic moments the parity is $(-1)^{L+1}$ (Krane, 1988).

Since the discovery of the atomic nucleus and the subsequent identification of the neutron and proton as its primary constituents, a longstanding goal has been that of deducing nuclear properties from those of these constituents (Frank, 1978). Unfortunately, a typical nucleus, being composed

of many nucleons, possesses several hundred degrees of freedom that may be specified in a variety of ways. It is the hope of the theorist that a proper method of specification will leave him with only a handful of coordinates that need be actively considered.

The discovery of nuclear fission in 1939 and its subsequent interpretation in terms of the surface and Coulomb energies of a deformed, charged liquid droplet, indicated that individual nucleons were capable of taking part in large scale cooperative phenomena (Frank, 1978). As experimental techniques were refined, evidence for low energy collective behavior began to accumulate, particularly in nuclei far removed from shell closures. Anomalously large quadrupole moments and electric quadrupole transition rates were observed.

The low energy spectra of many nuclei were found to contain sequences of levels resembling the rotational and vibrational bands known to occur in the excitations of molecules. Such discoveries emphasized the importance of taking the nuclear collective degrees of freedom into direct account. Aage Bohr recognized that collective coordinates, used to specify the shape and orientation of the nuclear surface, could be treated as dynamical variables (Frank, 1978). In particular, he studied the lowest order (quadrupole) surface vibrations of a liquid droplet about a spherical equilibrium shape, introducing the intrinsic coordinates (β, γ, θ_i) as a means to specify an arbitrary quadrupole surface.

The three Euler angles, θ_i, serve to orient a set of body-fixed (BF) principal axes within the nuclear droplet, while β and γ describe the appearance of the surface to a BF observer, β is a measure of the overall deformation from sphericity, and the angle γ describes the rotational asymmetry about the BF z-axis (Frank, 1978).

The building blocks of nuclei are neutrons and protons, two aspects, or quantum states, of the same particle, the nucleon (Samuel, 2004). Since a neutron does not carry any net electric charge and is unstable as an isolated particle, it was not discovered until 1932. The only charged particles inside a nucleus are protons, each of which carries a positive charge of the same magnitude, but opposite in sign, as an electron, since only positive charges are present, the electromagnetic force inside a nucleus is repulsive and the nucleons cannot be held together unless there is another source of force that is attractive and stronger than Coulomb force.

Both gravitational and electromagnetic forces are infinite in range and their interaction strengths diminish with the square of the distance of separation (Samuel, 2004). Clearly, nuclear force cannot follow the same radial dependence, else nucleons in one atom would have felt the attraction of those in nearby atoms. Being much stronger, it would have pulled the nucleons in different nuclei together into a single unit and destroy all the atomic structure we are familiar with. In fact, nuclear force has a very short range, not much beyond the confine of the nucleus itself, in marked contrast to the fundamental forces that were familiar at the time.

Nucleons interact with each other through two-body interactions (Samuel, 2004). That is, the force between nucleons acts only between a pair of them at a time. The absence of one-body terms in the potential can be seen by contrasting with atomic electrons. In an atom, the electrons are bound to a central electrostatic potential provided by the protons in the nucleus. As a result, there is a force acting on an electron even in cases where it is the only one present, such as the hydrogen atom. This is not true for nuclei, as there is no external source to provide a force on the individual nucleon. The only one-body operator in a nuclear Hamiltonian is the kinetic energy arising from

the motion of each nucleon. On the other hand, it is not possible to rule out completely three-body and higher particle-rank terms in the nuclear interaction.

Protons and neutrons are the lowest energy bound states of quarks and gluons. When we put two or more of these particles together, they interact, scatter and sometimes form bound states due to the strong interactions. If one is interested in the low-energy region where the nucleons hardly get excited internally, we can treat the nucleons as inert (non-interacting), structureless elementary particles, and we can understand many of the properties of the multi-nucleon systems by the nucleon-nucleon interactions (Samuel, 2004).

If the nucleons are non-relativistic, the interaction can be described by a potential. Since the fundamental theory governing the nucleon-nucleon interactions is Quantum Chromo Dynamics (QCD), the interactions shall be calculable from the physics of quarks and gluons. Nonetheless, the problem is quite complicated and only limited progress has been made from the first principles so far. Therefore, the approach we are going to take is a phenomenological one: One first tries to extract the nucleon- nucleon interaction from the nucleon-nucleon scattering data or few nucleon properties, and then one tries to use these interactions to make predictions for the nuclear many-body system (Samuel, 2004).

The atomic nucleus is a very complex system (Casten, 1990; Heyde, 1999; Jean, James & Michel, 2005; Nazarewicz, 1998), and a theoretical study is confronted with some severe basic problems. The nucleon-nucleon interaction acting inside the nucleus as an effective force is not well understood yet. Actually, the nucleon-nucleon interaction is not one of nature's basic forces, but it is the result of the strong force that acts between the quarks of which the nucleon is composed.

At low nuclear excitation energies however, quarks do not seem to play an explicit role in determining the nuclear structure properties.

The nuclear force is at first glance a mysterious one (Casten, 1990) since it has few if any recognizable consequences in macroscopic matter (i.e., everyday phenomena). And, in fact, the exact nature of this force is still largely unknown. Nevertheless, it is remarkable how much we can learn about it from a few simple empirical facts. We have already stated that the very existence of nuclei implies a new force, the strong interaction that can overcome the Coulomb repulsion between protons.

Nuclei are extremely small, and for all practical purposes, the nuclear force can be neglected when considering atomic and molecular phenomena (Casten, 1990). These two facts tell us that the nuclear force must be short range. So, the nuclear force is predominantly attractive and short range. A more general characteristic of the nuclear force is charge independence, which means that the p-p, n-n, and p-n forces are equal. The concept of the proton and neutron as merely two states of the same particle, the nucleon, leads to the concept of isospin, which is similar to intrinsic spin.

The properties of the simplest bound nuclear system, the deuteron, tell us still more about the nuclear force (Casten, 1990). The nonzero quadrupole moment of the deuteron is our first indication of the tendency of the proton-neutron interaction to lead to nonspherical nuclear shapes. Moreover, it is an indication that the nuclear force cannot be completely described by a spherically symmetric central potential. In the particular case of the deuteron the finite quadrupole moment is evidence for tensor forces that couple a spin dependent component to a central potential.

The Pauli principle is of fundamental importance to nuclear structure (Casten, 1990). It is essential in determining which nuclei are stable, that it provides a justification for the idea of independent particle motion in a dense nucleus. It explains why all even-even nuclei have 0^+ ground states, why the low-lying states of these nuclei increase in energy with spin, why most low lying negative parity states have odd spin, and, remarkably, the entire systematic of where collectivity, phase transitions, and deformation occur in nuclei.

The Pauli principle embodies the notion that no two identical nucleons can occupy the same place at the same time. More formally, no two nucleons can have identical quantum numbers because nucleons are fermions. In this second form it plays an important role in proton-neutron systems where the two nucleons can be treated as two states of the same nucleon. Many applications of the Pauli principle, however, are best expressed in terms of a generalized mathematical formulation of it that the nuclear wave function must be totally antisymmetric totally meaning antisymmetric in all coordinates, spatial, spin, and isospin (i.e., that the wave function must reverse its sign if all these coordinates are interchanged) (Casten, 1990).

Just as we learn about atoms by studying their excited states, we study nuclear structure in part through the properties of nuclear excited states (Krane, 1988). And like atomic excited states, the nuclear excited states are unstable and decay rapidly to the ground state.

Nucleons in a nucleus do not behave like classical particles, colliding like billiard balls (Krane, 1988). Instead, the wave behavior of the nucleons determines the properties of the nucleus, and to analyze this behavior requires that we use the mathematical techniques of quantum mechanics. From a variety of scattering experiments, we know that the nucleons in a nucleus are in motion

with kinetic energies of the order of 10 MeV. This energy is small compared with the nucleon rest energy (about 1000 MeV), and so we can with confidence use nonrelativistic quantum mechanics.

The internal structure of the atomic nucleus varies greatly and often suddenly with the number of constituent protons and neutrons (Caprio, 2003). These changes in structure are associated with corresponding changes in the nuclear excitation spectrum and in the decay properties of the excited states. The predominant undertaking of the field of nuclear structure physics is to extract from observed properties of the ground and excited states of the nucleus an understanding of the physical structure of these states and to develop a comprehensive theoretical description of the nuclear system.

In principle, all the properties of a nucleus are contained in the nuclear Hamiltonian (Hodgson et al., 1997). Unfortunately, however, we do not know the nuclear Hamiltonian, and even if we did know it, the mathematical difficulties of obtaining its Eigen functions and eigenvalues would be inseparable. Even if these could be overcome, the amount of information we would obtain would be unmanageable with the technology in hand.

A nuclear state (Hodgson et al., 1997) is normally in its state of lowest energy called the ground state. It can also exist in many states of higher energy called excited states. Each nuclear state is characterized by its structure that is by the arrangement of its nucleons and the coupling of their spins. This can be described in various ways. In principle, of course, the nucleus is completely specified by its total wave function. Except for the very lightest nuclei this is, however, far too complicated an object to be accurately estimated. It is thus usual to express the structure of a nucleus in terms of nuclear models.

The structure of nuclei is a fingerprint (Neugart & Neyens, 2006) of how protons and neutrons in these many-particle systems interact in order to form a bound nucleus. Fundamentally, the behavior of the aggregate nuclear system is entirely determined by the interaction of its constituents, but it is largely impossible to deduce even the most basic structural behavior of the system directly from the intrinsic properties of these constituents. This limitation arises in part since the underlying interactions of protons and neutrons in the nuclear medium are not entirely understood.

Consequently, there is a need for phenomenological models of nuclear structure, which require some degree of empirical input regarding the properties of the nuclear system in order to make predictions of further properties (Neugart & Neyens, 2006). These models serve at the least to provide a rough conceptual understanding of the properties of nuclei and ideally can allow detailed quantitative descriptions to be obtained.

Until the mid-1970s the two principle strains of nuclear structure theory were embodied in the shell model and the collective model pioneered by Aage Bohr and Benjamin Mottelson. In nuclei far from closed shells where the shell model is either intractable or unreliable, one normally takes recourse in other theoretical frameworks. One of the significant and most fruitful of these approaches can be called geometrical or collective models, which bypass the shell model by taking a more macroscopic approach of assigning a specific shape to the nucleus and examining the rotations and vibrations of such a, generally non-spherical, shape (Casten, 1990).

The shell model is generally considered the fundamental nuclear model (Casten, 1990; Nazarewicz, 1998). Historically, it was the first model to have considerable, detailed success. Of

course, this is not accidental. The shell model works best for light nuclei. More fundamental to the shell model's central position in nuclear physics is that it provides a well-defined procedure for the calculation of basic nuclear observables. Since the shell model is the only broadly applicable microscopic model available, it is the standard against which others are compared. A collective model that can be shown to be inconsistent with the shell model is discarded with little delay.

Many features of nuclei indicate that the nuclear motion does not consist of only the simple single particle excitations (Liu, 2010). Instead, there are a few typical effects that imply a collective motion, where all or at least a large part of nucleons in a nucleus move coherently with well-defined phases. Two important types of the collective motions are the surface vibration of the nuclear shape that is a motion of nucleons from one region of the nuclear sphere to another one and the rotation of the entire nucleus.

The assumption of a non-spherical macroscopic nuclear shape is a phenomenological or ad hoc one, while the enormous successes of the collective model, its demonstrated predictive power, and the numerous progeny it has produced over in the last years leave little doubt that it aptly describes the nuclear structure of perhaps the majority of nuclei, one is left with an uneasiness about the apparent incompatibility of an independent particle picture such as we have been discussing and the clearly collective and coherent motion involved in macroscopic rotations and vibrations (Liu, 2010).

From the observed properties of nuclei over a large mass range, A, it can be seen that there are two major types of collective nuclear behavior (Liu, 2010). Firstly, in the region of $A < 150$ the nuclei are known as vibrational since they vibrate about a spherical equilibrium. In the region $150 < A <$

190 and also A > 220 is rotational. They are known as rotational nuclei due to their non-spherical shape at equilibrium. Opposed to the spherical shape of the rotational nuclei, these nuclei are ellipsoidal; either a prolate ellipsoid (Figure 2.1 (a)) or of oblate form (Figure 2.1 (b)) but will always be symmetric about both semi-major and semi-minor axis.

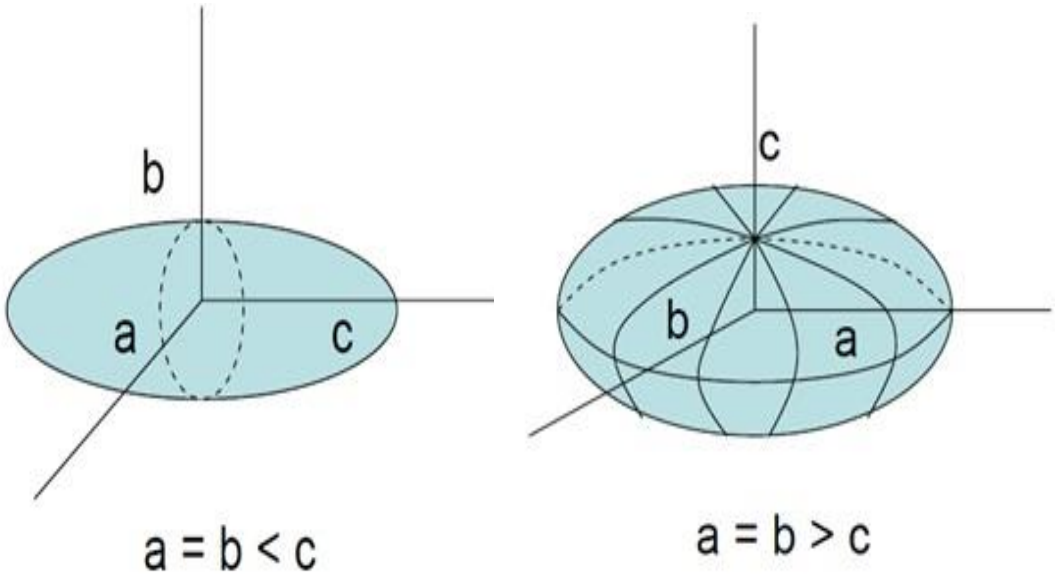

(a) (b)

Figure 2.1. a) A prolate ellipsoid, defined by the semi-major axis, c, being greater than the semi-minor axis. b) An oblate ellipsoid is defined by the semi major axis, c, being smaller than the semi-minor axis.

The most obvious characteristic of non-spherical nuclei is that they can undergo rotations about an axis perpendicular to the symmetry axis (Liu, 2010). They can, of course, also vibrate and, moreover, rotations can be superimposed on vibrational motion. It has been shown by the study of even-even nuclei in the regions A <= 150 and A >= 190 that the properties of their excited levels can be accounted for by considering the rotational motion of non-axial (non-axially symmetric) nuclei or nuclear vibrations.

A new collective theory of the behavior of nuclei has been developed by Davydov and Filippov (DF) taking into account possible violations of the axial symmetry of the nucleus (Pearson, 2008). This violation affects the rotational spectrum of the axial even-even nucleus, and some new rotational states with total angular momenta of 2, 3, 4, … appear. A deformed nucleus has a rotational degree of freedom. For even-even nuclei, the 0^+ state is always the ground state. Then, the next states are $I^\pi = 2^+, 4^+, 6^+, 8^+, \ldots$; on symmetry grounds.

Even-even nuclei are known to have 0^+ ground states and several low-energy integer spin states (Allmond, 2007). The transition strengths between these levels are sufficiently strong and well established to support the view that most nuclei are collective. While the full and true structure of these nuclei is not known, the structure is clearly dominated by low spin degrees of freedom. To establish a reference frame in which we can discuss and compare data, models of adiabatic rotations are by far the most useful.

The asymmetric rotor model of Davydov- Filippov (DF) has been employed to study the reduced transition probabilities, meanlives and energies of excited states in the rotational excited state band even-even nuclei of lanthanide and actinide series. Basic nuclear properties of excited nuclear states such as excitation energy, angular momentum (spin) and parity can be measured using conservation laws and electromagnetic selection rules (Paddy, 2003). In addition, the determination of decay probabilities of nuclear states (i.e. their lifetimes) gives direct information on the make-up of the initial and final states and can reveal highly collective, deformed structures within the nucleus.

2.1. Nuclear Angular Momentum

It is necessary to consider the basic properties that define nuclear quantum states. Those properties, which for stationary states can be measured experimentally, are constants of the motion (Nemirovskii, 1963). In stationary states, the nucleus obviously possesses a definite energy. However, a theoretical interpretation of nuclear-level spectra is an extremely hard task. As is known, in a central field the constant of motion is the angular momentum; in the nucleus, it is the total angular momentum representing the sum of the orbital momenta and the spins of all the nucleons. In non-spherical nuclei the angular momentum projection onto the nuclear symmetry axis is conserved.

In classical mechanics as well as in quantum mechanics (John & Victor, 1979), the angular momentum of a system is conserved if the equations of motion are invariant under rotations of the coordinate system which is used to describe the motion. This is true of any isolated system, such as a nucleus. It is not true of a system subject to external forces, such as an applied electric or magnetic field, which distinguishes one direction in space from all others. Angular momentum plays a critical role (Nouredine, 2009) in the description of molecular rotations, the motion of electrons in atoms and the motion of nucleons in nuclei. Thus, the quantum theory of angular momentum is a prerequisite for studying molecular, atomic and nuclear systems.

To describe the interplay between the motion of the particles and the collective rotation, consider an axially symmetric deformed nucleus rotating around the x-axis, with orbiting valence nucleon as shown in Figure 2.2. The total angular momentum, I, of the nucleus is given by (Obed, 2011)

$$I = R + J \tag{2.1}$$

where R is the angular momentum generated by the collective rotation of many nucleons (core) around the x-axis, and J is the intrinsic angular momentum that is generated by the valence nucleon.

If there are more than one valence nucleons, the intrinsic angular momentum of the valence nucleons J is represented as the sum of the angular momenta of the individual valence nucleons (Obed, 2011), i.e.

$$J = \sum_{i=1}^{A} j_i \tag{2.2}$$

The total angular momentum of a nucleus is formed from the sum of the individual constituents' orbital angular momentum and spin angular momentum (Alex, 2005). Since neutron and proton spins are half-integral, and orbital angular momentum is integral, it follows that I is half-integral for odd - A nuclei, and integral for even - A nuclei. The total angular momentum may be composed of the sum of orbital and intrinsic spins, or it may be composed of the sum of the angular momenta for two or more nucleons. The projection of the total angular momentum I on to the symmetry axis is K, and is the same as the projection of J. The projection of the angular momentum j_i, of a valence nucleon is Ω_i, thus

$$K = \sum_{i=1}^{A} \Omega_i \tag{2.3}$$

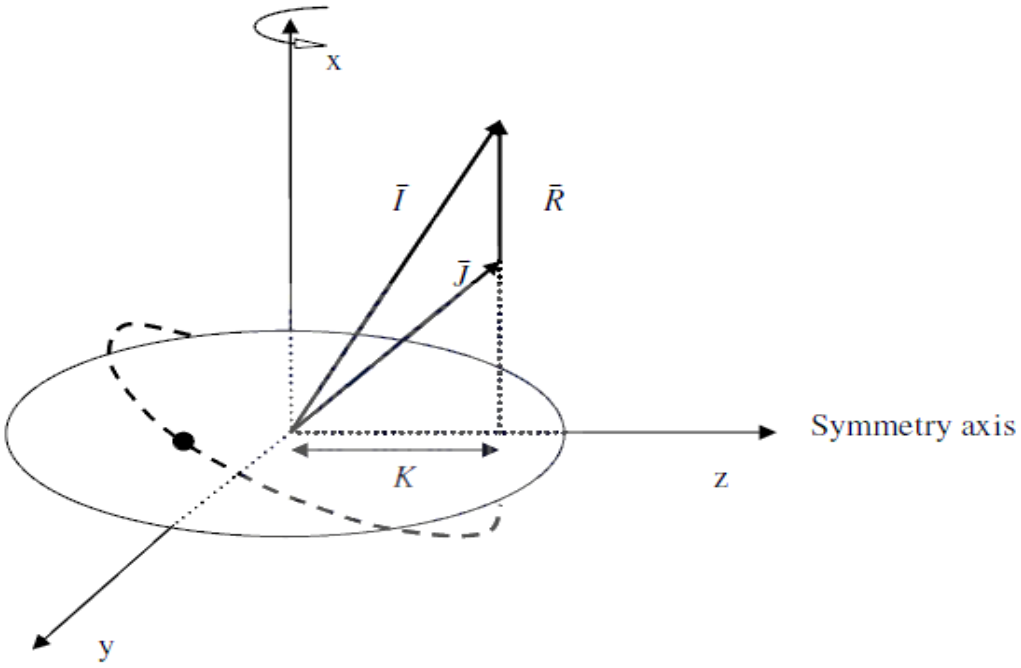

Figure 2.2. Schematic of the coupling of the collective angular momentum $\vec{R}$, and the intrinsic angular momentum of valence nucleons $\vec{J}$. The projection of the total angular momentum $\vec{I}$, on to the symmetry axis is K.

The projection of the total angular momentum on to the rotational axis is given by

$$I_x = \left\{\sqrt{I(I+1) - K^2}\right\}\hbar \tag{2.4}$$

and it is known as the aligned angular momentum.

2.2. Nuclear Models

The nucleus with its constituents, protons and neutrons, constitutes the core of an atom (Serkan, 2009). Nuclei exhibit quantized states similar to atoms. However, the excitation energy of nuclei is far greater than atoms, ranging from keV to MeV, and the excitation pattern is different. Due to

the complexity of the nucleus, models are needed to explain of their structure. Models have to be consistent with observed quantum properties of the nucleus and they have to have predictive power. Usually, one of the models is dominant for that particular region compared to the other models.

Nuclear models are developed to interpret specific features observed in nuclei in different mass regions (Obed, 2011). A good model is the one that could predict most of the features that nuclei exhibit. Usually in order to describe all features exhibited by all nuclei, more than one nuclear model is needed. The reason for this is that every nuclear model has its own limitations or shortcomings. The spherical shell model, for example, is only applicable to magic nuclei or nuclei near closed shell (i.e. near-spherical nuclei) and fails for nuclei whose particle number of protons Z and neutrons N are located far away from magic numbers. To predict features observed for nuclei located far away from shell gaps other models are needed. Up to the present there are varieties of nuclear models that one can use, but the applicability of the model rests on how the model relates to the physical properties of the nucleus.

There are two complementary approaches to describe the nucleus (Heyde, 1999; Thomas, 2009). The first is a microscopic approach, where nucleons are treated as independent particles moving in a central potential arising from the interaction of each nucleon with all other nucleons. One of the simplest such models is the so called Fermi gas model in which the nucleons are considered as non-interacting particles in a 3-dimensional square well potential. This model can be seen as predecessor of the successful shell model.

The second is a macroscopic approach where the nucleus is treated like a macroscopic (or geometric) object. One of the earliest nuclear models, the liquid drop model, belongs in this category. There, the nucleus is described similar to a drop of an incompressible liquid. The observed masses and binding energies can be well deduced from it. In this model the nucleus has a surface and a shape and excitations can be described in terms of collective vibration and rotation. These ideas are also essential in the collective model by Bohr and Mottelson (Heyde, 1999).

Nuclear structure is generally explained on the basis of two nuclear models (Varshney, 1982), the shell model and the collective model. In the shell model one performs detailed calculations with specific potentials and residual interactions to explain not only general features displayed by nuclei over fairly wide regions but also to explain and predict properties of individual nuclei. In the collective model one considers quantized fluid with certain properties and subjects it to certain boundary conditions in order to predict gross characteristics which depend upon most of the nucleons in a system.

Generally, in order to test the validity of such models, a survey of selected nuclear properties like binding energies, excitation energies, nuclear moments, transition probabilities etc. is done. It is well known that different nuclear models are applicable to different regions of mass number with varying degree of success in explaining different nuclear properties. The collective model was a result of two major works: the liquid drop model for describing nuclear fission, which was developed largely by A. Bohr and initiated the possibility of deformation, and the observation of large electric quadrupole moments in nuclei by J. Rainwater. These two works provided the basis for the Bohr collective model (Varshney, 1982).

Historically (Irving, 1962), the liquid drop model was the first model developed to describe the nuclear properties. It describes the bulk properties (binding energies) and collective phenomena, such as vibrations and rotations of the nucleus. The idea came mainly from the consideration that nuclear forces exhibit a saturation properties and from the fact that the nucleus has a low compressibility and a well-defined nuclear surface. The binding energy per nucleon as a function of mass number A is found to be fairly constant (≃ -8.5 MeV) (Beiser, 2003), which indicates the saturation properties of nuclear force.

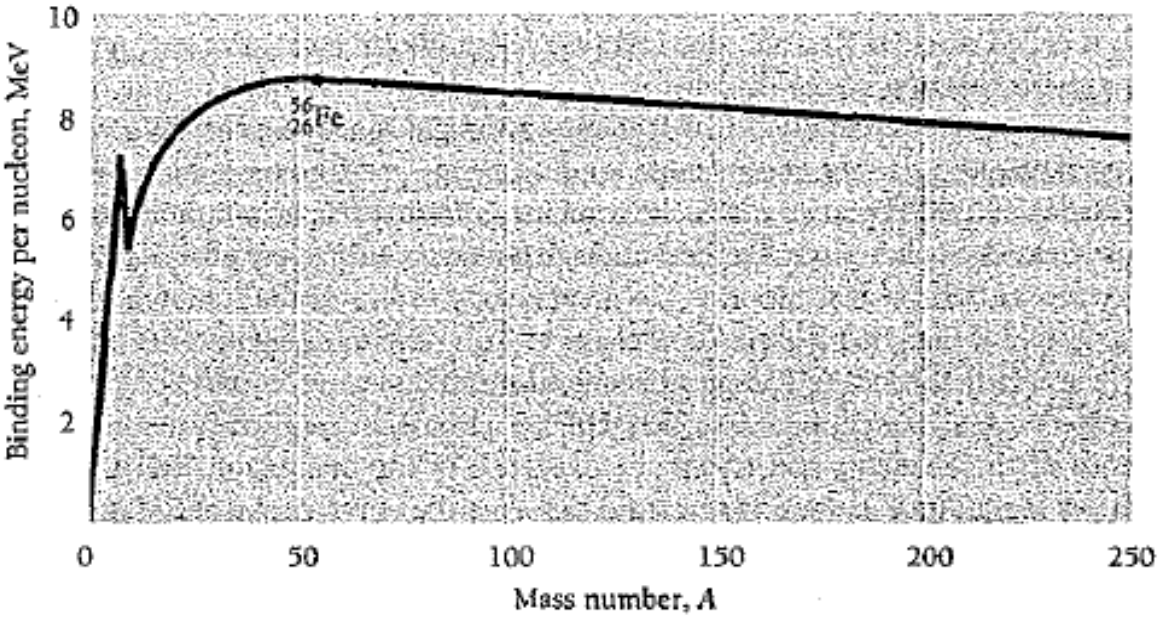

Figure 2.3. Binding energy per nucleon as a function of mass number. The peak at A = 4 corresponds to the exceptionally stable $^{4}_{2}$He nucleus, which is the alpha particle. The binding energy per nucleon is a maximum for nuclei of mass number A = 56. Such nuclei are the most stable.

Many different models have been proposed to interpret experimental phenomena in nuclear physics (Irving, 1962; Shaohua, 2010). Roughly, these models can be classified into two main types: the shell model and the collective model, which describe single nucleon motions and collective motions of nucleons in a specific nucleus, respectively.

2.2.1. Nuclear Shell Model

The shell model forms the basis for various theoretical models (Obed, 2011). This model was first developed in the 1940s and many unsuccessful attempts were made in constructing a nuclear potential that will fit the observed properties of the nuclei. Mayer, Haxel, Jensen and Suess further developed this model in 1949 by introducing a spin-orbit interaction in the nuclear potential. It now accounts very well for the observed nuclear properties such as nuclear transitions, spins and parities of the states.

The shell model is also called a single-particle model because it treats the nucleons individually. The occurrence of so-called magic numbers (N or Z is equal to 2, 8, 20, 28, 50, 82, 126, …) has, from the experimental point of view, been one of the strongest motivations for the formulation of the nuclear shell model. The shell model proposes that (Obed, 2011) a valence nucleon moves in an attractive potential well created by the other nucleons in the nucleus. The most often discussed potential wells are an isotropic harmonic oscillator, infinite or finite square well and Woods-Saxon potential.

The Shell model of the nucleus originated from the theoretical attempts to explain the extra stability of certain nuclei having nucleon numbers equal to the magic numbers (2, 8, 20, 28,50, 82, 126, …), which are analogous to the inert gases in atomic physics. This model is based on the mean field approximation, where each nucleon is assumed to move independently in a potential that represents an average interaction with the other nucleons in the nucleus. Unlike the atomic case where the central mean field is provided by the Coulomb field of the heavy nucleus at the center of mass, in the nuclear case the mean field is produced by the nucleons themselves (Obed,

2011). This model was capable of explaining not only the magic numbers but also many other nuclear properties such as spin, magnetic moment and energy levels.

The spherical shell model was first introduced by Mayer and Jensen (Shaohua, 2010). Evidence of the existence of nuclear shells has been observed experimentally in many aspects, such as nuclide abundance, neutron and proton separation energies, and the α-decay energies. For example, sudden drops are seen in neutron and proton separation energies at certain numbers of neutrons or protons, like 50, 82, and 126 for neutrons. These numbers are known as magic numbers.

The first job was to find an appropriate potential that would reproduce these corresponding magic numbers correctly. This goal was not fulfilled until Mayer and separately Jensen found that the proper potential like the harmonic oscillator potential must include the spin-orbit interaction, a term of $\hat{\imath}.\hat{s}$ with the opposite sign and much larger magnitude than the spin-orbit interaction of electrons in atoms. A realistic finite potential, the Woods-Saxon potential, with spin-orbit coupling is widely used in the form of (Shaohua, 2010),

$$U(r) = \frac{U_0}{1+\exp[\frac{r-R_0}{a}]} + \frac{U_{ls}}{r_0}\frac{1}{r}\frac{d}{dr}\{\frac{1}{1+\exp[\frac{r-R_0}{a}]}\}\,\hat{\imath}.\hat{s} \qquad (2.5)$$

A typical set of parameters is $U_0 = [-51 + 33(N - Z)/A]$ MeV, $U_{ls} = -0.44U_0$, a = 0.67 fm, and $R_0 = r_0A^{1/3}$ with r_0 = 1.27fm.

The spin-orbit interaction results in individual energy levels to split in such a way that at magic numbers, 2, 8, 20, 28, 50, 82, 126, are large gaps in the energy spacings. It is easy to understand

that nuclei in the shell model have a spherical shape. The Woods-Saxon potential (Obed, 2011) is an intermediate between the harmonic oscillator and square well potentials and represents a more realistic shape of the nucleus.

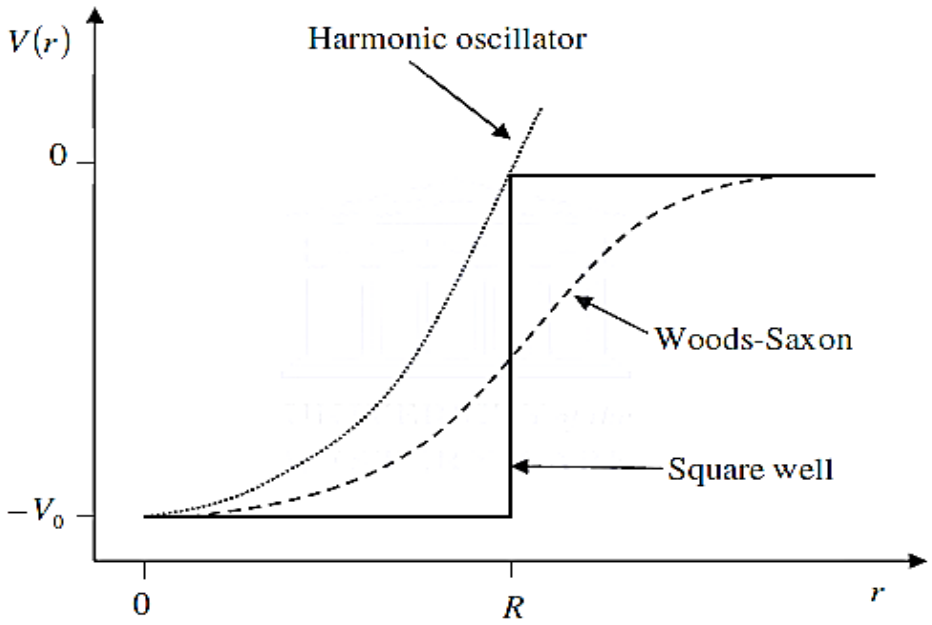

Figure 2.4. A comparison of one-dimensional harmonic oscillator potential, square well potential and Woods-Saxon potential.

Besides its ideal reproduction of magic numbers, the shell model has been used to successfully interpret nuclear properties in more ways than one, such as the magnetic dipole moments, the electric quadrupole moments, the spin-parity assignments of ground states of odd-A nuclei, the isomer distributions, and the γ-ray transition probabilities. The shell model can also be used to predict and interpret excited states as well. Excited states are often calculated by considering nucleons outside a specific magic or doubly-magic core as single particles. It is assumed that nucleons up to the closed major shells or sub-shells are too tightly bound to contribute to nuclear excitations (Obed, 2011).

However, despite its success, the shell model still has some limitations because it simply treats nucleons as independent particles (Obed, 2011), moving in a spherical mean potential produced by themselves. Even after including the pairing effect, the residual interaction and the possibilities of the configuration mixture, the shell model still cannot predict or interpret some features and phenomena of nuclei, such as larger quadrupole moments observed in nuclei far away from magic numbers, and certain distinguishing properties in low-energy excitations or high-energy excitations.

2.2.2. Nuclear Collective Models

The shell model, as described above, has been quite successful in explaining nuclei close to the magic numbers (Obed, 2011). However, while moving away from the closed shells, some simple and systematic features start to show up, which could not be understood in terms of shell model. These include large ground state quadrupole moment, enhanced E2 transition probabilities rotor like energy spectrum etc. These observations suggest that in these nuclei, such large effects can arise through a coherent participation of all the nucleons. To understand the collective features away from the closed shells, Aage Bohr and Benjamin Mottelson had developed Collective model.

One of the most characteristic empirical facts of nuclear systematics is that the shell model picture of nearly independent particle motion under the influence of weak residual interactions in simple configurations breaks down as one adds more and more valence nucleons past magic numbers (Casten, 1990). Simply put, the residual interactions among a growing number of valence nucleons build up to such an extent that they obliterate much of the underlying shell structure.

The shell model wave functions become a poor first-order approximation to the real nuclear wave functions (Casten, 1990). In short, they no longer serve as the most appropriate basis states. In general, in a physical system, one always searches for some suitable set of basis states such that the realistic wave functions are dominated by one or a few components and any admixtures of basis states can be treated as relatively small perturbations. This is not to say that the shell model cannot provide a valid microscopic description of such collective excitations.

Many nuclear phenomena indicate that the nuclear motion does not consist of only the simple single particle excitations (Shaohua, 2010). Instead, there are a few typical effects that imply a collective motion, where all or at least large parts of nucleons in a nucleus move coherently with well-defined phases. Nearly all nuclei with neutron numbers at mid shell between two major magic numbers show some degree of collective behaviors. Two important types of the collective motions are the surface vibration of the nuclear shape that is a motion of nucleons from one region of the nuclear sphere to another one and the rotation of the entire nucleus.

The first step of the collective model was made by Bohr and Mottelson in the 1950s (Shaohua, 2010). One important Hamiltonian of a collective motion including vibrational motions, rotational motions and their interactions, namely the rotation-vibration model, is given by

$$\hat{H}_{coll} = \hat{H}_{rot} + \hat{H}_{vib} + \hat{H}_{vib\ rot.} \tag{2.6}$$

In even-even nuclei, strong indicators for the collectively rotational motions are, for example, the ratios of the lowest 4^+ to 2^+ state energies and the large 2^+ state electric quadrupole moments.

Evidence of the rotational and vibrational motions is shown in Figure 2.5 (Shaohua, 2010), where the ratios of the first 4^+ to 2^+ level energies are shown.

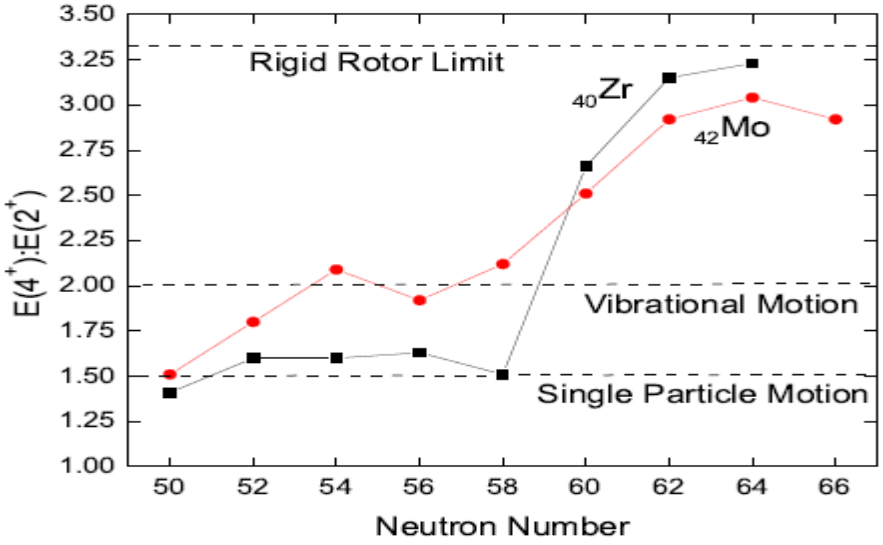

Figure 2.5. E (4+): E (2+) of yrast bands of even-even Zr and Mo isotopes.

2.2.2.1. Bohr - Mottelson Model

The most striking evidence of the collective phenomenon in nuclei was provided by the existence of rotational bands in the nuclear spectra observed in the Coulomb excitation studies (Varshney, 1982). The Coulomb excitation studies also revealed the systematic occurrence of strong E2 transition in nuclei outside the rotational regions. The low energy spectra of even-even nuclei outside the rotational regions could be interpreted, at least qualitatively, in terms of quadrupole vibrations about a spherical equilibrium.

Large values of quadrupole moments can be obtained if the nuclei are assumed to be deformed so that they have permanent non-spherical shapes. Rainwater noted that the many number of protons

in nucleus can give large value of electric quadrupole moments as a result of the polarizing action of one or more loosely bound nucleons on the remaining nucleus, which is the basic of collective behavior (Varshney, 1982).

Bohr-Mottelson have developed a single model called the unified model. It is an extension of shell model. In this model the shell model potential is assumed non-spherical (Varshney, 1982). The energies of the single particle in this non-spherical potential are calculated, and the distortion which gives the minimum energy is taken as the actual distortion. The long range correlations are replaced by the assumption of a permanently distorted potential. The model necessarily represents the collective effects of the nucleons in the nucleus. This model is a symmetric rotor type.

Bohr and Mottelson (Demille et al., 1959; Shaoshua, 2010) have shown that even-even nuclei with spheroidal shapes may be expected to exhibit rotational states with energy levels given by

$$E_{rot} = \frac{\hbar^2}{2\Im} I(I+1), \qquad I = 0, 2, 4, 6, \ldots \tag{2.7}$$

where $\Im$ is the effective moment of inertia and I the total nuclear angular momentum.

2.2.2.2. Asymmetric Rotor Model

The models we have discussed so far incorporate excursions from axial symmetry that are both small and dynamic (Casten, 1990). Certainly, such an approach accounts reasonably well for the deviations of most well-deformed nuclei from the properties of the pure axial rotor. However, there have long been indications that larger and possibly permanent (static) asymmetries also occur.

Naturally, this would lead to more radical departures from the energy and transition rate expressions we have considered. In fact, in certain limiting cases of large asymmetry, new selection rules appear. In another sense, however, such models for larger asymmetry are extensions of the small excursions from axiality dealt with so far, and their predictions go over into the latter as $y \rightarrow 0°$.

The asymmetry parameter γ of ARM determines the deviation in shape of the nucleus from axial symmetry and it varies between 0 and $\pi/3$. When the asymmetry parameter γ is equal to zero, the energy spectrum is found to be identical to an axially symmetric nucleus and the ARM model produces the symmetric rotor "γ -band" (non-staggered) energies (Parveen & Harish, 2015).

The deviation of axial symmetry of even-even nuclei (i.e., as the asymmetry parameter γ increases) only slightly affects the rotational spectrum of the axial nucleus; however, a few new rotational energy states with spin 2, 3, 4, etc. may be visible. This effect becomes large when the asymmetry parameter $\gamma = 20^0$. The nucleus gets more deformed with increase in γ and finally the nucleus becomes triaxial near $\gamma = 30^0$ (Parveen & Harish, 2015).

Bohr and Mottelson (Bohr & Mottelson, 1998) have developed the hydrodynamic model in a completely general fashion restricting the treatment to axial symmetry when they considered the coupling of the odd nucleon to the core. Bohr-Mottelson model was unable to explain the very large deviations from the rule for B(E2) branching ratios. This leads Davydov and Filippov take a quite different path in extending the collective vibrations of spherical nuclei to the deformed region. Davydov and Filippov postulated the existence of the triaxial nuclei, that is, nuclei with fixed β and γ-deformations. They calculated the energy spectra and B(E2) transition probabilities

resulting from the asymmetric rotator. Although some physicists have been skeptical of such hypothesis on theoretical grounds, the fact is that the calculations with the Davydov-Filippov model have led to quite impressive agreements with experimental data.

The best known model of fixed stable asymmetry (triaxiality) is that of Davydov and co-workers developed around 1960 (Casten, 1990). Here, the potential V(γ) is envisioned to have a steep, deep minimum at a particular value of γ so that the nucleus takes on a rigid shape with that asymmetry.

A general form of the Hamiltonian for nuclear collective motion can be written as (Casten, 1990; Hassan, Hadi & Akpan, 2017; Ikot, Sobhani & Hassanabadi, 2017; Yigitoglu & Dennis, 2011)

$$H = -\frac{\hbar^2}{2B}\left[\frac{1}{\beta^4}\frac{\partial}{\partial\beta}\left(\beta^4\frac{\partial}{\partial\beta}\right) + \frac{1}{\beta^2\sin(3\gamma)}\frac{\partial}{\partial\gamma}\left(\sin(3\gamma)\frac{\partial}{\partial\gamma}\right) - \frac{1}{4\beta^2}\sum_{k=1}^{3}\frac{{I_k}^2}{\sin^2\left(\gamma - \frac{2\pi}{3}k\right)}\right] + V(\beta,\gamma) \quad (2.8)$$

in which, intrinsic deformation coordinates are denoted by β (departure from the spherical shape), γ (departure from axial symmetry) and I_k (k = 1, 2, 3) the operators of the total angular momentum projections in the intrinsic reference, and B is mass parameter.

The solution of this equation is quite complicated (Sukomal, 1973). Different nuclear models use different approximations to solve this Schrodinger equation. Davydov and Filippov have assumed fixed values of β and γ for the rotating nucleus that is the intrinsic structure of the nucleus remained unchanged during rotation called the adiabatic approximation. The Schrodinger equation in this case can be written as

$$-\frac{\hbar^2}{8B\beta^2}\left[\sum_{k=1}^{3}\frac{I_k{}^2}{\sin^2\left(\gamma-\frac{2\pi}{3}k\right)}\right]\psi = E\psi \tag{2.9}$$

Here k denotes the nuclear fixed axis (1, 2, 3). For the asymmetric rotor, k is not a good quantum number. The eigenfunctions can be written as a sum over the various values of k,

$$\psi_{IM} = \sum_k g^I_{ki}(\gamma)|KMI> \tag{2.10}$$

where $g^I_{ki}(\gamma)$'s are the various amplitudes.

For a given I, K runs over all even integers less than or equal to I, except for the odd I, where K=0 is excluded. Consequently, there are no I = 1 states and I = 3 has a fixed value of K, namely 2. The subscript I indicates that for other values of I there are more than one states, corresponding to different allowed values of K. Thus, there is one 0^+ state, two 2^+ states, one 3^+ state, three 4^+ states, two 5^+ states, and so on.

Solving for the angular momentum matrix elements in explicit form the following equation arises and its solutions give the energies for the various states (Sukomal, 1973):

$$g^I_{k+2}(\Im_2-\Im_1)\,\Im_3[(I-K)(I-K-1)(I+K+1)(I+K+2)]^{\frac{1}{2}} + g^I_k[2(\Im_1+\Im_2)\,\Im_3(I^2+I-K^2) + 4\Im_1\Im_2K^2 - 8(\tfrac{E}{\hbar^2})\,\Im_1\Im_2\Im_3] + g^I_{k-2}\,(\Im_2-\Im_1)\,\Im_3[(I+K)(I+K-1)(I-K+1)(I-K+2)]^{\frac{1}{2}} = 0 \tag{2.11}$$

Where $\Im_1$, $\Im_2$ and $\Im_3$ represent the moment of inertia for the three axes, refer Eqn. (2.26) for their explicit form. The determinant of the coefficients of $g_k's$ must be zero for a solution. For I = 2, the following equation emerges which has two roots giving two energies for this spin value,

$$(\frac{E}{\hbar^2})^2\text{-}2(\frac{E}{\hbar^2})\,(\Im_1^{-1}+\Im_2^{-1}+\Im_3^{-1}) + \frac{3}{8}\,[\Im_1^{-2}+\Im_2^{-2}+6\Im_1^{1}\Im_2^{-1}+ 8(\Im_1^{-1}+\Im_2^{-1})\,\Im_3^{-1}] = 0 \qquad (2.12)$$

$\gamma = 0^o$, corresponds to the axially symmetric case and $\Im_1 = \Im_2 = \Im, \text{and } \Im_3 = 0$ for this case. The roots of the above equation for this situation turns out to be of the form

$$E_I = \frac{\hbar^2}{2\Im}\,I(I+1) \quad \text{for K= 0} \qquad (2.13)$$

2.3. Nuclear Shapes and Deformations

Many nuclei, particularly those away from the closed shells, are appreciably deformed, and this affects many of their properties (Hodgson et al., 1997). Therefore, there is a need for a convenient way of defining the deformation, and then go on to see how it affects the measurable properties.

The nuclear shapes and deformations have been interesting topics to the nuclear physicists, since the identification of nucleus. The highly complicated nature of structure and properties of nuclei may be one of the reasons for this (Girija, 2012). Moreover, shape is one of the fundamental properties of nuclei. Till date, no theory is developed to describe the nuclear structure and properties completely, since the knowledge about the forces which shape the nucleus is very limited. The configuration dependent forces present inside the nucleus are mainly the nuclear force between nucleons and Coulomb force between protons.

The shell effects and pairing correlation also contribute to the determination of nucleonic configuration. The atomic nuclei exhibit spherical, quadrupole and higher order multipole deformed shapes, even though the quadrupole deformed shapes are mostly discussed. Due to the interplay between single particle and collective degrees of freedom, the coexistence of different shapes at the same spin and similar energies is also not rare (Girija, 2012).

Nuclei having spherical shape in their ground state are few in number. The deformed nuclei are classified into prolate, oblate and tri-axial. Prolate and oblate nuclei are axially symmetric. If the third axis of the nucleus is longer than the others, the nucleus is prolate and if it is shorter, the nucleus is oblate. For triaxial nuclei, the three axes are different. In nature, prolate nuclei dominate over oblate ones. It is found that 86% (Girija, 2012) of the even-even nuclei are prolate in the ground state and triaxial shapes are very rare for them.

The effect of Coulomb repulsion between protons is to deform the nucleus more into an elongated shape than to a flattened shape. The difference in the volume element of the collective coordinates between prolate and oblate shapes is pointed out to be another reason for the prolate dominance over oblate shape. The spin-orbit coupling potential between nucleons plays a role favoring stable prolate shape for nuclei. The shell structure of nuclei is also responsible for the variety of shapes, depending on the position of Fermi level between two closed shells. Prolate shape occurs just after closed shells and towards the end of closed shells, oblate shape is observed (Girija, 2012).

Nuclear deformation is characterized by two collective parameters, the deformation parameter β and the triaxiality parameter γ (Girija, 2012). The deformation parameters β and γ of the collective model (Singh et al., 2011) are basic description of the nuclear equilibrium shape and structure. It

has been shown by the study of even-even nuclei in the regions A <=150 and A >=190 that the properties of their excited levels can be accounted for by considering the rotational motion of non-axially symmetric nuclei or nuclear vibrations.

Properties of excited states: energy levels, spins, values of the electric multipole transitions, average values of electric multipole moments etc. are determined by the shape of nucleus and the nuclear deformability. The shape is a fundamental property of the nucleus and, while the majority of nuclei are thought to be axially symmetric, triaxial deformation has been a subject of much recent interest in nuclear structure studies (Nadirbekov & Yuldasheva, 2014).

The presence of triaxial deformation at or near the ground state has been studied extensively in the past (Obed, 2011), primarily via Coulomb excitation of stable nuclei, without reaching definitive conclusions for any region of the nuclear chart as the nuclei involved are more commonly viewed as γ-soft rather than as rigidly triaxial. The excitation spectra of even-even nuclei in the energy range ≤ 2 MeV show characteristic band structures that are interpreted as vibrations and rotations of the nuclear surface in the geometrical collective model first proposed by Bohr and Mottelson and elaborated by Faessler and Greiner.

The collective model, extends the liquid drop model by including motions of the whole nucleus such as rotations and vibrations. The collective model emphasizes the coherent behavior of all of the nucleons. The moving nuclear surface may be described quite generally by an expansion in spherical harmonics. This model is based on the concept of a nuclear surface defined by the surface coordinate R in the (θ, ϕ) as (Malin, 2016; Obed, 2011)

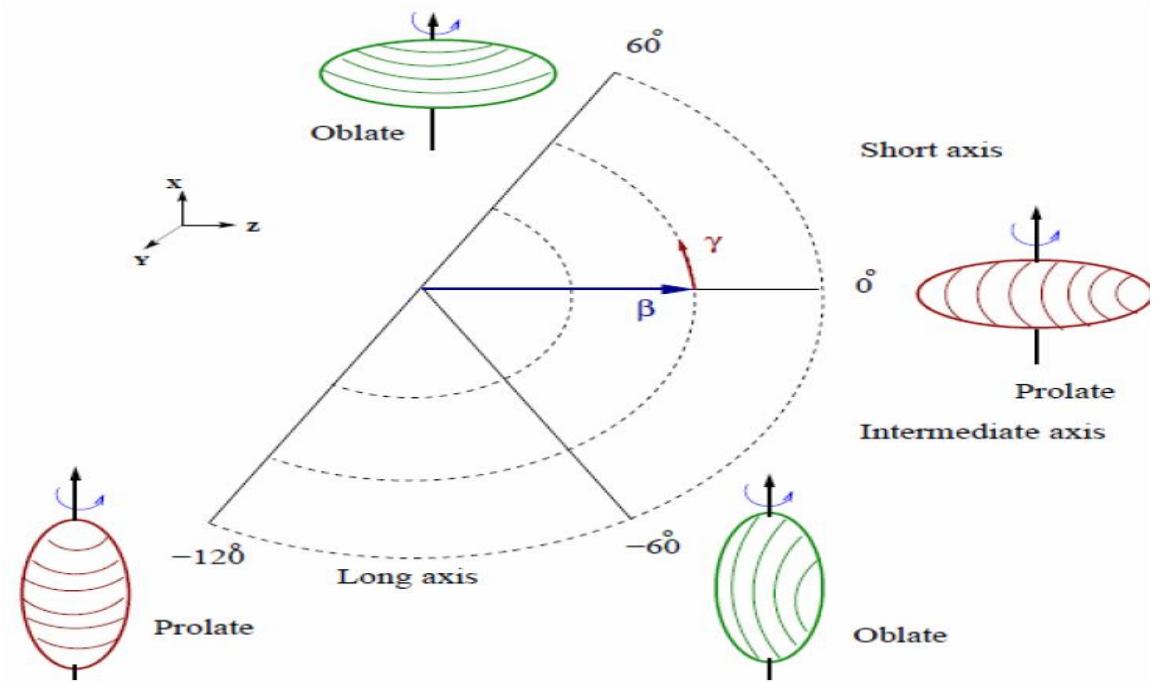

Figure 2.6. Various nuclear shapes in (β - γ) plane. On the top left is shown the principal axes of intrinsic frame.

$$R(\theta, \phi) = R_0[1 + \sum_{\mu} \alpha_{\lambda\mu} Y_{2\mu}(\theta, \phi)] \quad (2.14)$$

where R_0 is the radius of the spherical nucleus. The $\alpha_{\lambda\mu}$ represent the expansion of any general function of the angels (θ, ϕ) in terms of the complete set of spherical harmonics $Y_{\lambda\mu}(\theta, \phi)$, λ is multi-polarity of the shape oscillations, and μ is the projection of λ.

The $\lambda = 0, 1$ terms are called as monopole mode and dipole mode, respectively. These monopole and dipole terms can be discarded based on the arguments of incompressibility and translational symmetry, respectively. Considering $\lambda = 2$ term in the expansion and making suitable transformation to intrinsic frame with axis 1, 2 and 3, the five coefficients of $\alpha_{2\mu}$ reduces to two real independent deformation parameters α_{20} and $\alpha_{22} = \alpha_{2-2}$ for axially symmetric quadrupole deformation (Obed, 2011).

Nuclear shape is usually specified in terms of the two nuclear deformation parameters β and γ. The β parameter represents the extent of quadrupole deformation, while γ gives the degree of axial asymmetry. Nuclear triaxiality is associated with the breaking of axial symmetry of the quadrupole deformation (Nadirbekov, 2016; Nadyrbekov & Bozarov, 2017). These two parameters can be expressed in terms of the Hill-Wheeler (David & John, 1953) co-ordinates β and γ as:

$$\alpha_{2,0} = \beta\cos\gamma, \quad \alpha_{2,2} = \frac{1}{\sqrt{2}}\beta\sin\gamma \tag{2.15}$$

such that,

$$\sum_{\mu} |\alpha_{2,\mu}|^2 = \alpha_{2,0}^2 + 2\alpha_{2,2}^2 = \beta^2 \tag{2.16}$$

β represents the extent of quadrupole deformation, while γ gives the degree of axial asymmetry.

The expression for the radius, Eqn. (2.14), using the spherical harmonics $Y_{2,0}$ and $Y_{2,\pm2}$ in the intrinsic frame can be written as:

$$R(\theta, \phi) = R_0 [1 + \alpha_{20} Y_{2,0}(\theta, \phi) + \alpha_{22} Y_{2,2}(\theta, \phi) + \alpha_{2-2} Y_{2,-2}(\theta, \phi)] \tag{2.17}$$

$$R(\theta, \phi) = R_0[1 + \beta\sqrt{\frac{5}{16\pi}}(\cos\gamma\,(3\cos^2\theta - 1) + \sqrt{3}\sin\gamma\sin^2\theta\cos2\phi)] \tag{2.18}$$

Increment in length $\delta_R = R(\theta, \phi) - R_0$ along the three body fixed axes can be written (From Eqn. (2.13)) as,

$$\delta R_k = R_0 \sqrt{\frac{5}{4\pi}} \beta \cos(\gamma - \frac{2\pi}{3}k) \tag{2.19}$$

where, k = 1, 2, 3.

Two distinct axially symmetric shapes are possible for different orientations in space, viz,

- Prolate Shapes: for $\gamma = 0^0$, 120^0 and 240^0
- Oblate Shapes: for $\gamma = 60^0$, 180^0 and 300^0

In Figure 2.6, we have shown nuclear shapes in the $\beta - \gamma$ plane for $\lambda = 2$. In this figure, Lund conventions have been used (Obed, 2011). $\gamma = 0^0$ (-60^0) correspond to collective prolate (collective oblate), whereas the $\gamma = 60^0$ (-120^0) describes the non-collective oblate (non-collective prolate). If the value of γ is not a multiple of 60^0, then triaxial shapes occur. Due to discrete symmetries, the interval $0^0 \leq \gamma \leq 60^0$ is sufficient to describe all the quadrupole shapes.

Therefore, the parameter β, related to the quadrupole deformation, is a measure of the deviation of the nuclear shape from spherical. The larger β is the more quadrupole deformation a nucleus has. Since $\alpha_{22} = \frac{1}{\sqrt{2}}\beta \sin\gamma$ vanishes for the axially symmetric quadrupole deformation, the parameter γ describes the departure from axial symmetry. Further, for axially symmetric shapes, the only remaining $\alpha_{\lambda 0}$ can be simplified as $\alpha_{\lambda 0} = \beta_\lambda$. Without going into details, it is known that in the (β, γ) plane = $0^0 - 60^0$ is sufficient to describe all ellipsoidal shapes. The different 60^0 sectors only

correspond to a different labeling of the three principal axes. The z-axis is chosen as the symmetry axis here. The nucleus is a prolate ellipsoid for $\gamma = 0^0$ or an oblate ellipsoid for $\gamma = 60^0$. If $0^0 < \gamma < 60^0$, the nucleus is expected to be triaxial with maximum triaxiality at $\gamma = 30^0$ (Shaohua, 2010).

The nuclear parameter β can be either positive or negative for axially symmetric nuclei (Shaohua, 2010). In this case, the positive β corresponds to prolate while the negative to oblate. In addition, one can obtain the relationship between β and the electric quadrupole moment in quadrupole deformations as

$$Q_0 \approx \frac{3}{\sqrt{5\pi}} eZR_0^2\beta \tag{2.20}$$

Therefore, the nucleus is prolate (or oblate) if its Q_0 is positive (or negative). The Q_0 is called the intrinsic electric quadrupole moment, to differentiate the experimental (or laboratory) electric quadrupole moment Q, which can be measured experimentally. In the unified model, the relationship between these quantities is expressed as

$$Q(I) = \frac{3K^2 - I(I+1)}{(I+1)(2I+3)} Q_0 \tag{2.21}$$

for different levels with spins I.

The electric quadrupole moment is a measure of the deviation from spherical symmetry of the nuclear charge density distribution inside the nucleus, and it has the dimensions of area and is measured in m^2 or barns (Alya'a, 2016). Then the Q(I) is an important property of nuclei and from

the quadrupole moment we can determine whether the nucleus is spherical Q(I) = 0, deformed oblate Q(I) < 0 or prolate Q(I) > 0 shapes.

The Q_0 can be derived from the B(E2) value and given by

$$Q_0 = [\frac{16\pi}{5} B(E2)]^{\frac{1}{2}} \quad (2.22)$$

2.4. Nuclear Rotation and Moment of Inertia

An interesting feature of nuclear structure is deformation. It has been known for a long time, that heavy nuclei with many valence nucleons of both kinds tend to take on a static prolate axially symmetric quadrupole deformation in their ground state. Regular rotational excitation bands are beautiful evidence of this fact. Excitations and behavior of deformed even-even nuclei can be very successfully described using collective models (Bohr & Mottelson, 1998).

A collective excitation is characterized by the movement of a large number of nucleons. Rotation is a typical example of collective degree of freedom in nuclei (Bohr & Mottelson, 1998). The shape variation of nuclei can be considered as another collective degree of freedom. Since nuclear deformation is a collective property, only collective models can successfully describe the behavior of deformed nuclei. One cannot define collective rotation around a symmetry axis, since such a rotation would change only a trivial phase factor in the wave function.

Such an unchanged wave function is in contrast to collective rotation (Bohr & Mottelson, 1998). Instead, collective rotation is characterized by small angular momentum contributions from a large

number of particles, i.e., the wave functions of these particles change slowly with increasing angular momentum. This implies that only deformed nuclei can rotate collectively and if the nucleus is axially symmetric, the only possible rotation axis is perpendicular to the symmetry axis.

For collective rotation of a nucleus (Girija, 2012),

$$H_{rot} = \frac{L^2}{2\Im} \tag{2.23}$$

where $\Im$ is the moment of inertia and L is the collective angular momentum, which equals the total angular momentum I (total spin) in pure collective rotation. The simple collective model prediction for the energy dependence of the rotational levels of an axially symmetric nucleus is given by (Girija, 2012; Gregory, 1965):

$$E_I = \frac{\hbar^2}{2\Im} I(I+1) \tag{2.24}$$

Since only deformed nuclei exhibit rotational spectra, it should be possible to determine deformation from the occurrence of rotational bands. The moment of inertia can also be extracted from measured rotational bands. A rotational band is a group of closely spaced states differing in angular momentum slightly. In deformed nuclei, the valence particles add their spin to the angular momentum due to rotation.

Numerous experiments (Yuri, 2005) have shown that many nuclei have electric quadrupole moments much greater than predicted by the shell model. Large quadrupole moments of nuclei are caused by the deviation of these nuclei from spherical symmetry. Indeed, if a nucleus has the form

of an ellipsoid, then its electric quadrupole moment will be proportional to the amount of deformation.

Nuclei with all nucleon shells filled are spherically symmetric (Yuri, 2005). If a nucleus has one or a few nucleons above the closed shells, these nucleons can deform the nucleus via their interaction with the core. It was theoretically proved that one nucleon above the closed shell could have lower energy if its potential well was not spherical. Therefore, the nucleus consisting of a core with closed shells and an additional nucleon (or nucleons) can achieve a state with lower energy if the core becomes non-spherical.

Two types of collective motions of nucleons can be observed in nuclei (Yuri, 2005). First, there are the vibrations of the nucleus, namely the vibration of its shape, which is not accompanied by changes in density because nuclear matter is in fact incompressible. Non-spherical nuclei can vibrate as well as spherical ones. The energy spectra of many nuclei have levels of a vibrational origin. The properties of such levels are predicted by the collective model of a nucleus.

Another type of collective motion of nucleons is the rotation of non-spherical nuclei. If the rotation of a non-spherical nucleus is rather slow, as it is in many cases, then such rotation will not substantially influence the motions of separate nucleons inside the nucleus and the possible small vibrations of the nuclear surface. Under these conditions the rotational energy can be explicitly extracted from the total energy of a nucleus (Yuri, 2005). In other words, the energy spectrum of a non-spherical nucleus comprises, besides the levels of a stationary nucleus, also the levels of its rotation. The intervals between the rotational levels turn out to be small compared to those for the levels of a stationary nucleus (one-particle levels).

If the nucleus takes the shape of a rotational ellipsoid, then such a quantum mechanical system can rotate only around the axis perpendicular to its axis of symmetry. Indeed, rotation of the nucleus around its axis of symmetry does not alter its orientation in space, thus its states are not distinguishable and the energy of a system does not change (Yuri, 2005). Any rotation about an axis that is inclined at a definite angle to the axis of symmetry can always be represented as a result of rotations about the axis of symmetry and the axis perpendicular to the axis of symmetry. Since a change in the spatial orientation of a nucleus takes place only in the second case, a rotation of a non-spherical nucleus about an arbitrary axis becomes, in fact, a rotation about the axis perpendicular to the axis of symmetry.

A spherical nucleus cannot rotate, so it has no rotational degrees of freedom. This statement also concerns any spherically symmetric quantum system whose states are indistinguishable upon spatial rotation. Further from closed shells, the accumulating p-n interaction strength leads to additional configuration mixing and deviations from spherical symmetry even in the ground state, and so we now turn to consider nuclei with stable and permanent deformations (Casten, 1990; Samuel, 2004). The lowest applicable shape component is a quadrupole distortion. There can also be octupole and hexadecapole shapes in the nuclear deformation.

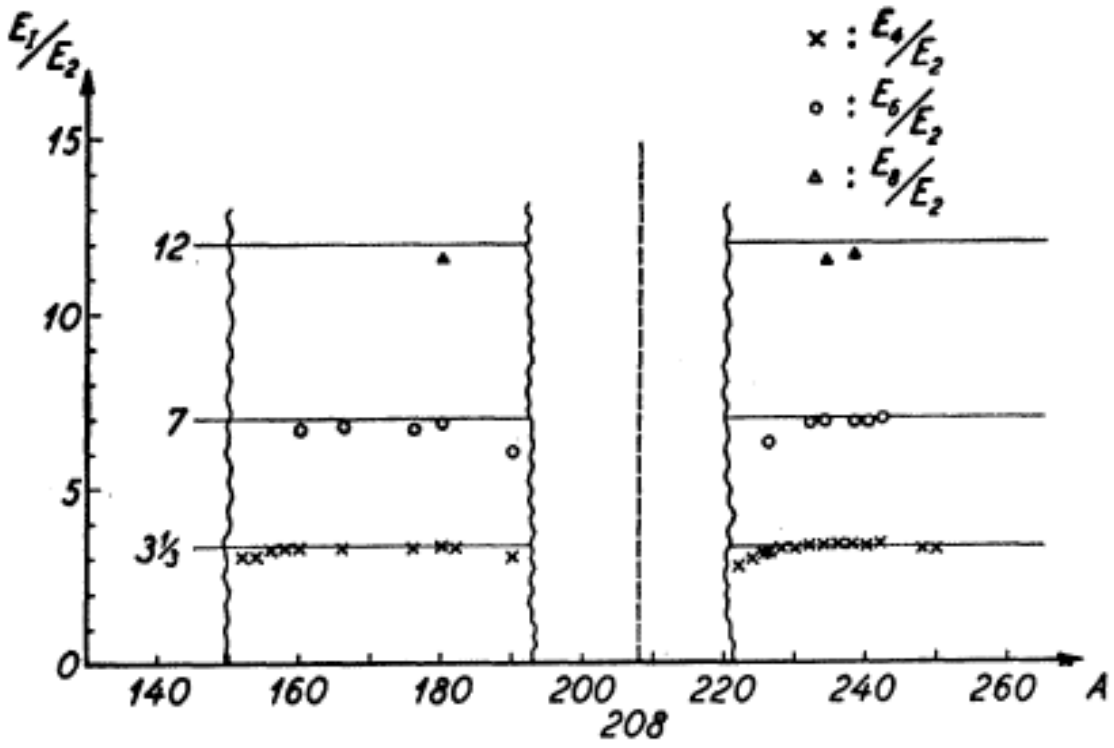

Figure 2.7. Experimentally observed energy ratios for excited states in rotational bands in even-even nuclei.

The experimental evidence on the rotational spectra of even-even nuclei is shown in Figure 2.7. This gives the ratio of the measured excitation energies of the excited states to the energy observed for the first excited, 2^+, states in these nuclei.

- $2.23 < E(4^+)/E(2^+) < 3.33$: Deformed Region
  - ✓ $3 < E(4^+)/E(2^+) < 3.33$: Rotation Region
  - ✓ $2.4 < E(4^+)/E(2^+) < 3$: Transition Region
  - ✓ $2 < E(4^+)/E(2^+) < 2.4$: Vibration Region
- $1.82 < E(4^+)/E(2^+) < 2.23$: Spherical Region
- $1.00 < E(4^+)/E(2^+) < 1.82$: Magic Region

The most important property distinguishing non-spherical from spherical nuclei is the presence in non-spherical nuclei of rotational energy levels (Alex, 1997). Whereas the general features of the rotational spectra, for example, the ratios of the energies, the values of the spins and parities, the symmetry of the states, etc. are entirely determined by the rotational nature of the levels, the absolute values of the rotational energies, that is, the magnitudes of the moments of inertia, depend essentially on the internal structure of the nuclei.

A detailed comparison of the observed excitation spectra of deformed nuclei with the predictions of the rotational model in which the nucleus is regarded as an axially symmetric rotator has shown that, although the rotational model does reproduce well the features of the rotational spectra for many nuclei, there is, nevertheless, disagreement between the observed picture and the predictions of the simple rotational model for certain nuclei. Attempts to explain the discrepancy by including corrections for the non-adiabaticity of the rotation have been unsuccessful (Alex, 1997).

Davydov and Filippov have shown that the difficulties can be removed if the assumption of axial symmetry of the deformed nuclei is discarded (Davydov & Filippov, 1958). They developed a theory of non-axial nuclei, in which the fundamental assumption is that the deformed nucleus is a triaxial ellipsoid whose rotation determines the spectrum of the collective excitations of the nucleus. This theory has made it possible to describe the principal features of the spectra of the excited states of most even-even nuclei.

In the adiabatic approximation, when the rotational motion can be separated from the vibrations of the nuclear surface and from the one particle motion, the shape of the nucleus can be assumed fixed; then the Hamiltonian describing the rotation of an even-even nucleus can be written in the form (Alex, 1997)

$$H_r = \sum_{k'} \frac{\hbar^2}{2\Im_{k'}} I_{k'}^2 \tag{2.25}$$

where $I_{k'}$ are the projections of the total angular momentum operator along the principal axes of the ellipsoid and $\Im_{k'}$ are the moments of inertia about the principal axes, given by

$$\Im_{k'} = 4B\beta^2 \sin^2(\gamma - \frac{2\pi}{3}k') \tag{2.26}$$

These three moments of inertia of the nucleus are assumed to be all different. The rotational energy operator Eqn. (2.25) acts only on the Euler angles and is the Hamiltonian operator of a rigid non-axial rotator (asymmetric top).

The operator H_r and the commutation relations Eqn. (2.25) for the projections $I_{k'}$ of the total angular momentum along the principal axes are invariant under the transformations of the group D_2 (See Appendix A) consisting of the three rotations through an angle of 180^0 about the axes (Alex, 1997). The Hamiltonian commutes with all the operations of the group D_2. Since each element of the group D_2 forms a class of the group, and the number of classes of a group is equal to the number of irreducible representations, there are in all four one dimensional irreducible representations of the group D_2.

It is well known (Alex, 1997) that there is a close connection between the eigenfunctions of the stationary states and the irreducible representations of a group of transformations which commute with the Hamiltonian. The energy states of the system can be classified according to the irreducible representations corresponding to these states. It is clear that the degeneracy of an energy level coincides with the dimensionality of the representation, that is, with the number of basis functions of the representation. All these functions belong to the same energy value. Thus, knowing the irreducible representations of the symmetry group according to which the stationary state wave functions transform, we can find certain properties of these functions without solving the Schrodinger equation.

In the case under consideration, all the irreducible representations of the group D_2 are one-dimensional, and so the energy states of the corresponding physical system are non-degenerate (Alex, 1997). Since there are four irreducible representations in all, the stationary-state wave functions can be classified by their symmetry properties into four types. Those states which belong to the irreducible representation are unchanged under the action of any of the operations of the group D_2. These states are called fully symmetric states, and the representation corresponding to them is called the fully symmetric representation. Usually, the ground state of the system belongs to the fully symmetric representation.

The wave functions of the collective motions in even-even nuclei depend only on the spatial coordinates of the nucleons. Since the spins of two identical nucleons in the same one-particle (orbital) state have opposite orientations, the coordinate wave function will be symmetric. In as much as the spatial coordinates of the nucleons are interchanged by the operations Rj'(π), the wave function describing the rotation of the nucleus must belong to the fully symmetric representation

of the group D_2, since only in this case will the wave function of the collective motions be transformed into itself, with the same sign, under any operation of the group D_2 (Alex, 1997).

It should be noted that the nucleus is not a rigid body (Obed, 2011), and measured moments of inertia are less than rigid body values at low spins. This is due to the effects of the pairing interactions, which make the nucleus behave like a superfluid. Experimental moments of inertia are larger than those of the corresponding irrotational flow of a superfluid, showing that the nucleus is somewhere between these two extremes. As the nucleus rotates, it is found that the moment of inertia changes as a function of spin.

Rotational energy spectra can be discussed in terms of three spin-dependent moments of inertia, which are related to the zero-, first- and second-order derivatives of the excitation energy with respect to the aligned angular momentum. The overwhelming success of the rotational model leaves little doubt that it is fundamentally correct (David, 2010; Heyde, 1999). But in formulating the model one does not really face up to the question of exactly how the nucleus is supposed to rotate. As we shall see, the moment of inertia is very sensitive to the character of the rotational motion. A major goal of any rotational theory must therefore be to predict this parameter successfully.

2.5. Internal Conversion Coefficient

A competing process to gamma-ray emission in the decay of bound nuclear states is internal conversion where an atomic electron emitted (Paddy, 2003). Here the electromagnetic (EM) field of the nucleus interacts with an atomic electron and the energy released by the nuclear decay is

transferred to the electron causing it to be ejected from the atom. The electron is released with a kinetic energy equal to the energy difference between the nuclear states minus the atomic binding energy for the electron shell from which it was emitted. Experimentally, electron conversion coefficients are very useful as they are dependent on the multipolarity of the transition and can thus give information on the spin and parity of nuclear states.

Internal conversion coefficients (ICC) convey important information about the atomic nucleus (Kibedi, Burrows, Trzhaskovskaya Nestor & Davidson, 2007). Through comparison of experimental ICCs with corresponding theoretical values, multi-polarities and mixing ratios of nuclear transitions are determined. As well as nuclear structure research, knowledge of accurate coefficients is needed in, for example, the determination of total transition rates (required for the normalization of decay schemes), Mossbauer spectroscopy (CEMS), or nuclear reaction calculations.

In the simplest way (Kibedi et al., 2007) the ICC is defined as

$$\alpha = \frac{\mathrm{ICE}}{\mathrm{I}_\gamma} \tag{2.27}$$

where ICE and Iγ are the electron and γ-ray intensities, respectively. The ICE represents the number of electrons ejected from an atomic shell (K, L1, L2, ...), a major shell (L, M, etc.), or the sum of all shells (total), or can be the intensity of the electron-positron pairs.

The internal conversion coefficient depends on the atomic number of the emitting nucleus (Z), the transition energy (Eγ), the transition multi-polarity (πL) and, in the case of internal conversion, the

atomic shell involved (Kibedi et al., 2007). Often the ratio of different ICCs, for example αK/αL or αL1/αL2, was used to determine the multi-polarity and/or the mixing ratio. Internal conversion coefficients also can be deduced from the intensity of x-rays or Auger electrons, which are emitted as the atomic vacancies are filled. There are a number of techniques developed to measure internal conversion coefficients, which usually require the knowledge of the intensity of two radiations, including conversion electrons, γ-rays, x-rays, β-rays, etc.

For many of the E2 transitions the total internal conversion coefficients, α_T, have been deduced by combining the reduced E2 electromagnetic transition probability, B(E2), obtained from Coulomb excitation with the half-life of the level, $T_{1/2}$, from lifetime measurements. The basic formula of the so called CEL method is defined by (Raman et al., 2001) as:

$$T_{1/2}(\text{ns})*(1+\alpha_T) = \frac{2.829\times10^{11}*E_\gamma^{-5}(\text{keV})}{B(E2)\uparrow(e^2b^2)} \qquad (2.28)$$

BrIcc has been primarily developed (Kibedi et al., 2007) to help Evaluated Nuclear Structure Data File (ENSDF) evaluators to calculate conversion coefficients using the best available theoretical data. The ENSDF (Kibedi, Burrows, Trzhaskovskaya, Davidson, & Nestor, 2008), is a computer-based file system, which is maintained by the National Nuclear Data Center at Brookhaven National Laboratory. The content of the file is regularly updated by the Network of Nuclear Structure and Decay Data (NSDD) network. For each isotope the ENSDF file usually contains a number of data sets. Each data set refers to a particular reaction or decay mode of a nucleus. The adopted level and gamma-ray properties are given in the adopted data set.

Conversion coefficients can be easily obtained at the BrIcc web interface at BrIcc-ANU. This interface also allows to generate chart of conversion coefficient (or ratios of conversion coefficients) vs transition energy, which can be useful to explore the sensitivity of ICC values to multi-polarities. A silent version of the code, BrIccS has also been developed to provide an easy and simple way to obtain conversion coefficients from computer programs running on various operating systems. BrIcc was developed in an ANU – NNDC (National Nuclear Data Center) - Petersburg – ORNL (Oak Ridge National Laboratory) collaboration for the International Network of Nuclear Structure and Decay Data (NSDD) Evaluators (Kibedi et al., 2008).

The total internal conversion coefficient has been calculated using online software known as Bricc v2.35 (conversion coefficient calculator), specifically RpIcc was used (Australian National University, 2011). The internal conversion coefficient is the ratio of the electron emission rate to the gamma emission rate. They are known to depend on four parameters: (1) the charge of the decaying nucleus, (2) the energy of the nuclear transition, (3) the atomic subshell out of which the orbital electron is ejected and finally, (4) the multi-polarity and parity of the nuclear transition.

The size of the electron conversion coefficient increases with (a) decreasing transition energy, (b) increasing Z of the nucleus and (c) increasing multipolarity (Paddy, 2003). Internal conversion coefficients provide important information about the atomic nucleus. Through comparison of experimental values with corresponding theoretical ones, multi-polarities and mixing ratios of nuclear transitions are determined. As well as nuclear structure research, knowledge of accurate coefficients is needed, for example, in the determination of total transition rates.

CHAPTER 3. Electric Transitions of Rotational Nuclear States

3.1. Introduction

In rotational model, electromagnetic transitions between two members of a band can take place by a change in the rotational frequency and, hence, the spin, without any modifications to the intrinsic state. We shall concentrate here on electric quadrupole (E2) transitions, as these are the most commonly observed intra-band transitions (Samuel, 2004).

As is well known (Davydov & Filippov, 1958), measurements of the transition probabilities between electric rotational nuclear states in a nucleus yield important information on the nature of the excited states. In particular, for elucidation of the nature of the second excited state of spin 2 in an even-even nucleus one may study the relative probability for transition from this level directly to the ground state or to the first excited state with a spin of 2. It has been assumed in a number of investigations that the first two spin 2 levels observed experimentally refer to one-phonon and two-phonon vibrations of the nuclear surface. In this case, transition from the second state to the ground state can take place only as a result of violation of the oscillator approximation.

One of the fundamental properties of the nuclei is their shapes (Akkoyun, Bayram & Kara, 2015). Nuclei with magic numbers of neutron and proton have a closed shell. Nuclei with neutron (N) or proton (Z) numbers far from a magic number generally have deformed shape. The simplest deformations are called quadrupole deformations where the nuclei can either take an oblate or a prolate shape.

The reduced electric quadrupole transition probability (B(E2)↑) includes nuclear information about energy of low-lying levels of nuclei. The first excited states of the even-even nuclei are 2^+. So, the transition from this state to the 0^+ ground state is important. It is highly related to nuclear quadrupole deformation parameter (β), mean lifetime (τ) and electric quadrupole moment (Q_0).

Accurate calculations of B(E2)↑ values represent a challenge for nuclear theory (Pritychenko, Birch, Singh & Horoi, 2013; Pritychenko, Birch & Singh, 2017). Therefore, it is warranted to explore nuclear systematics for realistic estimates of collectivities in even-even nuclei. The deformations of nuclei are important for understanding their shapes (prolate, oblate etc.) and structures. The lifetimes of the levels are useful for determining the energy levels in nuclei. So, there is much attention in B(E2)↑ value. The reduced electric quadrupole transition probability is measured, experimentally, by inelastic electron scattering, muonic x-ray measurement, Mössbauer spectroscopy, Coulomb excitation, lifetime measurement or resonance fluorescence.

Even-even nuclei are known to have 0^+ (zero angular momentum and even parity) ground states and several low-energy integer spin states (Bohr & Mottelson, 1998; James, 2007). The transition strengths between these levels are sufficiently strong and well established to support the view that most nuclei are collective. While the full and true structure of these nuclei is not known, the structure is clearly dominated by low spin degrees of freedom. To establish a reference frame in which we can discuss and compare data, models of adiabatic rotations are by far the most useful. To first order this is the best starting point for viewing selection rules and transition strengths.

The quantity B(Eλ), is known as the reduced transition probability and it is unique to the structure of a specific nucleus (James, 2007). For quadruple transitions (which is the dominant mode for

collective nuclei), it is common to use B(E2)'s to test and compare models, and it is done in units of $e^2.b^2$ (where 1b = 100 fm^2) or in units of w.u. (where $e^2.b^2 = (5.94\times10^{-6})A^{4/3}$ w.u.).

The aim of this particular work is to apply the Davydov-Fillipov model for calculating the values of the reduced electric quadrupole transition probability B(E2) for the rotational excited ground band states even-even nuclei of lanthanide and actinide series. We have employed the model dependent intrinsic quadrupole moment Q_0 in plotting our systematics which reflects the asymmetric spirit of the model in true sense.

3.2. Methods

The experimental transition probabilities in units of $e^2.b^2$ is related to the experimental mean-life by the expression (Raman et al., 2001; Varshney, 1982)

$$B(E2:I+2\rightarrow I)_{exp} = \frac{0.08162}{E\gamma 5(1+\alpha_T)T} \quad (3.1)$$

where Eγ is the energy involved in the transition and is expressed in MeV, Ƭ is the mean-life of the excited state in Ps, and α_T are the total internal conversion coefficients (calculated using Bricc online software named BrIcc v2.3S Conversion Coefficient Calculator (Australian National University, 2011)).

Mean-life of states can be calculated from half-life using the well-known relations $T_{1/2} = \ln2/\lambda$ and $T = 1/\lambda$ (Marton & Marton, 1963), where λ is the decay constant. From these relations we obtained

$$T = T_{1/2}/\ln2 \text{ or } T_{1/2} = \ln2 * T \quad (3.2)$$

Using these relations, we can rewrite the experimental transition probability as

$$B(E2:I+2\rightarrow I)_{exp} = \frac{0.0566}{E\gamma 5(1+\alpha_T)T_{1/2}} \tag{3.3}$$

This experimental formula has been derived to incorporate the half-life rather than the mean-life of rotational excited states to compute the values of B(E2).

Using Eqn. (3.1), we can rewrite the experimental mean-life as

$$\tau = \frac{0.08162}{E_\gamma{}^5(1+\alpha_T)B(E2:I+2\rightarrow I)_{exp}} \tag{3.4}$$

The electric quadrupole transition probabilities for transitions inside the ground state rotational band between two states of spin I and I' are described by the following empirical formula (Varshney, 1982):

$$B(E2: I \rightarrow I')_{emp} = \frac{5e^2Q_0^2}{32\pi}(2I00|I'0)^2\{1+\frac{3-2\sin^2(3\gamma)}{[9-8\sin^2(3\gamma)]^{1/2}}\} \tag{3.5}$$

where $(2I00|I'0)$ are Clebsch-Gordon coefficients in the notation (2Jmm'|J'm') (See Appendix A).

For transition between two states of ground state rotational band, the Clebsch-Gordon coefficients have the form

$$(2I00|I'0)^2 = \frac{3}{2}\frac{(I+1)(I+2)}{(2I+3)(2I+5)} \tag{3.6}$$

in decay or de-excitation from I+2 → I.

Hence,

$$B(E2: I+2 \rightarrow I)_{emp} = \frac{15e^2Q_0^2}{64\pi}\frac{(I+1)(I+2)}{(2I+3)(2I+5)}\{1+\frac{3-2\sin^2(3\gamma)}{[9-8\sin^2(3\gamma)]^{1/2}}\} \tag{3.7}$$

where Q_o is the intrinsic quadrupole moment given by (Raman et al., 2001)

$$Q_o = \left[\frac{16\pi}{5}\frac{B(E2)\uparrow}{e^2}\right]^{1/2} \tag{3.8}$$

where B(E2)↑is the reduced electric quadrupole moment transition probability between the 0^+ ground state and the first 2^+ state in even-even nuclides. The B(E2)↑values are basic experimental quantities that do not depend on nuclear models.

The intrinsic quadrupole moment can also be given by

$$Qo = \frac{3}{\sqrt{5\pi}} ZR_0^2\beta\ (1+ 0.16\beta) \tag{2.9}$$

to second order in β, and where $Ro \approx 1.2\ A^{\frac{1}{3}}$ fm.

There are four common methods used for evaluating the non-axiality parameter γ. These methods are: a) from the energy ratio $E2^{+'}/ E2^{+}$, b) from the energy ratio $E4^{+}/ E2^{+}$, c) from the energy ratio $E2^{+'}/ E4^{+}$ or $E6^{+}$, d) from the values of $E2^{+}$, B(E2: $2^{+} \rightarrow 0^{+}$) and model dependent Q_0. In this research, we have employed the most widely used method (a) to calculate the asymmetry parameter γ, which is used in our empirical calculation. The asymmetry parameter is evaluated from the ratio of two band head energies $E2^{+'}/ E2^{+}$ (Gupta, Varshney & Gupta, 1982; Parveen & Harish, 2015; Singh et al., 2013; Varshney et al., 2011),

where $$E2^{+'} = \frac{9}{\sin^2(3\gamma)}\left[1+\sqrt{1-\frac{8\sin^2(3\gamma)}{9}}\right]\frac{\hbar^2}{4B\beta^2} \text{ and}$$

$$E2^{+} = \frac{9}{\sin^2(3\gamma)}\left[1-\sqrt{1-\frac{8\sin^2(3\gamma)}{9}}\right]\frac{\hbar^2}{4B\beta^2} \tag{3.10}$$

So that we can write for the asymmetric parameter as

$$\gamma = \frac{1}{3}\sin^{-1}\left\{\frac{9}{8}\left[1-\frac{(m-1)^2}{(m+1)^2}\right]\right\}^{1/2} \tag{3.11}$$

where m is the energy ratio $E2^{+'}/E2^{+}$.

3.3. Result and Discussion

In this section the B(E2) values computed have been tabulated and figured. Table 3.1 gives asymmetric parameter calculated results and energy ratio $4^{+} / 2^{+}$, Table 3.2 gives B(E2) values for transition from rotational level 2^{+} to 0^{+} ground state rotational band, and Table 3.3 gives values

for transitions between $2^+ \rightarrow 0^+$, $4^+ \rightarrow 2^+$, $6^+ \rightarrow 4^+$,$8^+ \rightarrow 6^+$, $10^+ \rightarrow 8^+$, and $12^+ \rightarrow 10^+$ rotational ground state bands for the 57 lanthanides and actinides series, included in this study.

Table 3.1. Calculated results of asymmetric parameter γ

S/No.	Nuclide	Energy (keV)			$4^+ / 2^+$	Asymmetric Parameter (γ)
		2^+	$2^{+'}$	4^+		
1.	$^{150}_{62}$Sm	333.863	1193.84	773.238	2.316034	20.42^0
2.	$^{152}_{62}$Sm	121.7817	1085.84	366.4795	3.009315	13.23^0
3.	$^{154}_{62}$Sm	81.976	1440.04	266.76	3.254123	9.54^0
4.	$^{152}_{64}$Gd	344.2789	1109.20	755.3958	2.194139	19.76^0
5.	$^{154}_{64}$Gd	123.0714	996.26	371.005	3.014551	13.86^0
6.	$^{156}_{64}$Gd	88.9666	1154.15	288.1799	3.239192	11.05^0
7.	$^{158}_{64}$Gd	79.51	1187.14	261.44	3.28814	10.32^0
8.	$^{160}_{64}$Gd	75.26	988.40	248.52	3.302153	10.98^0
9.	$^{154}_{66}$Dy	334.58	1027.04	747.04	2.232769	21.98^0
10.	$^{156}_{66}$Dy	137.83	890.50	404.18	2.932453	15.42^0
11.	$^{158}_{66}$Dy	98.918	946.32	317.139	3.20608	12.79^0
12.	$^{160}_{66}$Dy	86.788	966.17	283.8236	3.270309	11.89^0
13.	$^{162}_{66}$Dy	80.66	888.16	265.665	3.29364	11.96^0
14.	$^{164}_{66}$Dy	73.392	761.82	242.23	3.300496	12.30^0
15.	$^{160}_{68}$Er	125.8	854.40	389.9	3.099364	15.07^0
16.	$^{162}_{68}$Er	102.04	900.72	329.61	3.230204	13.3^0
17.	$^{164}_{68}$Er	91.4	860.25	299.44	3.276149	12.9^0
18.	$^{166}_{68}$Er	80.577	785.91	264.991	3.288668	12.68^0
19.	$^{168}_{68}$Er	79.804	821.17	264.089	3.30922	12.36^0
20.	$^{170}_{68}$Er	78.591	934.03	260.131	3.309934	11.53^0
21.	$^{166}_{70}$Yb	102.37	932.38	330.5	3.228485	13.09^0
22.	$^{168}_{70}$Yb	87.73	984.00	286.551	3.266283	11.85^0
23.	$^{170}_{70}$Yb	84.25474	1145.72	277.44	3.292871	10.80^0
24.	$^{172}_{70}$Yb	78.7427	1465.88	260.268	3.305297	9.27^0
25.	$^{174}_{70}$Yb	76.471	1633.97	253.117	3.309974	8.66^0
26.	$^{176}_{70}$Yb	82.13	1260.89	271.7	3.30817	10.18^0
27.	$^{166}_{72}$Hf	158.5	809.96	470.3	2.967192	17.23^0
28.	$^{168}_{72}$Hf	124	875.94	385.6	3.109677	14.79^0
29.	$^{170}_{72}$Hf	100.8	961.30	321.99	3.194345	12.81^0
30.	$^{172}_{72}$Hf	95.22	1075.29	309.24	3.247637	11.81^0
31.	$^{174}_{72}$Hf	90.985	1226.77	297.38	3.268451	10.85^0
32.	$^{176}_{72}$Hf	88.351	1341.31	290.18	3.2844	10.24^0
33.	$^{178}_{72}$Hf	93.18	1174.63	306.619	3.29061	11.20^0

34.	$^{182}_{74}W$	100.106	1221.40	329.4267	3.290779	11.38^0
35.	$^{184}_{74}W$	111.208	903.31	364.056	3.273649	13.84^0
36.	$^{186}_{74}W$	122.33	737.96	396.34	3.239925	15.94^0
37.	$^{180}_{76}Os$	132.3	870.44	408.9	3.090703	15.29^0
38.	$^{182}_{76}Os$	127	890.61	400.4	3.152756	14.84^0
39.	$^{184}_{76}Os$	119.8	942.87	383.77	3.203422	14.05^0
40.	$^{186}_{76}Os$	137.159	767.48	434.088	3.164852	16.51^0
41.	$^{188}_{76}Os$	155.021	633.02	477.94	3.083066	19.16^0
42.	$^{190}_{76}Os$	186.718	557.98	547.854	2.934125	22.28^0
43.	$^{228}_{90}Th$	57.759	968.38	186.823	3.234526	9.76^0
44.	$^{230}_{90}Th$	53.2	781.38	174.1	3.272556	10.40^0
45.	$^{232}_{90}Th$	49.369	785.25	162.12	3.283842	10.01^0
46.	$^{234}_{92}U$	43.498	926.72	143.351	3.295577	8.68^0
47.	$^{236}_{92}U$	45.242	957.90	149.476	3.303921	8.71^0
48.	$^{238}_{92}U$	44.91	1060.27	148.41	3.304609	8.25^0
49.	$^{238}_{94}Pu$	44.08	1028.54	145.96	3.311252	8.30^0
50.	$^{240}_{94}Pu$	42.824	900.32	141.69	3.308659	8.23^0
51.	$^{242}_{94}Pu$	44.54	1102.00	147.3	3.30714	8.07^0
52.	$^{244}_{94}Pu$	46	1015.00	156.9	3.41087	8.53^0
53.	$^{244}_{96}Cm$	42.965	1020.76	142.348	3.313115	7.84^0
54.	$^{246}_{96}Cm$	42.852	1124.26	142.01	3.313964	8.23^0
55.	$^{248}_{96}Cm$	43.38	1131.00	143.8	3.314892	7.88^0
56.	$^{250}_{98}Cf$	42.722	1031.85	141.885	3.321123	8.16^0
57.	$^{252}_{98}Cf$	45.72	804.80	151.73	3.318679	9.58^0

Figure 3.1 gives the graphical representation of experimental energy ratios ($4^+/2^+$) for rotational excited ground state bands (refer Table 3.1 for the experimental values of 2^+ and $2^{+'}$). These energy ratios are very important in determining the observed excitation spectra of deformed (rotation, transition and vibration), spherical and magic region.

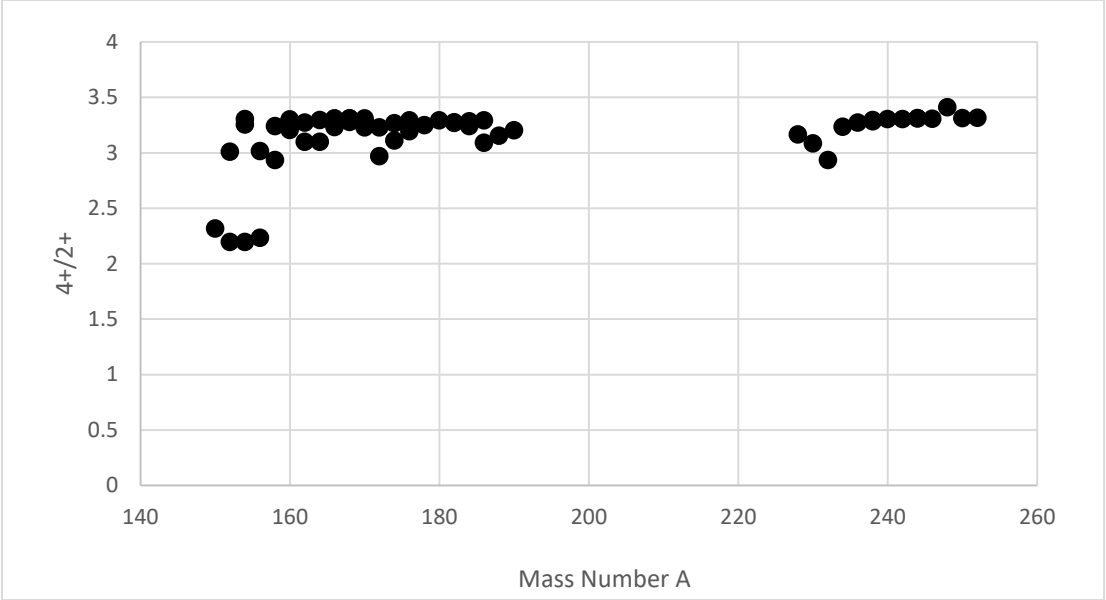

Figure 3.1. Experimental energy ratios for rotational excited ground state bands in even-even nuclei.

The experimental reduced transition probability values are either extracted from half-life data using the derived relation (Eqn. (3.3)) or which are taken from references (Raman et al., 2001) and (Varshney, 1982) are presented along with the experimentally calculated B(E2) values obtained from the Davydov-Fillipov model.

Table 3.2. Reduced transition probability B(E2) values for $2^+ \rightarrow 0^+$ transition, intrinsic quadrupole moment (Q_o), nuclear deformation parameter (β) and internal conversion coefficient (ICC).

S/No	Nuclide	Experimental B(E2) Values *	B(E2) Values Present Work		B(E2) Values Previous Work **		Q_o*	Deformation Parameter (β)*	ICC
			Experimental ***	Empirical	Experimental	Empirical			
1.	$^{150}_{62}$Sm	0.270 (30)	0.271	0.252	0.274 (6)	0.265	3.684	0.1931	0.0408
2.	$^{152}_{62}$Sm	0.692 (6)	0.696	0.662	0.670 (15)	0.657	5.90	0.3061	1.17
3.	$^{154}_{62}$Sm	0.872 (5)	0.854	0.850	0.922 (40)	0.911	6.620	0.3410	4.93
4.	$^{152}_{64}$Gd	0.334 (14)	0.347	0.311	0.394 (26)	0.368	4.09	0.206	0.0399

5.	$^{154}_{64}$Gd	0.778 (7)	0.768	0.743	0.770 (16)	0.760	6.25	0.3120	1.20
6.	$^{156}_{64}$Gd	0.928 (5)	0.934	0.910	0.914 (10)	0.918	6.830	0.3378	3.92
7.	$^{158}_{64}$Gd	1.004 (5)	1.010	0.980	0.994 (10)	0.948	7.104	0.3484	6.00
8.	$^{160}_{64}$Gd	1.050 (6)	1.035	1.020	1.030 (10)	1.015	7.265	0.3534	7.42
9.	$^{154}_{66}$Dy	0.478 (13)	0.476	0.447			4.90	0.237	0.0467
10.	$^{156}_{66}$Dy	0.742 (40)	0.748	0.702	0.753		6.107	0.2929	0.85
11.	$^{158}_{66}$Dy	0.932 (5)	0.942	0.895	0.980 (70)	0.969	6.844	0.3255	2.85
12.	$^{160}_{66}$Dy	1.026 (11)	0.979	0.991	0.998 (60)	0.961	7.18	0.3387	4.68
13.	$^{162}_{66}$Dy	1.070 (11)	1.045	1.030	1.089 (30)	1.061	7.33	0.3430	6.21
14.	$^{164}_{66}$Dy	1.120 (5)	1.125	1.080	1.140	1.095	7.503	0.3481	9.00
15.	$^{160}_{68}$Er	0.876 (20)	0.865	0.830	0.840 (40)	0.795	6.63	0.304	1.27
16.	$^{162}_{68}$Er	1.002 (6)	1.175	0.960	0.976 (49)	0.933	7.097	0.3222	2.76
17.	$^{164}_{68}$Er	1.090 (6)	1.174	1.044	1.150 (70)	1.135	7.402	0.3333	4.21
18.	$^{166}_{68}$Er	1.166 (5)	1.177	1.120	1.122 (40)	1.076	7.656	0.3420	6.89
19.	$^{168}_{68}$Er	1.158 (10)	1.157	1.114	1.170 (40)	1.150	7.63	0.3381	7.16
20.	$^{170}_{68}$Er	1.164 (10)	1.176	1.124	1.185 (30)	1.160	7.65	0.3363	7.62
21.	$^{166}_{70}$Yb	1.048 (31)	1.033	1.001	1.05 (150)	1.010	7.25	0.315	2.98
22.	$^{168}_{70}$Yb	1.116 (30)	1.167	1.105	1.080 (50)	1.050	7.49	0.322	5.44
23.	$^{170}_{70}$Yb	1.158 (13)	1.141	1.130	1.040 (20)	1.010	7.63	0.3258	6.39
24.	$^{172}_{70}$Yb	1.208 (7)	1.225	1.180	1.186 (56)	1.160	7.792	0.3302	8.40
25.	$^{174}_{70}$Yb	1.188 (6)	1.174	1.170	1.148	1.130	7.727	0.3249	9.50
26.	$^{176}_{70}$Yb	1.060 (19)	1.075	1.030	1.050	1.030	7.30	0.305	7.08
27.	$^{166}_{72}$Hf	0.700 (20)	0.691	0.660	0.86		5.93	0.250	0.646
28.	$^{168}_{72}$Hf	0.860 (23)	0.850	0.815	0.836		6.57	0.275	1.57
29.	$^{170}_{72}$Hf	1.060 (12)	1.025	1.020	1.26		7.3	0.301	3.47
30.	$^{172}_{72}$Hf	0.894 (33)	0.872	0.862	0.928		6.70	0.276	4.35
31.	$^{174}_{72}$Hf	0.976 (31)	0.892	0.950	0.935 (44)	0.932	7.00	0.286	5.22
32.	$^{176}_{72}$Hf	1.054 (10)	1.070	1.025	1.215 (35)	1.20	7.28	0.2953	5.87

33.	$^{178}_{72}$Hf	0.964 (6)	0.948	0.933	0.998	0.980	6.961	0.2803	4.74
34.	$^{182}_{74}$W	0.840 (8)	0.829	0.812	1.029 (11)	1.02	6.50	0.2503	3.96
35.	$^{184}_{74}$W	0.756 (13)	0.737	0.720	0.667 (12)	0.660	6.16	0.2362	2.57
36.	$^{186}_{74}$W	0.700 (12)	0.716	0.660	0.669 (9)	0.660	5.93	0.2257	1.784
37.	$^{180}_{76}$Os	0.720 (8)	0.711	0.680			6.0	0.226	1.456
38.	$^{182}_{76}$Os	0.772 (35)	0.780	0.730	1.702		6.22	0.234	1.700
39.	$^{184}_{76}$Os	0.646 (16)	0.620	0.616	0.569		5.70	0.213	2.13
40.	$^{186}_{76}$Os	0.580 (10)	0.587	0.550	0.63 (6)	0.630	5.40	0.2000	1.271
41.	$^{188}_{76}$Os	0.510 (5)	0.492	0.460	0.568 (6)	0.580	5.06	0.1862	0.810
42.	$^{190}_{76}$Os	0.470 (6)	0.484	0.442	0.496 (4)	0.510	4.86	0.1775	0.420
43.	$^{228}_{90}$Th	1.412 (24)	1.410	1.380	1.41		8.42	0.2301	153.2
44.	$^{230}_{90}$Th	1.608 (10)	1.638	1.560	1.60 (400)	1.57	8.99	0.2441	228
45.	$^{232}_{90}$Th	1.856 (10)	1.705	1.810	1.850 (80)	1.82	9.66	0.2608	327
46.	$^{234}_{92}$U	2.132 (20)	2.021	2.087	2.030 (90)	1.98	10.35	0.2718	713
47.	$^{236}_{92}$U	2.322 (15)	2.160	2.276	2.320 (80)	2.27	10.80	0.2821	589
48.	$^{238}_{92}$U	2.418 (20)	2.498	2.370	2.380 (50)	2.33	11.02	0.2863	610
49.	$^{238}_{94}$Pu	2.522 (17)	2.438	2.475	2.520		11.26	0.2861	787
50.	$^{240}_{94}$Pu	2.604 (30)	2.645	2.550	2.530 (70)	2.47	11.44	0.2891	905
51.	$^{242}_{94}$Pu	2.680 (16)	2.728	2.630	2.68 (110)	2.63	11.61	0.2917	748
52.	$^{244}_{94}$Pu	2.736 (16)	2.766	2.684	2.770 (70)	2.71	11.73	0.2931	640
53.	$^{244}_{96}$Cm	2.934 (17)	3.791	2.882			12.14	0.2972	1050
54.	$^{246}_{96}$Cm	2.988 (19)	3.040	2.930	3.010 (90)	2.94	12.26	0.2983	1064
55.	$^{248}_{96}$Cm	2.998 (19)	3.036	2.950		2.98	12.28	0.2972	1002
56.	$^{250}_{98}$Cf	3.200 (16)	3.183	3.150			12.7	0.299	1274
57.	$^{252}_{98}$Cf	3.340 (11)	3.355	3.260			12.95	0.304	917

* Taken from adopted value of Reference (Raman et al., 2001), ** Taken from Reference (Varshney, 1982), and *** are extracted from experimental equation (3.3).

Table 3.3. Reduced transition probability B(E2) values for various transitions of the present work (experimental and empirical), and the previous (experimental and empirical) data.

S/No.	Nuclide	Transition State	Present Work		Previous Work *	
			Experimental **	Empirical	Experimental	Empirical
1.	$^{150}_{62}$Sm	$2^+ \rightarrow 0^+$	0.270	0.252	0.274 (6)	0.265
		$4^+ \rightarrow 2^+$	0.520	0.360	0.521 (39)	0.391
		$6^+ \rightarrow 4^+$		0.397		
		$8^+ \rightarrow 6^+$		0.415		
		$10^+ \rightarrow 8^+$		0.426		
		$12^+ \rightarrow 10^+$		0.434		
2.	$^{152}_{62}$Sm	$2^+ \rightarrow 0^+$	0.696	0.662	0.670 (15)	0.657
		$4^+ \rightarrow 2^+$	1.010	0.946	1.03 (1)	0.938
		$6^+ \rightarrow 4^+$	1.181	1.042	1.16 (2)	1.00
		$8^+ \rightarrow 6^+$	1.372	1.100	1.41 (7)	1.19
		$10^+ \rightarrow 8^+$	1.525	1.120	1.54 (14)	1.78
		$12^+ \rightarrow 10^+$		1.140		
3.	$^{154}_{62}$Sm	$2^+ \rightarrow 0^+$	0.854	0.850	0.922 (40)	0.911
		$4^+ \rightarrow 2^+$	1.199	1.215	1.18 (3)	1.30
		$6^+ \rightarrow 4^+$	1.428	1.340	1.31 (4)	1.30
		$8^+ \rightarrow 6^+$	1.559	1.400	1.54 (15)	1.56
		$10^+ \rightarrow 8^+$	1.539	1.440		
		$12^+ \rightarrow 10^+$	1.381	1.464		
4.	$^{152}_{64}$Gd	$2^+ \rightarrow 0^+$	0.347	0.311	0.394 (26)	0.368
		$4^+ \rightarrow 2^+$	0.645	0.444		
		$6^+ \rightarrow 4^+$	0.951	0.489		
		$8^+ \rightarrow 6^+$		0.512		
		$10^+ \rightarrow 8^+$		0.526		
		$12^+ \rightarrow 10^+$		0.536		
5.	$^{154}_{64}$Gd	$2^+ \rightarrow 0^+$	0.768	0.743	0.770 (16)	0.760
		$4^+ \rightarrow 2^+$	1.204	1.061	1.18 (4)	1.086
		$6^+ \rightarrow 4^+$	1.395	1.170	1.36 (5)	1.17
		$8^+ \rightarrow 6^+$	1.529	1.223	1.50 (5)	1.40
		$10^+ \rightarrow 8^+$	1.749	1.260		
		$12^+ \rightarrow 10^+$		1.280		
6.	$^{156}_{64}$Gd	$2^+ \rightarrow 0^+$	0.934	0.910	0.915 (10)	0.918
		$4^+ \rightarrow 2^+$	1.316	1.293	1.29 (2)	1.32
		$6^+ \rightarrow 4^+$	1.470	1.424	1.47 (3)	1.36
		$8^+ \rightarrow 6^+$	1.598	1.491	1.61 (11)	1.65
		$10^+ \rightarrow 8^+$	1.568	1.532		
		$12^+ \rightarrow 10^+$	1.495	1.560		
7.	$^{158}_{64}$Gd	$2^+ \rightarrow 0^+$	1.010	0.980	0.994 (10)	0.948
		$4^+ \rightarrow 2^+$	1.470	1.400	1.37 (11)	1.361
		$6^+ \rightarrow 4^+$		1.540		

		$8^+ \rightarrow 6^+$	1.648	1.610	1.69 (13)	1.66
		$10^+ \rightarrow 8^+$	1.699	1.650	1.77 (9)	1.73
		$12^+ \rightarrow 10^+$	1.556	1.681	1.57 (12)	1.50
8.	$^{160}_{64}$Gd	$2^+ \rightarrow 0^+$	1.035	1.020	1.030 (10)	1.015
		$4^+ \rightarrow 2^+$		1.460		
		$6^+ \rightarrow 4^+$		1.604		
		$8^+ \rightarrow 6^+$		1.680		
		$10^+ \rightarrow 8^+$		1.724		
		$12^+ \rightarrow 10^+$		1.755		
9.	$^{154}_{66}$Dy	$2^+ \rightarrow 0^+$	0.476	0.447		
		$4^+ \rightarrow 2^+$	0.771	0.640		
		$6^+ \rightarrow 4^+$	0.975	0.704		
		$8^+ \rightarrow 6^+$	1.058	0.740		
		$10^+ \rightarrow 8^+$	0.874	0.760		
		$12^+ \rightarrow 10^+$	0.855	0.771		
10.	$^{156}_{66}$Dy	$2^+ \rightarrow 0^+$	0.747	0.702	0.753	
		$4^+ \rightarrow 2^+$	1.305	1.003		
		$6^+ \rightarrow 4^+$	0.997	1.104		
		$8^+ \rightarrow 6^+$	1.443	1.160		
		$10^+ \rightarrow 8^+$	1.829	1.200		
		$12^+ \rightarrow 10^+$	1.903	1.210		
11.	$^{158}_{66}$Dy	$2^+ \rightarrow 0^+$	0.942	0.895	0.980 (70)	0.969
		$4^+ \rightarrow 2^+$	1.350	1.280	1.29 (16)	1.385
		$6^+ \rightarrow 4^+$	1.745	1.410		
		$8^+ \rightarrow 6^+$	1.720	1.474		
		$10^+ \rightarrow 8^+$	1.623	1.514		
		$12^+ \rightarrow 10^+$	1.590	1.541		
12.	$^{160}_{66}$Dy	$2^+ \rightarrow 0^+$	0.999	0.991	0.998 (60)	0.961
		$4^+ \rightarrow 2^+$	1.483	1.420	1.49 (13)	1.40
		$6^+ \rightarrow 4^+$	1.228	1.560	1.23 (6)	1.46
		$8^+ \rightarrow 6^+$	1.874	1.632	1.57 (10)	1.74
		$10^+ \rightarrow 8^+$	1.695	1.680	1.65 (15)	1.77
		$12^+ \rightarrow 10^+$	1.607	1.710	1.29 (79)	1.60
13.	$^{162}_{66}$Dy	$2^+ \rightarrow 0^+$	1.045	1.030	1.089 (30)	1.061
		$4^+ \rightarrow 2^+$	1.513	1.470	1.53 (9)	1.52
		$6^+ \rightarrow 4^+$	1.577	1.620	1.38 (16)	1.59
		$8^+ \rightarrow 6^+$	1.818	1.700	1.91 (8)	1.89
		$10^+ \rightarrow 8^+$	1.835	1.741	1.79 (11)	1.93
		$12^+ \rightarrow 10^+$	1.705	1.772	1.48 (8)	1.47
14.	$^{164}_{66}$Dy	$2^+ \rightarrow 0^+$	1.125	1.080	1.140	1.095
		$4^+ \rightarrow 2^+$	1.446	1.540	1.57	1.622
		$6^+ \rightarrow 4^+$	1.618	1.700	1.67 (6)	1.697
		$8^+ \rightarrow 6^+$	1.602	1.771	1.69 (12)	2.02
		$10^+ \rightarrow 8^+$	1.899	1.820	1.89 (10)	2.05
		$12^+ \rightarrow 10^+$	1.768	1.850	1.87 (3)	1.86

15.	$^{160}_{68}$Er	$2^+ \rightarrow 0^+$	0.865	.0830	0.840 (40)	0.795
		$4^+ \rightarrow 2^+$	1.237	1.184	1.17 (6)	1.14
		$6^+ \rightarrow 4^+$	1.352	1.304	1.36 (12)	1.25
		$8^+ \rightarrow 6^+$	1.523	1.365	1.17 (28)	1.49
		$10^+ \rightarrow 8^+$	1.508	1.400	1.09 (55)	1.43
		$12^+ \rightarrow 10^+$	1.480	1.430		
16.	$^{162}_{68}$Er	$2^+ \rightarrow 0^+$	1.175	0.960	0.976 (49)	0.933
		$4^+ \rightarrow 2^+$		1.370		
		$6^+ \rightarrow 4^+$		1.510		
		$8^+ \rightarrow 6^+$		1.580		
		$10^+ \rightarrow 8^+$		1.620		
		$12^+ \rightarrow 10^+$		1.650		
17.	$^{164}_{68}$Er	$2^+ \rightarrow 0^+$	1.174	1.044	1.150 (70)	1.135
		$4^+ \rightarrow 2^+$	1.383	1.500	1.40 (13)	1.62
		$6^+ \rightarrow 4^+$		1.640		
		$8^+ \rightarrow 6^+$	1.831	1.720	1.83 (13)	2.06
		$10^+ \rightarrow 8^+$	1.903	1.770	2.97 (12)	2.05
		$12^+ \rightarrow 10^+$	1.411	1.800	1.20 (9)	1.84
18.	$^{166}_{68}$Er	$2^+ \rightarrow 0^+$	1.177	1.120	1.122 (40)	1.076
		$4^+ \rightarrow 2^+$	1.690	1.600	1.69 (11)	1.57
		$6^+ \rightarrow 4^+$	1.465	1.760	1.60	1.66
		$8^+ \rightarrow 6^+$	1.982	1.850	1.85 (11)	1.98
		$10^+ \rightarrow 8^+$	2.009	1.900	2.10 (2)	1.99
		$12^+ \rightarrow 10^+$	2.040	1.930	1.97 (15)	1.79
19.	$^{168}_{68}$Er	$2^+ \rightarrow 0^+$	1.157	1.114	1.170 (40)	1.150
		$4^+ \rightarrow 2^+$	1.755	1.600	1.67 (10)	1.64
		$6^+ \rightarrow 4^+$	2.415	1.750		
		$8^+ \rightarrow 6^+$	1.929	1.840	2.10 (18)	2.04
		$10^+ \rightarrow 8^+$	1.661	1.885		
		$12^+ \rightarrow 10^+$	1.849	1.920		
20.	$^{170}_{68}$Er	$2^+ \rightarrow 0^+$	1.176	1.124	1.185 (30)	1.160
		$4^+ \rightarrow 2^+$		1.61	1.55 (4)	1.66
		$6^+ \rightarrow 4^+$		1.770		
		$8^+ \rightarrow 6^+$	2.075	1.850	2.21 (16)	2.06
		$10^+ \rightarrow 8^+$	1.790	1.902	1.83 (12)	2.11
		$12^+ \rightarrow 10^+$	2.097	1.940	2.12 (10)	1.92
21.	$^{166}_{70}$Yb	$2^+ \rightarrow 0^+$	1.033	1.001	1.060 (150)	1.010
		$4^+ \rightarrow 2^+$	1.475	1.430	1.47 (5)	1.45
		$6^+ \rightarrow 4^+$	1.575	1.580	1.57 (6)	1.55
		$8^+ \rightarrow 6^+$	1.747	1.650	1.75 (2)	1.84
		$10^+ \rightarrow 8^+$	1.650	1.700	1.65 (109)	1.84
		$12^+ \rightarrow 10^+$	1.451	1.724	1.46 (102)	1.64
22.	$^{168}_{70}$Yb	$2^+ \rightarrow 0^+$	1.167	1.100	1.080 (50)	1.050
		$4^+ \rightarrow 2^+$		1.540		
		$6^+ \rightarrow 4^+$		1.700		

		$8^+ \rightarrow 6^+$		1.770		
		$10^+ \rightarrow 8^+$		1.820		
		$12^+ \rightarrow 10^+$		1.850		
23.	$^{170}_{70}$Yb	$2^+ \rightarrow 0^+$	1.141	1.130	1.040 (20)	1.010
		$4^+ \rightarrow 2^+$		1.610		
		$6^+ \rightarrow 4^+$		1.770		
		$8^+ \rightarrow 6^+$	2.039	1.853	1.61 (14)	1.79
		$10^+ \rightarrow 8^+$	1.993	1.904	2.03 (13)	1.84
		$12^+ \rightarrow 10^+$	1.496	1.940	1.51 (12)	1.68
24.	$^{172}_{70}$Yb	$2^+ \rightarrow 0^+$	1.225	1.180	1.186 (50)	1.160
		$4^+ \rightarrow 2^+$	1.716	1.683		
		$6^+ \rightarrow 4^+$	1.825	1.854		
		$8^+ \rightarrow 6^+$	2.179	1.941		
		$10^+ \rightarrow 8^+$	2.073	1.994		
		$12^+ \rightarrow 10^+$	2.392	2.030		
25.	$^{174}_{70}$Yb	$2^+ \rightarrow 0^+$	1.743	1.170	1.148 (56)	1.130
		$4^+ \rightarrow 2^+$	1.622	1.670		
		$6^+ \rightarrow 4^+$	2.126	1.840		
		$8^+ \rightarrow 6^+$	2.237	1.920		
		$10^+ \rightarrow 8^+$	1.956	1.972		
		$12^+ \rightarrow 10^+$	2.117	2.010		
26.	$^{176}_{70}$Yb	$2^+ \rightarrow 0^+$	1.075	1.030	1.050	1.030
		$4^+ \rightarrow 2^+$	1.580	1.473		
		$6^+ \rightarrow 4^+$	1.730	1.622		
		$8^+ \rightarrow 6^+$	1.740	1.700		
		$10^+ \rightarrow 8^+$	1.860	1.744		
		$12^+ \rightarrow 10^+$	1.800	1.780		
27.	$^{166}_{72}$Hf	$2^+ \rightarrow 0^+$	0.691	0.660	0.86	
		$4^+ \rightarrow 2^+$	1.062	0.940	1.10 (7)	1.165
		$6^+ \rightarrow 4^+$	1.110	1.040	1.14	1.31
		$8^+ \rightarrow 6^+$	1.340	1.084	1.38 (56)	1.568
		$10^+ \rightarrow 8^+$	1.370	1.113	1.42 (99)	1.44
		$12^+ \rightarrow 10^+$	0.840	1.133	0.84 (64)	1.26
28.	$^{168}_{72}$Hf	$2^+ \rightarrow 0^+$	0.850	0.815	0.836	
		$4^+ \rightarrow 2^+$	1.145	1.164	1.14 (13)	1.138
		$6^+ \rightarrow 4^+$	1.304	1.280	1.28 (13)	1.24
		$8^+ \rightarrow 6^+$	1.390	1.340	1.42 (15)	1.47
		$10^+ \rightarrow 8^+$	1.421	1.380	1.50 (21)	1.42
		$12^+ \rightarrow 10^+$	1.784	1.400	1.59 (4)	1.27
29.	$^{170}_{72}$Hf	$2^+ \rightarrow 0^+$	1.025	1.020	1.26	
		$4^+ \rightarrow 2^+$	1.430	1.453		
		$6^+ \rightarrow 4^+$	1.446	1.600		
		$8^+ \rightarrow 6^+$	1.665	1.700		
		$10^+ \rightarrow 8^+$	1.726	1.720		
		$12^+ \rightarrow 10^+$	1.581	1.751		

30.	$^{172}_{72}$Hf	$2^+ \rightarrow 0^+$	0.872	0.862	0.928	
		$4^+ \rightarrow 2^+$		1.232		
		$6^+ \rightarrow 4^+$		1.360		
		$8^+ \rightarrow 6^+$		1.420		
		$10^+ \rightarrow 8^+$		1.460		
		$12^+ \rightarrow 10^+$		1.485		
31.	$^{174}_{72}$Hf	$2^+ \rightarrow 0^+$	0.892	0.950	0.935 (44)	0.932
		$4^+ \rightarrow 2^+$		1.350		
		$6^+ \rightarrow 4^+$		1.500		
		$8^+ \rightarrow 6^+$		1.560		
		$10^+ \rightarrow 8^+$		1.600		
		$12^+ \rightarrow 10^+$		1.630		
32.	$^{176}_{72}$Hf	$2^+ \rightarrow 0^+$	1.070	1.025	1.215 (35)	1.20
		$4^+ \rightarrow 2^+$		1.464		
		$6^+ \rightarrow 4^+$		1.613		
		$8^+ \rightarrow 6^+$		1.700		
		$10^+ \rightarrow 8^+$		1.734		
		$12^+ \rightarrow 10^+$		1.765		
33.	$^{178}_{72}$Hf	$2^+ \rightarrow 0^+$	0.948	0.933	0.998	0.980
		$4^+ \rightarrow 2^+$		1.333		
		$6^+ \rightarrow 4^+$	1.300	1.470		
		$8^+ \rightarrow 6^+$	1.408	1.540		
		$10^+ \rightarrow 8^+$	1.527	1.580		
		$12^+ \rightarrow 10^+$	1.523	1.610		
34.	$^{182}_{74}$W	$2^+ \rightarrow 0^+$	0.829	0.812	1.029 (11)	1.02
		$4^+ \rightarrow 2^+$	1.203	1.160	1.235 (90)	1.714
		$6^+ \rightarrow 4^+$	1.228	1.280	1.22 (13)	1.77
		$8^+ \rightarrow 6^+$	1.278	1.340		
		$10^+ \rightarrow 8^+$	1.246	1.374		
		$12^+ \rightarrow 10^+$	1.173	1.400		
35.	$^{184}_{74}$W	$2^+ \rightarrow 0^+$	0.737	0.720	0.667 (12)	0.660
		$4^+ \rightarrow 2^+$	0.998	1.030	0.954 (9)	0.946
		$6^+ \rightarrow 4^+$	1.201	1.135	1.24 (13)	1.02
		$8^+ \rightarrow 6^+$	1.482	1.200		
		$10^+ \rightarrow 8^+$	1.803	1.220		
		$12^+ \rightarrow 10^+$		1.242		
36.	$^{186}_{74}$W	$2^+ \rightarrow 0^+$	0.716	0.660	0.669 (9)	0.660
		$4^+ \rightarrow 2^+$	0.905	0.943	0.892 ()	0.945
		$6^+ \rightarrow 4^+$	1.151	1.040	1.36 ()	1.05
		$8^+ \rightarrow 6^+$	1.100	1.090		
		$10^+ \rightarrow 8^+$	0.941	1.120		
		$12^+ \rightarrow 10^+$	1.183	1.140		
37.	$^{180}_{76}$Os	$2^+ \rightarrow 0^+$	0.711	0.680		
		$4^+ \rightarrow 2^+$	1.159	0.970		
		$6^+ \rightarrow 4^+$	0.938	1.070		

		$8^+ \rightarrow 6^+$	0.377	1.120		
		$10^+ \rightarrow 8^+$		1.150		
		$12^+ \rightarrow 10^+$		1.170		
38.	$^{182}_{76}$Os	$2^+ \rightarrow 0^+$	0.780	0.730	1.702 ()	
		$4^+ \rightarrow 2^+$		1.043		
		$6^+ \rightarrow 4^+$		1.150		
		$8^+ \rightarrow 6^+$		1.203		
		$10^+ \rightarrow 8^+$		1.240		
		$12^+ \rightarrow 10^+$		1.260		
39.	$^{184}_{76}$Os	$2^+ \rightarrow 0^+$	0.619	0.626	0.569 ()	
		$4^+ \rightarrow 2^+$	0.846	0.880	0.84 (26)	0.774
		$6^+ \rightarrow 4^+$		0.970		
		$8^+ \rightarrow 6^+$		1.014		
		$10^+ \rightarrow 8^+$		1.040		
		$12^+ \rightarrow 10^+$		1.060		
40.	$^{186}_{76}$Os	$2^+ \rightarrow 0^+$	0.587	0.550	0.63 (6)	0.630
		$4^+ \rightarrow 2^+$	0.846	0.780	0.90 ()	0.904
		$6^+ \rightarrow 4^+$	1.164	0.860	1.16 ()	1.02
		$8^+ \rightarrow 6^+$	1.096	0.900		
		$10^+ \rightarrow 8^+$	1.203	0.920		
		$12^+ \rightarrow 10^+$	1.084	0.940		
41.	$^{188}_{76}$Os	$2^+ \rightarrow 0^+$	0.492	0.460	0.568 (6)	0.580
		$4^+ \rightarrow 2^+$	0.774	0.660	0.79 ()	0.841
		$6^+ \rightarrow 4^+$	0.841	0.722		
		$8^+ \rightarrow 6^+$	0.918	0.760		
		$10^+ \rightarrow 8^+$	1.220	0.780		
		$12^+ \rightarrow 10^+$		0.800		
42.	$^{190}_{76}$Os	$2^+ \rightarrow 0^+$	0.484	0.442	0.496 (4)	0.510
		$4^+ \rightarrow 2^+$	0.620	0.630	0.62 ()	0.774
		$6^+ \rightarrow 4^+$	0.664	0.700	1.03 ()	0.94
		$8^+ \rightarrow 6^+$	0.827	0.730		
		$10^+ \rightarrow 8^+$	0.759	0.750		
		$12^+ \rightarrow 10^+$		0.760		
43.	$^{228}_{90}$Th	$2^+ \rightarrow 0^+$	1.410	1.380	1.41 ()	
		$4^+ \rightarrow 2^+$	2.033	1.970	1.72 (7)	1.96
		$6^+ \rightarrow 4^+$		2.165		
		$8^+ \rightarrow 6^+$		2.270		
		$10^+ \rightarrow 8^+$		2.33		
		$12^+ \rightarrow 10^+$		2.370		
44.	$^{230}_{90}$Th	$2^+ \rightarrow 0^+$	1.638	1.560	1.60 (400)	1.57
		$4^+ \rightarrow 2^+$	2.222	2.230	2.29 (7)	2.26
		$6^+ \rightarrow 4^+$		2.460		
		$8^+ \rightarrow 6^+$		2.572		
		$10^+ \rightarrow 8^+$		2.640		
		$12^+ \rightarrow 10^+$		2.700		

45.	$^{232}_{90}$Th	$2^+ \rightarrow 0^+$	1.705	1.810	1.850 (80)	1.82
		$4^+ \rightarrow 2^+$	2.466	2.600		
		$6^+ \rightarrow 4^+$	2.802	2.840		
		$8^+ \rightarrow 6^+$	2.918	2.980		
		$10^+ \rightarrow 8^+$	3.068	3.060		
		$12^+ \rightarrow 10^+$	3.113	3.110		
46.	$^{234}_{92}$U	$2^+ \rightarrow 0^+$	2.021	2.087	2.030 (90)	1.98
		$4^+ \rightarrow 2^+$		3.000		
		$6^+ \rightarrow 4^+$		3.280		
		$8^+ \rightarrow 6^+$		3.440		
		$10^+ \rightarrow 8^+$		3.530		
		$12^+ \rightarrow 10^+$		3.600		
47.	$^{236}_{92}$U	$2^+ \rightarrow 0^+$	2.160	2.276	2.320 (80)	2.27
		$4^+ \rightarrow 2^+$	3.094	3.250		
		$6^+ \rightarrow 4^+$	3.338	3.600		
		$8^+ \rightarrow 6^+$	3.410	3.750		
		$10^+ \rightarrow 8^+$	3.163	3.850		
		$12^+ \rightarrow 10^+$	3.535	3.920		
48.	$^{238}_{92}$U	$2^+ \rightarrow 0^+$	2.498	2.370	2.380 (50)	2.33
		$4^+ \rightarrow 2^+$		3.400		
		$6^+ \rightarrow 4^+$		3.730		
		$8^+ \rightarrow 6^+$		3.900		
		$10^+ \rightarrow 8^+$		4.010		
		$12^+ \rightarrow 10^+$		4.080		
49.	$^{238}_{94}$Pu	$2^+ \rightarrow 0^+$	2.438	2.475	2.520 ()	
		$4^+ \rightarrow 2^+$		3.540		
		$6^+ \rightarrow 4^+$		3.900		
		$8^+ \rightarrow 6^+$		4.080		
		$10^+ \rightarrow 8^+$		4.200		
		$12^+ \rightarrow 10^+$		4.260		
50.	$^{240}_{94}$Pu	$2^+ \rightarrow 0^+$	2.645	2.550	2.530 (70)	2.47
		$4^+ \rightarrow 2^+$		3.650		
		$6^+ \rightarrow 4^+$		4.020		
		$8^+ \rightarrow 6^+$		4.210		
		$10^+ \rightarrow 8^+$		4.320		
		$12^+ \rightarrow 10^+$		4.400		
51.	$^{242}_{94}$Pu	$2^+ \rightarrow 0^+$	2.728	2.630	2.68 (110)	2.63
		$4^+ \rightarrow 2^+$		3.760		
		$6^+ \rightarrow 4^+$		4.140		
		$8^+ \rightarrow 6^+$		4.340		
		$10^+ \rightarrow 8^+$		4.450		
		$12^+ \rightarrow 10^+$		4.540		
52.	$^{244}_{94}$Pu	$2^+ \rightarrow 0^+$	2.766	2.684	2.770 (70)	2.71
		$4^+ \rightarrow 2^+$		3.830		
		$6^+ \rightarrow 4^+$		4.220		

		$8^+ \rightarrow 6^+$		4.420		
		$10^+ \rightarrow 8^+$		4.540		
		$12^+ \rightarrow 10^+$		4.620		
53.	$^{244}_{96}$Cm	$2^+ \rightarrow 0^+$	3.791	2.882		
		$4^+ \rightarrow 2^+$		4.120		
		$6^+ \rightarrow 4^+$		4.540		
		$8^+ \rightarrow 6^+$		4.750		
		$10^+ \rightarrow 8^+$		4.880		
		$12^+ \rightarrow 10^+$		4.960		
54.	$^{246}_{96}$Cm	$2^+ \rightarrow 0^+$	3.040	2.930	3.010 (90)	2.94
		$4^+ \rightarrow 2^+$		4.200		
		$6^+ \rightarrow 4^+$		4.620		
		$8^+ \rightarrow 6^+$		4.830		
		$10^+ \rightarrow 8^+$		4.960		
		$12^+ \rightarrow 10^+$		5.05		
55.	$^{248}_{96}$Cm	$2^+ \rightarrow 0^+$	3.036	2.950	3.000	2.98
		$4^+ \rightarrow 2^+$	3.663	4.210		
		$6^+ \rightarrow 4^+$	5.153	4.640		
		$8^+ \rightarrow 6^+$	6.034	4.860		
		$10^+ \rightarrow 8^+$	3.908	4.990		
		$12^+ \rightarrow 10^+$	4.881	5.080		
56.	$^{250}_{98}$Cf	$2^+ \rightarrow 0^+$	3.183	3.150		
		$4^+ \rightarrow 2^+$		4.500		
		$6^+ \rightarrow 4^+$		4.960		
		$8^+ \rightarrow 6^+$		5.190		
		$10^+ \rightarrow 8^+$		5.330		
		$12^+ \rightarrow 10^+$		5.42		
57.	$^{252}_{98}$Cf	$2^+ \rightarrow 0^+$	3.355	3.260		
		$4^+ \rightarrow 2^+$		4.650		
		$6^+ \rightarrow 4^+$		5.120		
		$8^+ \rightarrow 6^+$		5.360		
		$10^+ \rightarrow 8^+$		5.510		
		$12^+ \rightarrow 10^+$		5.600		

* Taken from adopted value of Reference (Raman et al., 2001) and ** are extracted from experimental equation (3.3).

In the following two figures below, we are going to show the relationship between the input parameters employed in this particular study for computing the experimental B(E2) values.

Figure 3.2 illustrates the relationship between the energy involved in the transition, the total internal conversion coefficient and half-life of six transitions for selected nuclides of lanthanide series, while Figure 3.3 demonstrates the energy involved in the transition, the total internal conversion coefficient and the half-life of six transitions for selected nuclides of actinide series.

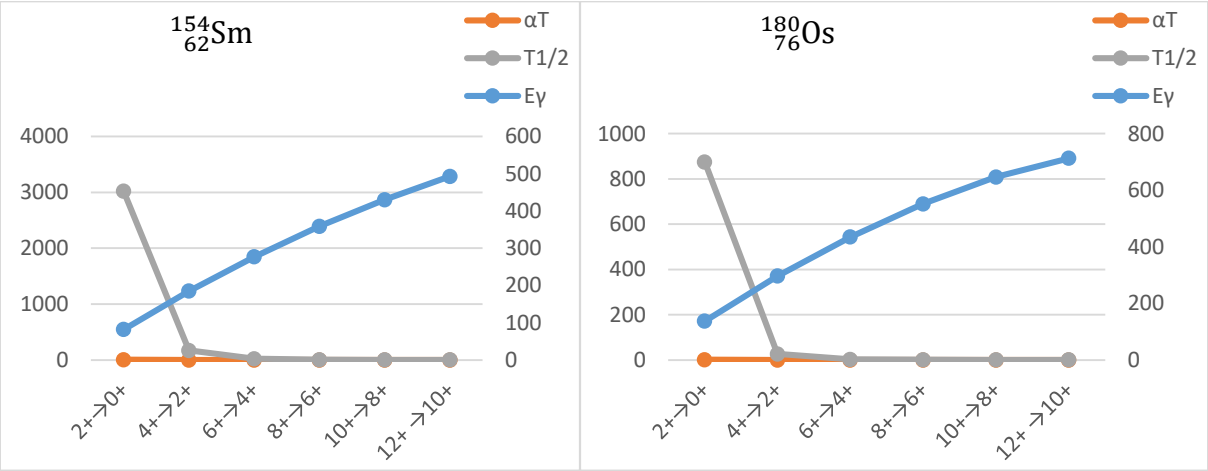

Figure 3.2. Comparison of energy involved in the transition (Eγ), the total internal conversion coefficient (α_T) and half-life ($T_{1/2}$) of the transitions for lanthanide nuclides.

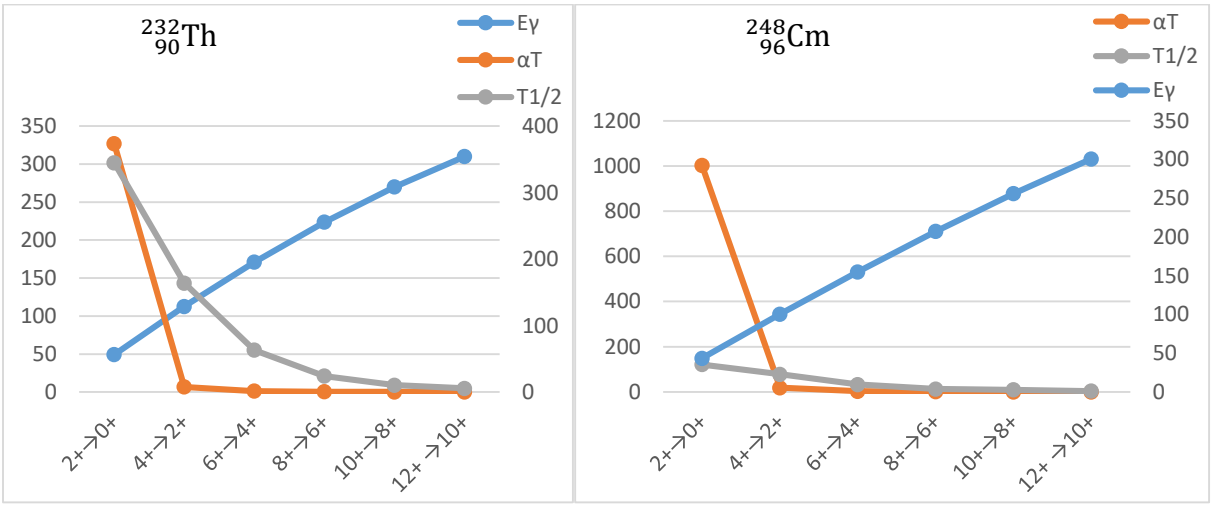

Figure 3.3. Comparison of energy involved in the transition (Eγ), the total internal conversion coefficient (α_T) and half-life ($T_{1/2}$) of the transitions for actinide nuclides.

In this study, the half-life of nuclear excited state rather than mean-life has been employed in computing the experimental reduced transition probabilities, extracted from experimental equation. This is so, because usually experimental half-life of states will be provided in literatures rather than meanlives. We have never seen any report of B(E2) values calculated employing half-life. Moreover, this method of computing considered being a new approach in estimating the reduced transition probabilities. In addition, this formula has given due emphasis of the significant figures to make the obtained result as much accurate as possible. Therefore, the result obtained in this computation could be compared to the previous works that employed mean-life instead of half-life, because it is possible to convert mean-life to half-life and vice versa.

Moreover, the other point that makes this work somewhat peculiar is that the most recent and updated experimental data of energies and half-lives have been employed. This may also bring difference when compared to the calculated B(E2) values of previous works. Therefore, we can say that this work may not be accurately compared to others' work because the differences may arise due to the mentioned reasons. There is no experimental data reported for higher transitions except for $2^{+} \rightarrow 0^{+}$ transition to compare with the current computed data, except the report of (Varshney, 1982).

The experimentally calculated B(E2) values are evidently seen to depend, inversely, upon the transition gamma energy to the power of five, the total internal conversion coefficient and half-life of the rotational excited state (See Eqn. (3.3)). It is easily observed that the total internal conversion coefficient is inversely proportional to the transition gamma energy (See Figure 3.2 and Figure 3.3). This is because the internal conversion coefficient decreases as the gamma energy get increases, keeping the atomic number same. This could be easily verified from the calculated

values of the coefficient using Bricc online software. It is also possible to observe from the experimental half-life of the rotational excited states that the half-life get decreases while the transition gamma energy increases, as the nuclear spin increases.

It is also easy to observe that the limiting factors of the experimentally calculated B(E2) values are the input parameters in the denominator. The numerator part has no effect since it is a constant number for each transition.

It has been seen that the experimental B(E2) values get increases until the transition $6^{+} \rightarrow 4^{+}$ for most cases and decreases for higher transitions. This may be ascribed to the difficulty in determining the exact ICC values for transition gamma energy greater than 400 keV using the Bricc software. The transition gamma energy get increases for higher transitions and are observed to be greater than the mentioned value especially for the rare earth series. Therefore, for the rare earth series, there is a difficulty in determining the exact value of ICC at higher transitions.

The ICC values are also known to depend upon the charge of decaying nucleus, the gamma energy of the transition, the atomic subshell out of which the orbital electron is ejected and the multi-polarity and parity of the nuclear transition. Therefore, it is important to take in to consideration all these parameters in order to have a full description of the transition magnitude.

In the case of the theoretical (empirical) calculations, it can be seen from the corresponding formula that the B(E2) values are proportional to the square of the intrinsic quadrupole moment (Qo). This in turn is directly proportional to the elongation deformation parameter β (see Eqn. (3.9)). So in these empirical calculations both the asymmetric parameter γ and the elongation

parameter β have been employed. Actually, these two input parameters are so important in determining the actual nuclear deformation properties.

In this empirical calculation, we do observe that the first factor consisting Qo and the factor in parenthesis remain constant (See Eqn. (3.5)) for a nuclide under consideration since the Qo and γ parameters are constant regardless of the transition for a specific nuclide. Therefore, the limiting factor for different transitions is the nuclear spin dependent part. The empirical values are seen getting increase as the nuclear spin, I increase (See Table 3.3). The difference in the increase between successive transitions will actually decrease. So we do observe that the empirical values of B(E2) increases as transition state increase.

We also observe that for the nuclides with the same atomic number (isotopes) the asymmetric parameter increases as the mass number increases when the excitation energy (2^+) get increase (for most nuclides) even though the second excitation ($2^{+'}$) also do have power to determine the value (See Table 3.2). So we see that the empirical value of B(E2) increases (slowly) as the nuclear spin for transition states increases. For higher transition states, this increase gets much slower in opposition to the decrease in experimental values.

This present study reveals, by comparing the percentage difference between the available experimental data and the present experimentally calculated result, that the percentage difference is very less except for $^{162}_{68}$Er (17.27%) and for $^{244}_{96}$Cm (29.2%). For most nuclides, the percentage difference value lies below 3%. When the empirical result is compared to the experimentally calculated result we obtained less percentage difference as well, and for most cases, the value lies below 4%. Finally, the comparison between the present empirically obtained result and the

previous empirical data is found to be less except for $^{188}_{76}$Os (26.1%), and for most cases, it is less than 5%. This comparison show that the present study is in good agreement with the experimental available data and the reported, previous works, in literatures as well.

It can be seen that at high spin transitions the experimentally calculated B(E2) values seem closer to the available experimental data for the actinide series. This may be so, because the excitation energy of higher transitions will not exceed the limiting value (400 keV) of Bricc software. For the actinide series, the computed ICC values are more exact when compared to the rare earth ones, at higher spin transitions.

CHAPTER 4. Meanlives of Rotational Nuclear States

4.1. Introduction

The measurement of lifetime (or equivalently the transition rate) of nuclear levels has been an important branch of nuclear physics (Ralph, 1962). In fairly recent years much time and effort has been devoted to determination of these level lifetimes. Several reasons exist for this; one is the possibility of using lifetime measurements to clarify nuclear level schemes. For example, if some simple picture of the nucleus is used to predict transition rates, such as the single particle model, the transition rates obtained from lifetime measurements can be then compared with these single particle predictions any rate which goes against the trend may indicate a wrong level schema assumption.

Practically all E2 transition rates in medium and heavy nuclei are enhanced over the predicted rates by up to several orders of magnitude (Ralph, 1962). If a supposed E2 lifetime measurement leads to a retarded transition rate, then the multipolarity of the γ-ray and hence the assumed level schema may be wrong. Alternatively, the unusual transition rate may be tied up with other quantum numbers.

Another reason for lifetime measurements is the necessity of knowing transition rates for comparison with nuclear model predictions (Ralph, 1962). All theories of the nucleus must predict or explain properties of nuclei such as excited level schemes and γ-ray transitions between these levels. The transition rates are inversely proportional to the lifetimes of the levels, so the measurements of these lifetimes are often the easiest and quickest test of the model.

Historically (Ralph, 1962), these transition rates were among the first properties of nuclei to be predicted and are still an essential part of any general nuclear theory. Many modern theories are very successful in some regions, but less so in others, examples are the rotational model, applying to nuclei far from closed shells, and the non-axial rotor theory (the Davydov-Filippov model) applying to nuclei near closed shells.

There exist many modern techniques for measurement of lifetimes (Ralph, 1962), such as scattering of charged particles, direct nuclear recoil methods, Coulomb excitation, resonance fluorescence, etc. Perhaps the simplest in concept is the delayed coincidence method, in which the time difference is measured between a radiation leading to an excited level and a radiation which de-excites the level. This method became more important with development of modern photomultiplier and scintillator techniques. Most recent work has used a fast-slow coincidence arrangement similar to that of Bell, Graham and Petch. Currently, microwave techniques are being developed for application to lifetime measurements, but the fast-slow technique is most widely used.

Atomic nuclei are known to exhibit a variety of shapes (Smith, Durell, Phillips & Urban, 2012) whose deviation from sphericity can be well described as combinations of quadrupole and higher-order multipole deformations. Quadrupole deformations are the most common and may be expressed in terms of the parameters β and γ. Axially symmetric prolate deformations with the rotation axis perpendicular to the symmetry axis correspond to $\gamma = 0^0$, while $\gamma = 60^0$ describes an axially symmetric oblate shape and $\gamma = 30^0$ describes a maximally triaxial nucleus.

The shape that a particular nucleus takes up results from a delicate balance between the collective (macroscopic) and single particle (microscopic) energies and is therefore dependent on both the atomic number Z and the neutron number N (Smith et al., 2012). Also, because nuclear rotation perturbs the microscopic structure of the nucleus, it may be that the shapes favored by a particular nucleus will change with the nuclear spin I. This threefold sensitivity of the nuclear shape, to Z, N, and I, provides a severe test of current theoretical approaches to low-energy nuclear structure.

The measurement of the mean lifetimes of rotational states provides the means to probe the nuclear shape at intermediate to high spin, since the electric quadrupole transition matrix elements in a rotational band are simply related to the magnitude of the quadrupole deformation of the intrinsic nuclear state (Smith et al., 2012). Before the advent of large arrays of high-purity Ge detectors, most of the experimental information on the shapes of the neutron rich nuclei had been limited to low spins.

4.2. Methods

When the ratio of the experimental B(E2) values to the empirical B(E2) values versus γ-values are very close to unity the empirical B(E2) values may be used (Varshney, 1982) for the prediction of meanlives for those transitions where neither the experimental B(E2) values nor the meanlives are known.

Using Eqn. (3.1) we can rewrite the mean-life as

$$\tau = \frac{0.08162}{E\gamma 5(1+\alpha_T)B(E2{:}I+2\rightarrow I)_{exp}} \quad (4.1)$$

Thus, the experimental mean-life can be rewritten replacing the empirical reduced transition probability by the experimental as,

$$\tau = \frac{0.08162}{E_\gamma{}^5(1+\alpha_T)B(E2{:}I+2\rightarrow I)_{emp}} \tag{4.2}$$

This is an empirical relation used in this study to predict the meanlives of the transitions.

4.3. Result and Discussion

In this section, the energy ratio and B(E2) values ratio are figured, and the empirical meanlives computed, using Eqn. (4.2), have been tabulated. Table 4 gives meanlives for transitions between $2^+ \rightarrow 0^+$, $4^+ \rightarrow 2^+$, $6^+ \rightarrow 4^+$, $8^+ \rightarrow 6^+$, $10^+ \rightarrow 8^+$, and $12^+ \rightarrow 10^+$ rotational excited nuclear states.

In this particular study we have selected rotational nuclides. The nuclear rotational states are determined by the energy ratio E_4/E_2, as shown in Figure 4.1 (refer Figure 3.1 as well).

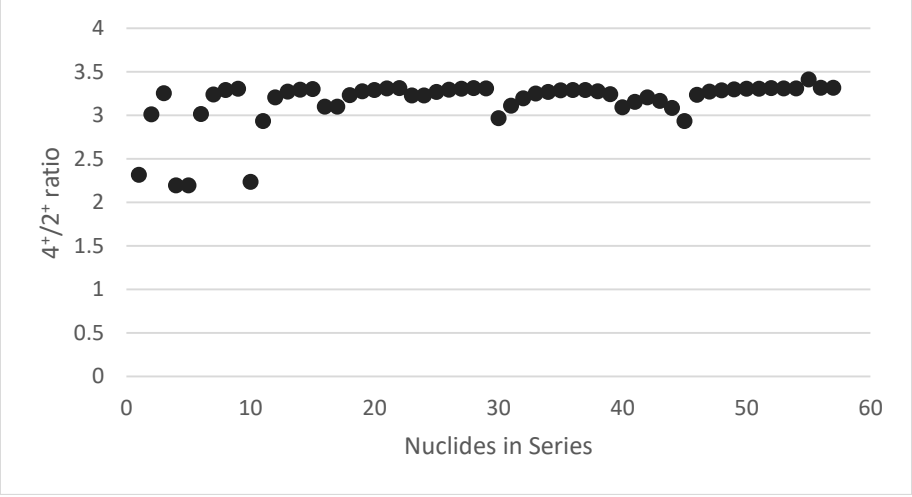

Figure 4.1. Energy ratio E_4/E_2 for nuclides.

The ratio of the experimental B(E2) to the empirical B(E2) values versus γ-values are shown in the Figure 4.2. It can be seen that the ratio is, in most cases, very close to unity.

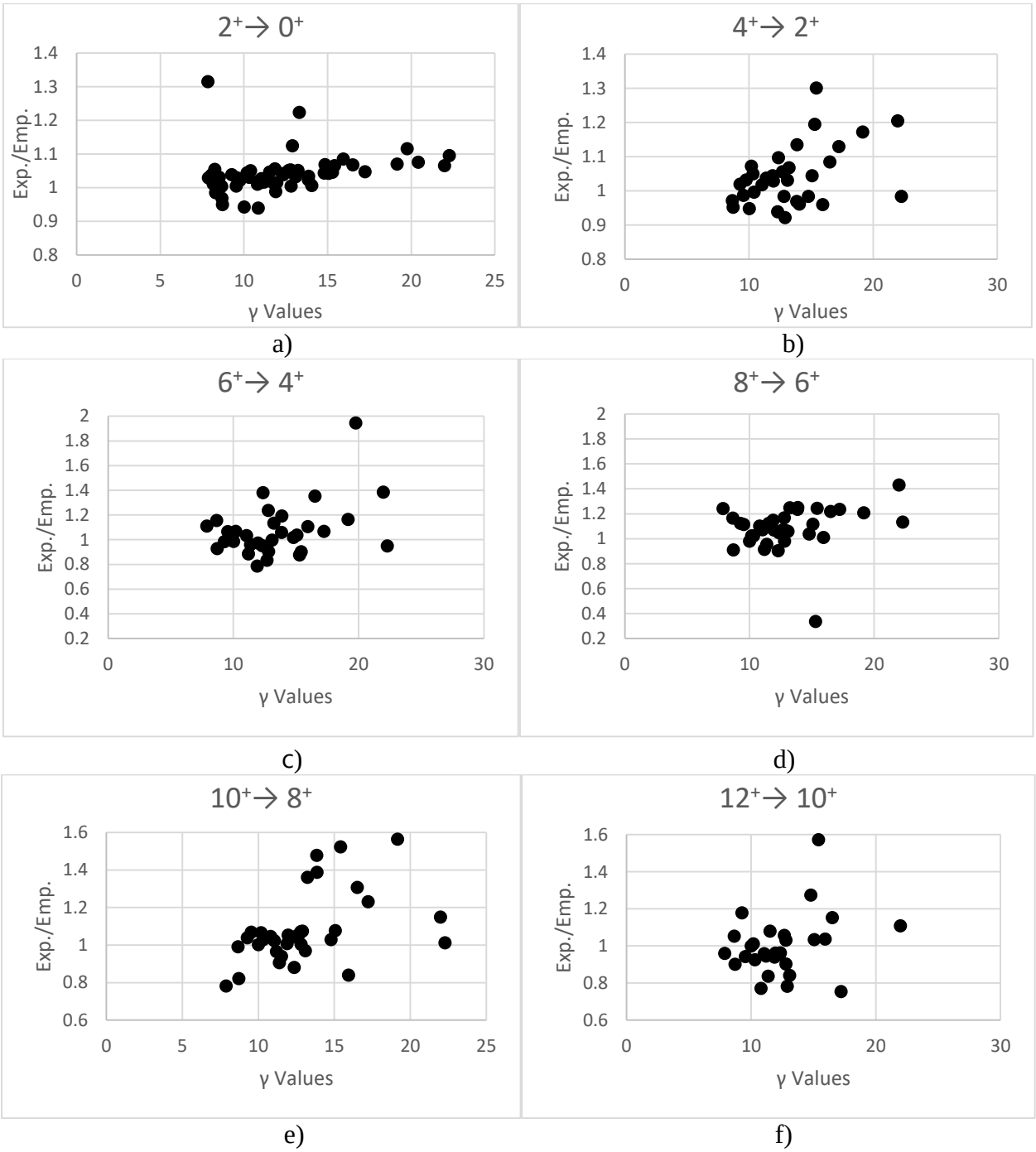

Figure 4.2. Ratio of experimental to empirical B(E2) values versus γ-values: a) $2^+ \rightarrow 0^+$, b) $4^+ \rightarrow 2^+$, c) $6^+ \rightarrow 4^+$, d) $8^+ \rightarrow 6^+$, e) $10^+ \rightarrow 8^+$ and f) $12^+ \rightarrow 10^+$.

Table 4. Experimental and empirical meanlives of transitions.

Nuclide	Theoretical Meanlives						Experimental Meanlives					
	$2^+ \rightarrow 0^+$	$4^+ \rightarrow 2^+$	$6^+ \rightarrow 4^+$	$8^+ \rightarrow 6^+$	$10^+ \rightarrow 8^+$	$12^+ \rightarrow 10^+$	$2^+ \rightarrow 0^+$	$4^+ \rightarrow 2^+$	$6^+ \rightarrow 4^+$	$8^+ \rightarrow 6^+$	$10^+ \rightarrow 8^+$	$12^+ \rightarrow 10^+$
$^{150}_{62}$Sm	75.02	13.60	6.15	3.60	2.52	2.12	69.83	9.38	2.02	-	-	-
$^{152}_{62}$Sm	2121.14	88.76	16.50	5.66	2.71	1.55	2019.77	83.24	14.57	4.55	1.99	-
$^{154}_{62}$Sm	4374.11	244.56	34.86	9.48	3.78	1.89	4356.94	248.14	32.75	8.51	3.54	2.01
$^{152}_{64}$Gd	52.18	15.29	7.01	4.16	2.95	2.23	46.74	10.53	3.61	-	-	-
$^{154}_{64}$Gd	1768.48	73.97	13.41	4.61	2.20	1.28	1711.04	65.21	11.25	3.69	1.59	-
$^{156}_{64}$Gd	3270.81	164.10	23.53	6.68	2.81	1.52	3188.36	161.44	22.80	6.23	2.74	1.59
$^{158}_{64}$Gd	3744.24	223.81	29.88	7.53	2.75	1.31	3635.59	213.52	23.08	7.36	2.67	1.41
$^{160}_{64}$Gd	3936.07	262.89	34.97	8.53	3.05	1.39	3880.85	-	-	-	-	-
$^{154}_{66}$Dy	41.61	10.42	4.61	2.76	1.99	1.49	39.10	8.66	3.33	1.93	1.73	1.34
$^{156}_{66}$Dy	1263.48	55.49	10.81	3.95	1.96	1.20	1187.34	42.70	11.97	3.17	1.28	0.77
$^{158}_{66}$Dy	2501.13	109.39	16.24	4.88	2.16	1.26	2394.87	103.87	13.13	4.18	2.03	1.23
$^{160}_{66}$Dy	2944.90	154.84	21.10	5.69	2.27	1.21	2922.90	148.60	26.83	4.95	2.25	1.28
$^{162}_{66}$Dy	3219.09	195.71	25.81	6.48	2.39	1.12	3173.93	190.44	26.55	6.06	2.27	1.17
$^{164}_{66}$Dy	3549.19	271.66	37.32	9.40	3.45	1.63	3448.04	289.98	39.24	10.39	3.30	1.70
$^{160}_{68}$Er	1374.96	48.64	8.07	2.73	1.35	0.87	1325.84	46.60	7.79	2.45	1.26	0.84
$^{162}_{68}$Er	2044.02	83.72	11.85	3.43	1.49	0.87	1687.95	-	-	-	-	-
$^{164}_{68}$Er	2352.49	114.17	15.15	3.97	1.55	0.78	2120.76	124.07	-	3.74	1.44	1.00
$^{166}_{68}$Er	2719.23	179.42	24.61	6.49	2.59	1.37	2625.70	170.24	29.60	6.06	2.45	1.30
$^{168}_{68}$Er	2773.95	179.92	23.07	5.44	1.88	0.86	2712.27	164.47	16.74	5.19	2.14	0.89
$^{170}_{68}$Er	2809.69	190.17	24.47	5.82	2.01	0.89	2728.14	204.00	-	5.19	2.14	0.82
$^{166}_{70}$Yb	1822.28	78.55	11.21	3.27	1.40	0.78	1788.94	76.32	11.25	3.09	1.44	0.92
$^{168}_{70}$Yb	2217.06	133.70	18.78	5.28	2.24	1.25	2120.76	-	-	-	-	-
$^{170}_{70}$Yb	2301.98	144.49	18.84	4.71	1.75	0.86	2315.53	-	-	4.29	1.67	1.11
$^{172}_{70}$Yb	2430.61	178.82	23.55	5.67	1.99	0.88	2380.45	176.01	23.95	5.05	1.90	0.75
$^{174}_{70}$Yb	2540.61	201.10	26.63	6.39	2.29	1.00	2582.42	207.75	23.08	5.48	2.31	0.95
$^{176}_{70}$Yb	2624.45	170.95	21.58	5.19	1.86	0.87	2539.14	158.70	20.20	5.05	1.73	0.85
$^{166}_{72}$Hf	751.06	27.51	5.40	2.15	1.25	0.96	717.02	24.24	5.05	1.73	1.01	1.30
$^{168}_{72}$Hf	1329.22	51.01	8.66	2.99	1.50	0.96	1284.00	51.94	8.51	2.89	1.46	0.75
$^{170}_{72}$Hf	1720.23	87.83	14.07	4.52	2.20	1.32	1731.23	89.45	15.58	4.62	2.19	1.46
$^{172}_{72}$Hf	2260.97	119.76	17.01	4.85	2.07	1.14	2236.18	-	-	-	-	-
$^{174}_{72}$Hf	2215.29	128.01	17.48	4.87	2.04	1.13	2394.87	-	-	-	-	-
$^{176}_{72}$Hf	2153.19	129.95	17.37	4.48	1.75	0.88	2063.05	-	-	-	-	-
$^{178}_{72}$Hf	2169.65	112.02	14.29	3.65	1.44	0.76	2135.19	-	16.16	4.00	1.49	0.81
$^{182}_{74}$W	2015.85	92.61	11.34	2.76	0.99	0.46	1975.05	89.45	11.83	2.90	1.10	0.55
$^{184}_{74}$W	1846.19	66.97	8.24	2.05	0.79	0.40	1804.81	69.25	7.79	1.66	0.53	-
$^{186}_{74}$W	1606.50	50.35	6.38	1.60	0.61	0.30	1494.63	52.51	5.77	1.59	0.72	0.29
$^{180}_{76}$Os	1194.09	46.49	8.47	3.35	2.01	1.48	1154.16	38.95	9.67	9.96	-	-
$^{182}_{76}$Os	1239.63	45.66	7.22	2.49	1.48	1.46	1172.91	-	-	-	-	-

$^{184}_{76}$Os	1699.20	63.70	8.89	2.50	1.03	0.54	1708.15	66.36	-	-	-	-
$^{186}_{76}$Os	1334.99	41.40	5.91	1.74	0.77	0.47	1262.36	38.23	4.37	1.43	0.59	0.40
$^{188}_{76}$Os	1088.37	32.78	5.20	1.69	0.86	0.67	1024.31	27.99	4.47	1.40	0.55	-
$^{190}_{76}$Os	570.99	20.01	3.56	1.24	0.69	-	523.70	20.34	3.75	1.10	0.68	-
$^{228}_{90}$Th	582.74	240.53	82.09	31.03	14.50	8.06	584.29	236.60	-	-	-	-
$^{230}_{90}$Th	536.14	238.55	84.48	30.77	13.57	7.03	510.71	239.49	-	-	-	-
$^{232}_{90}$Th	457.62	219.93	88.73	33.77	14.99	7.92	497.73	236.60	90.89	34.63	15.00	7.94
$^{234}_{92}$U	351.75	186.45	93.90	41.41	19.41	10.22	363.56	-	-	-	-	-
$^{236}_{92}$U	312.72	167.30	76.76	31.23	13.69	6.88	337.59	178.89	83.68	34.63	16.74	7.65
$^{238}_{92}$U	300.65	160.42	75.77	30.75	13.72	6.83	292.87	-	-	-	-	-
$^{238}_{94}$Pu	245.25	132.95	66.98	28.40	12.31	5.97	255.36	-	-	-	-	-
$^{240}_{94}$Pu	238.71	131.52	69.24	30.75	13.85	6.87	236.60	-	-	-	-	-
$^{242}_{94}$Pu	230.53	124.64	61.59	26.02	11.40	5.63	227.95	-	-	-	-	-
$^{244}_{94}$Pu	224.73	115.49	57.35	23.37	11.03	4.99	223.62	-	-	-	-	-
$^{244}_{96}$Cm	178.94	99.19	54.15	24.63	-	-	139.94	-	-	-	-	-
$^{246}_{96}$Cm	176.71	97.46	53.81	24.27	-	-	174.57	-	-	-	-	-
$^{248}_{96}$Cm	174.69	96.37	52.15	23.39	13.08	5.25	174.57	112.53	47.61	19.04	13.56	5.48
$^{250}_{98}$Cf	138.88	76.90	43.69	21.52	-	-	141.38	-	-	-	-	-
$^{252}_{98}$Cf	133.19	71.64	-	-	-	-	132.73	-	-	-	-	-

The experimental meanlives shown in this table are computed from half-lives of the transition states from table of Isotopes (Firestone, 1999) using the well-known relation,

$$\tau = \frac{T_{1/2}}{\ln 2} \tag{4.3}$$

In this study, the meanlives of rotational excited ground band states of even-even nuclei of rare earth and actinide series have been computed by making use of the empirically calculated reduced transition probabilities. This is because, as can be seen from Figure 4.2, the empirically calculated reduced transition probability ratio is very close to unity.

As clearly seen, from Figure 4.1, the energy ratio for almost all nuclides under the study fall beyond 2.5 where this is the rotational deformed region. So that almost all the nuclides considered in this

study are rotational in nature where nuclear deformation is highly observed, and that the asymmetric rotor model assumed to work best.

The meanlives of the transitions are dependent inversely upon the transition gamma energy (to the power of five), the total internal conversion coefficient, and the empirical reduced transition probability (See Eqn. (4.2)). The empirical reduced transition probability in turn is proportional to the square of the intrinsic quadrupole moment (Qo) (See Eqn. (3.7)). The intrinsic quadrupole moment, in turn, is directly proportional to the elongation deformation parameter β See Eqn. (3.9)). So in these empirical calculations both the asymmetric parameter γ and the elongation parameter β have been employed.

The empirical reduced transition probabilities calculated are in a very good agreement (Biniyam & Chaubey, 2017), especially for lower transitions. There is a difficulty in determining the total ICC values for transition gamma energy greater than 400 keV using the Bricc software. The transition gamma energy get increases for higher transitions and are observed to be greater than the mentioned value especially for the rare earth series.

We have found a very good agreement except for $^{150}_{62}$Sm & $^{152}_{64}$Gd at $4^+ \rightarrow 2^+$ and $6^+ \rightarrow 4^+$ transitions, $^{154}_{66}$Dy & $^{180}_{76}$Os at $8^+ \rightarrow 6^+$ transition, $^{156}_{66}$Dy, $^{184}_{74}$W & $^{188}_{76}$Os at $10^+ \rightarrow 8^+$ transition, and $^{156}_{66}$Dy at $12^+ \rightarrow 10^+$ transition. In these nuclides, the percentage difference is found to be large, in most cases greater than 40%. This large percentage difference observed in these nuclides may be attributed to the fact that most of these nuclides are not in a rotationally deformed category.

The percentage difference between the empirically calculated meanlives and experimental data available, in most cases, is found to be around 5%. This percentage difference get increases as the level of the transition get higher. This percentage difference could be attributed to the fact that the total internal conversion coefficient could not be computed for the transition gamma energy greater than 400 keV. This may be the real cause, for most cases, since the large percentage difference is observed for those transitions where the transition gamma energy is beyond the mentioned value.

It is observed that the percentage difference observed in actinide series is very small. This may be due to a smaller transition gamma energy than the minimum expected value in the Bricc online software.

CHAPTER 5. Energy States in Non-Axial Nuclei

5.1. Introduction

The energy levels of non-spherical nuclei corresponding to collective excitations not involving violation of axial symmetry of the nuclei were investigated on basis of the generalized nuclear model proposed by Aage Bohr and Benjamin Mottelson (Davydov & Filippov, 1958). It was shown that the rotational-vibrational energy of collective nuclear excited states is a function of only two parameters, viz., of the frequency of nuclear surface vibrations and of the ratio of the equilibrium deformation to the zero vibration amplitude. It seems natural to inquire to what extent these results are applicable if one takes into account possible violation of axial symmetry of the nucleus.

The problem of violation of axial symmetry of nuclei has been qualitatively treated in a number of papers. Recently it has even become usual to ascribe nuclear excited states to the so called γ-vibrations. This type of assignment is usually based on the spin values of these levels and on the large probability of electromagnetic transitions which confirms the collective nature of the levels. No quantitative theory of γ-vibrations has been proposed (Davydov & Filippov, 1958).

In the present paper, we investigate energy levels corresponding to rotation of the nucleus, which does not involve changes of its internal state. It will be shown that violation of axial symmetry of even-even nuclei only slightly affects the rotational spectrum of the axial nucleus although some new rotational states with total angular momenta of 2, 3, 4 ... do appear. If the deviations from axial symmetry are small these levels lie very high and are not excited. As the deviations from

axial symmetry are increased some of the additional levels become much lower. Thus, for example, the ratio of the second excited state with spin 2 to the first state (which also exists in axial nuclei), varies from infinity to two (Davydov & Filippov, 1958).

In recent years (James, 2007) the problem of the prediction of the nuclear rotational energy levels has attracted considerable interest. One of the main reasons is that the development of the high resolution solid state γ-detector has made it possible to follow the rotational bands of high spin. The new results showed that the energies of high spin rotational states deviate from the well-known rule of rigid rotor, namely

$$E_{rot} = \frac{\hbar^2 I(I+1)}{2\Im} \tag{5.1}$$

where $\Im$ is the effective moment of inertia and I is the nuclear spin.

Irrotational moments of inertia were introduced by Davydov and Filippov following the lead of A. Bohr in his original paper (James, 2007). It was extensively developed later. The Davydov and Filippov model directly correlates the inertia tensor to the E2 quadrupole tensor, via the parameters β and γ, by

$$\Im_k = 4B\beta^2 \sin^2(\gamma - k\frac{2\pi}{3}), \quad k = 1, 2, 3, \tag{5.2}$$

where B is the irrotational flow mass parameter and the dependence on γ gives the ratios of the components of the inertia tensor according to irrotational flow.

Irrotational flow is an idealization of nuclear rotation but it is more realistic than rigid flow. In comparison, the present triaxial rotor model assumes the electric quadrupole tensor and the inertia tensor are independently parameterized. Fitting to data reveals that these parameters are strongly correlated.

5.2. Methods

The Hamiltonian of the asymmetric rotor model (ARM) can be written as (Davydov & Filippov, 1958; Demille et al., 1959; Horacio, 1960; Moore & White, 1960; Parveen & Harish, 2015; Singh et al., 2007; Yan, Vogel, von Brentano & Gelberg, 1993; Yuvraj et al., 2013)

$$H = \frac{\hbar^2}{4B\beta^2} \sum_{\lambda=1}^{3} \frac{I_\lambda^2}{2\mathrm{Sin}^2(\gamma - \frac{2\pi}{3}\lambda)} \tag{5.3}$$

where B is the mass parameter, β is the nuclear quadrupole deformation parameter, γ varies between 0 and π/3 and determines the deviation of the shape of the nucleus from axial symmetry, and the I_λ are operators of the projections of the nuclear angular momenta on the axes of a coordinate system connected with the nucleus.

According to Eqn. (5.1), for $\gamma \neq 0$ or π/3 the nucleus should be regarded as an asymmetric top. In stationary states of the asymmetric top not one of the projections of the total angular momentum on axes 1, 2, 3 of the body-fixed coordinate system has a definite value and hence the energy levels cannot be specified by the values of $K = I_3$. Each value of the total angular momentum in the asymmetric top corresponds to 2I+1 different energy levels. These levels can be classified with

respect to the irreducible representations of group D_2 (See Appendix A). Thus, the energy levels of an asymmetric top split up into four types of levels that correspond to the four irreducible representations of group D_2.

In virtue of the symmetry conditions imposed on the wave function in even-even nuclei of the 2I+1 different levels only those energy levels with a given I can exist which correspond to a completely symmetric representation of group D_2. Rotation states of the required symmetry will not exist if I = 1. Two such states will exist for I = 2, one for I = 3, three for I = 4, two for I = 5, four for I = 6, etc.

If the energy is expressed in units of $A = \frac{\hbar^2}{4B\beta^2}$ the energy of two levels of the required symmetry are, for I = 2, defined by the expression

$$\mathcal{E}_1(2) = \frac{9(1-\sqrt{1-\frac{8}{9}\mathrm{Sin}^2(3\gamma)})}{\mathrm{Sin}^2(3\gamma)}\,,\ \mathcal{E}_2(2) = \frac{9(1+\sqrt{1-\frac{8}{9}\mathrm{Sin}^2(3\gamma)})}{\mathrm{Sin}^2(3\gamma)} \tag{5.4}$$

The energy of a level with angular momentum I = 3 is given by

$$\mathcal{E}(3) = \frac{18}{\mathrm{Sin}^2(3\gamma)} \tag{5.5}$$

The three spin 4 energy levels are the roots of the third degree equation

$$\mathcal{E}^3 - \frac{90}{\mathrm{Sin}^2(3\gamma)}\mathcal{E}^2 + \frac{48}{\mathrm{Sin}^4(3\gamma)}[27+26\mathrm{Sin}^2(3\gamma)]\mathcal{E} - \frac{640}{\mathrm{Sin}^4(3\gamma)}[27+7\mathrm{Sin}^2(3\gamma)] = 0 \tag{5.6}$$

The roots of this equation have been computed using wolfram Mathematica equation solver, online software (Stephen, 2017) and the solution has not been presented in this study because it is so lengthy.

The two spin 5 energy levels are given by the formula

$$\mathcal{E}_1(5) = \frac{45-9\sqrt{9-8\mathrm{Sin}^2(3\gamma)}}{\mathrm{Sin}^2(3\gamma)},\ \mathcal{E}_2(5) = \frac{45+9\sqrt{9-8\mathrm{Sin}^2(3\gamma)}}{\mathrm{Sin}^2(3\gamma)} \tag{5.7}$$

The energy levels of states possessing an angular momentum equal to 6 and 8 are defined by a fourth and fifth degree equation respectively.

The following simple relation between the spin 2 and spin 3 energy levels follows from Eqn. (5.4) and Eqn. (5.5) as

$$\mathcal{E}_1(2) + \mathcal{E}_2(2) = \mathcal{E}(3) \tag{5.8}$$

In the frame work of the rigid triaxial rotor model (Varshney, 1982), nuclear deformation parameters β and γ are extracted from both level energies and E2 transition rates in even-even nuclei. The rigid triaxial rotor model considers the nucleus as a rigid rotor with rigid triaxial asymmetry as specified by β and γ.

In this particular calculation as well, we have employed the most widely used method to compute the asymmetry parameter γ, which is evaluated from the ratio of two band head energies $E_2^{+'}/ E_2^{+}$,

(Singh et al., 2013; Varshney et al., 2011), as we have considered and showed in chapter three by Eqn. (3.9) and Eqn. (3.10).

The energies calculated are considered in two different units. The first is in an energy unit of A= $\frac{\hbar^2}{4B\beta^2}$ discussed in section (5.2) above. The second is in a unit of keV. It is possible to convert the energy calculated in a unit $\frac{\hbar^2}{4B\beta^2}$ to keV unit by considering the following empirical relation.

The hydrodynamic relation relates $E_2^{+'}$ with moment of inertia J_0 and asymmetric parameter γ for asymmetric nucleus ($\gamma \neq 0$) as (Singh et al., 2012)

$$E_2^{+'} = \frac{6\hbar^2}{2J_o} \frac{9-\sqrt{81-72\mathrm{Sin}^2(3\gamma)}}{4\mathrm{Sin}^2(3\gamma)} \tag{5.9}$$

where $J_o = 4B\beta^2$

Now we can rewrite Eqn. (5.9) to fit the energy unit we have considered in section (5.2) above as follows

$$\frac{\hbar^2}{4B\beta^2} = \frac{8}{6} \frac{E_2^{+'}}{\frac{9-\sqrt{81-72\mathrm{Sin}^2(3\gamma)}}{\mathrm{Sin}^2(3\gamma)}} \tag{5.10}$$

And we have approximated this equation as,

$$\frac{\hbar^2}{4B\beta^2} \approx \frac{E_2^{+'}}{\frac{9-\sqrt{81-72Sin^2(3\gamma)}}{Sin^2(3\gamma)}} \tag{5.11}$$

This empirical relation is used for this particular energy calculations and help us to convert the energy unit (A = $\frac{\hbar^2}{4B\beta^2}$) in to a convenient energy unit of keV.

5.3. Result and Discussion

In this section, we will present the calculated asymmetric parameter γ values in Figure 5.1, and the calculated band energies in a unit of (A = $\frac{\hbar^2}{4B\beta^2}$) in Figure 5.2. The empirical energy calculations, in a unit of A, is tabulated in Table 5.1, and the corresponding energies converted to a unit of keV is tabulated in Table 5.2.

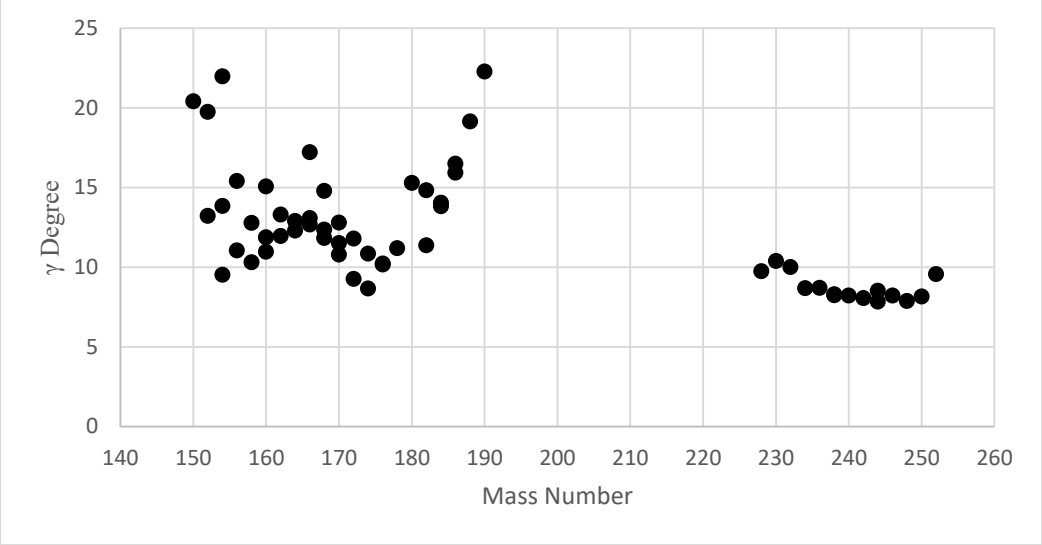

Figure 5.1. Mass number versus asymmetric parameter γ.

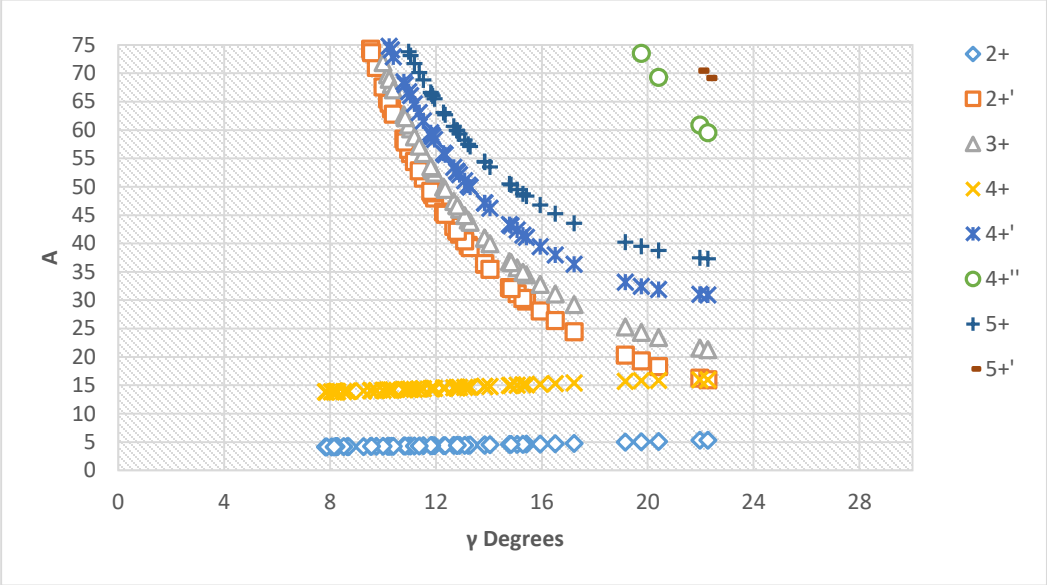

Figure 5.2. Energy (in a unit of A) versus asymmetric parameter γ.

Table 5.1. Calculated band energies (in a unit of A) of rare earth and actinide series.

S/No	Nuclide	Spin States							
		2^+	$2^{+'}$	3^+	4^+	$4^{+'}$	$4^{+''}$	5^+	$5^{+'}$
1.	$^{150}_{62}Sm$	5.12	18.29	23.41	15.86	31.90	69.31	38.77	78.29
2.	$^{152}_{62}Sm$	4.45	39.69	44.13	14.67	50.30	155.70	57.48	163.19
3.	$^{154}_{62}Sm$	4.23	74.22	78.45	14.05	84.26	293.95	91.14	301.12
4.	$^{152}_{64}Gd$	5.04	19.31	24.36	15.79	32.48	73.52	39.49	82.29
5.	$^{154}_{64}Gd$	4.49	36.37	40.86	14.79	47.14	142.37	54.35	149.97
6.	$^{156}_{64}Gd$	4.31	55.89	60.19	14.29	66.06	220.62	73.12	227.85
7.	$^{158}_{64}Gd$	4.27	63.75	68.01	14.16	74.12	251.38	80.82	259.25
8.	$^{160}_{64}Gd$	4.30	56.57	60.87	14.28	66.76	223.32	73.79	230.58
9.	$^{154}_{66}Dy$	5.30	16.29	21.59	15.99	31.05	60.91	37.49	70.44
10.	$^{156}_{66}Dy$	4.62	29.86	34.48	15.08	41.07	116.25	48.34	124.08
11.	$^{158}_{66}Dy$	4.42	42.30	46.72	14.60	52.75	166.23	59.97	173.61
12.	$^{160}_{66}Dy$	4.36	48.58	52.94	14.43	58.86	191.42	66.02	198.69
13.	$^{162}_{66}Dy$	4.36	48.04	52.40	14.45	58.35	189.21	65.49	196.52
14.	$^{164}_{66}Dy$	4.39	45.55	49.93	14.51	55.89	179.25	63.09	186.57
15.	$^{160}_{68}Er$	4.59	31.15	35.74	15.00	42.36	121.21	49.51	129.18
16.	$^{162}_{68}Er$	4.45	39.29	43.74	14.68	49.92	154.09	57.10	161.61
17.	$^{164}_{68}Er$	4.43	41.62	46.05	14.61	52.13	163.49	59.32	170.91
18.	$^{166}_{68}Er$	4.41	43.00	47.41	14.57	53.45	168.97	60.64	176.39
19.	$^{168}_{68}Er$	4.39	45.13	49.52	14.51	55.64	177.45	62.69	184.91

20.	$^{170}_{68}$Er	4.34	51.51	55.85	14.38	61.60	203.26	68.86	210.38
21.	$^{166}_{70}$Yb	4.44	40.49	44.93	14.65	51.04	158.94	58.24	166.39
22.	$^{168}_{70}$Yb	4.36	48.90	53.25	14.43	59.13	192.71	66.32	199.95
23.	$^{170}_{70}$Yb	4.29	58.40	62.70	14.25	68.50	230.73	75.58	237.90
24.	$^{172}_{70}$Yb	4.22	78.47	82.68	14.02	88.33	311.05	95.33	318.09
25.	$^{174}_{70}$Yb	4.19	89.61	93.80	13.93	99.66	355.17	106.36	362.63
26.	$^{176}_{70}$Yb	4.26	65.45	69.71	14.15	75.45	258.97	82.49	266.07
27.	$^{166}_{72}$Hf	4.78	24.45	29.24	15.41	36.32	94.45	43.58	102.59
28.	$^{168}_{72}$Hf	4.57	32.24	36.81	14.95	43.34	125.71	50.51	133.54
29.	$^{170}_{72}$Hf	4.42	42.18	46.60	14.60	52.61	165.77	59.85	173.13
30.	$^{172}_{72}$Hf	4.35	49.20	53.56	14.42	59.55	193.81	66.62	201.16
31.	$^{174}_{72}$Hf	4.30	57.88	62.18	14.26	68.01	228.61	75.07	235.81
32.	$^{176}_{72}$Hf	4.26	64.70	68.97	14.16	74.76	255.91	81.76	263.07
33.	$^{178}_{72}$Hf	4.32	54.47	58.79	14.32	64.61	214.97	71.74	222.19
34.	$^{182}_{74}$W	4.33	52.82	57.14	14.35	63.06	208.30	70.13	215.59
35.	$^{184}_{74}$W	4.49	36.47	40.97	14.79	47.20	142.84	54.44	150.38
36.	$^{186}_{74}$W	4.66	28.12	32.78	15.18	39.46	109.26	46.77	117.13
37.	$^{180}_{76}$Os	4.61	30.33	34.94	15.06	41.49	118.15	48.76	125.93
38.	$^{182}_{76}$Os	4.57	32.04	36.62	14.97	43.11	124.92	50.33	132.75
39.	$^{184}_{76}$Os	4.51	35.46	39.97	14.83	46.24	138.81	53.50	146.37
40.	$^{186}_{76}$Os	4.71	26.39	31.10	15.28	37.97	102.27	45.25	110.27
41.	$^{188}_{76}$Os	4.98	20.34	25.32	15.71	33.17	77.70	40.25	86.33
42.	$^{190}_{76}$Os	5.34	15.96	21.29	16.01	30.95	59.52	37.31	69.16
43.	$^{228}_{90}$Th	4.24	71.01	75.25	14.09	81.00	281.16	87.97	288.29
44.	$^{230}_{90}$Th	4.27	62.79	67.06	14.18	72.90	248.23	79.88	255.44
45.	$^{232}_{90}$Th	4.25	67.60	71.86	14.13	77.63	267.52	84.61	274.67
46.	$^{234}_{92}$U	4.19	89.22	93.41	13.93	99.02	354.05	105.97	361.07
47.	$^{236}_{92}$U	4.19	88.61	92.80	13.94	98.43	351.63	105.37	358.64
48.	$^{238}_{92}$U	4.17	98.51	102.68	13.88	108.33	391.20	115.19	398.22
49.	$^{238}_{94}$Pu	4.17	97.35	101.52	13.88	107.15	386.57	114.04	393.58
50.	$^{240}_{94}$Pu	4.17	98.98	103.15	13.87	108.80	393.09	115.66	400.10
51.	$^{242}_{94}$Pu	4.16	102.85	107.02	13.85	112.69	408.45	119.50	415.58
52.	$^{244}_{94}$Pu	4.18	92.28	96.46	13.91	102.11	366.29	109.01	373.31
53.	$^{244}_{96}$Cm	4.15	108.84	112.99	13.82	118.68	432.47	125.45	439.52
54.	$^{246}_{96}$Cm	4.17	98.98	103.15	13.87	108.80	393.09	115.66	400.10
55.	$^{248}_{96}$Cm	4.15	107.79	111.94	13.83	117.55	428.32	124.40	435.30
56.	$^{250}_{98}$Cf	4.17	100.67	104.83	13.87	110.41	399.93	117.33	406.84
57.	$^{252}_{98}$Cf	4.23	73.62	77.85	14.06	83.55	291.65	90.54	298.73

Table 5.2. Calculated empirical band energies (in keV) of rare earth and actinide series.

S/No.	Nuclide	Energy (keV)	Spin States							
			2^+	$2^{+'}$	3^+	4^+	$4^{+'}$	$4^{+''}$	5^+	$5^{+'}$
1.	$^{150}_{62}$Sm	Expt.	333.96	1193.84	1504.57	773.37				
		Emp.	333.87	1193.04	1526.90	1034.23	2080.55	4519.80	2528.50	5106.02
2.	$^{152}_{62}$Sm	Expt.	121.78	1085.84	1233.86	366.48	1371.74		1559.62	
		Emp.	121.78	1086.47	1208.26	401.63	1377.08	4262.57	1573.63	4467.65
3.	$^{154}_{62}$Sm	Expt.	81.98	1440.04	1539.19	266.82	1664.82		1804.99	
		Emp.	81.98	1439.17	1521.15	272.48	1633.73	5699.55	1767.08	5838.67
4.	$^{152}_{64}$Gd	Expt.	344.28	1318.42	1692.41	755.40	1550.16		1861.58	
		Emp.	344.28	1317.93	1662.20	1077.40	2216.41	5017.20	2695.04	5615.99
5.	$^{154}_{64}$Gd	Expt.	123.07	996.26	1127.80	371.00	1263.78		1432.59	
		Emp.	123.07	995.91	1118.98	404.91	1291.01	3898.63	1488.20	4106.72
6.	$^{156}_{64}$Gd	Expt.	88.97	1154.15	1248.01	288.19	1355.42		1506.86	
		Emp.	88.97	1154.05	1243.02	295.10	1364.11	4555.89	1509.92	4705.17
7.	$^{158}_{64}$Gd	Expt.	79.51	1187.14	1265.52	261.46	1358.47		1481.42	
		Emp.	79.51	1187.61	1267.12	263.82	1380.96	4683.34	1505.65	4829.96
8.	$^{160}_{64}$Gd	Expt.	75.26	988.40	1057.54	248.52	1147.78		1261.07	
		Emp.	75.26	989.07	1064.33	249.64	1167.27	3904.70	1290.11	4031.55
9.	$^{154}_{66}$Dy	Expt.	334.34	1027.04	1334.19	746.78	1442.28		1739.60	
		Emp.	334.58	1027.63	1362.21	1008.67	1959.26	3843.14	2365.94	4445.08
10.	$^{156}_{66}$Dy	Expt.	137.77	890.50	1022.08	404.19	1168.47		1335.56	
		Emp.	137.83	891.21	1029.05	450.01	1225.58	3469.23	1442.54	3702.69
11.	$^{158}_{66}$Dy	Expt.	98.92	946.32	1044.60	317.14	1163.75		1314.78	
		Emp.	98.92	947.12	1046.04	326.80	1181.20	3722.10	1342.79	3887.39
12.	$^{160}_{66}$Dy	Expt.	86.79	966.17	1049.10	283.82	1155.84		1288.66	
		Emp.	86.79	967.30	1054.09	287.41	1171.89	3811.23	1314.45	3956.00
13.	$^{162}_{66}$Dy	Expt.	80.66	888.16	962.94	265.66	1060.99		1182.76	
		Emp.	80.66	888.04	968.70	267.05	1078.62	3497.74	1210.68	3632.81
14.	$^{164}_{66}$Dy	Expt.	73.39	761.82	828.19	242.23	916.00		1024.64	
		Emp.	73.39	762.28	835.67	242.81	935.44	3000.05	1055.85	3122.50
15.	$^{160}_{68}$Er	Expt.	125.80	854.40	987.30	389.90			1316.70	
		Emp.	125.80	853.83	979.63	411.17	1161.03	3322.64	1357.03	3541.11
16.	$^{162}_{68}$Er	Expt.	102.04	900.72	1002.06	329.62	1128.11		1286.22	
		Emp.	102.04	900.22	1002.26	336.44	1143.86	3530.73	1308.38	3702.93
17.	$^{164}_{68}$Er	Expt.	91.38	860.25	946.40	299.43	1058.48		1197.46	
		Emp.	91.40	859.67	951.07	301.81	1076.77	3376.82	1225.27	3530.09
18.	$^{166}_{68}$Er	Expt.	80.58	785.91	859.39	264.99	956.23		1075.28	
		Emp.	80.58	785.54	866.11	266.26	976.60	3087.17	1107.85	3222.73
19.	$^{168}_{68}$Er	Expt.	79.80	821.17	895.79	264.09	994.75		1117.57	
		Emp.	79.80	820.57	900.38	263.81	1011.63	3226.58	1139.79	3362.09
20.	$^{170}_{68}$Er	Expt.	78.60	934.03	1010.54	260.15	1103.33		1236.61	
		Emp.	78.59	933.50	1012.09	260.58	1116.29	3683.53	1247.87	3812.60

21.	$^{166}_{70}$Yb	Expt.	102.37	932.38	1039.14	330.48	1162.74		1327.85	
		Emp.	102.37	933.81	1036.18	337.83	1177.18	3665.88	1343.29	3837.59
22.	$^{168}_{70}$Yb	Expt.	87.73	984.00	1067.15	286.55	1171.36		1302.30	
		Emp.	87.73	984.73	1072.46	290.60	1190.79	3880.87	1335.65	4026.65
23.	$^{170}_{70}$Yb	Expt.	84.25	1145.72	1225.35	277.43	1329.31		1459.75	
		Emp.	84.25	1145.90	1230.16	279.62	1344.02	4527.15	1482.92	4667.86
24.	$^{172}_{70}$Yb	Expt.	78.74	1465.88	1549.15	260.27	1657.79		1778.86	
		Emp.	78.75	1465.95	1544.69	261.88	1650.20	5811.14	1780.92	5942.54
25.	$^{174}_{70}$Yb	Expt.	76.47	1633.97	1709.42	253.12	1805.40		1926.00	
		Emp.	76.47	1636.71	1713.18	254.37	1820.14	6486.93	1942.59	6623.31
26.	$^{176}_{70}$Yb	Expt.	82.14	1260.89	1336.38	271.85	1435.50		1558.34	
		Emp.	82.13	1261.79	1343.92	272.83	1454.53	4992.28	1590.31	5129.28
27.	$^{166}_{72}$Hf	Expt.	158.64	809.96	1007.16	470.46	1332.41		1418.90	
		Emp.	158.50	810.44	968.94	510.66	1203.81	3130.39	1444.44	3400.26
28.	$^{168}_{72}$Hf	Expt.	124.10	875.94	1030.93	385.92	1216.50		1386.38	
		Emp.	124.00	875.54	999.54	406.04	1176.90	3413.45	1371.54	3626.16
29.	$^{170}_{72}$Hf	Expt.	100.80	961.30	1087.59	321.99	1227.30			
		Emp.	100.80	962.05	1062.85	333.03	1200.05	3781.19	1365.25	3949.01
30.	$^{172}_{72}$Hf	Expt.	95.22	1075.29	1180.87	309.24	1304.66		1462.88	
		Emp.	95.22	1076.04	1171.26	315.29	1302.40	4238.67	1456.92	4399.37
31.	$^{174}_{72}$Hf	Expt.	90.99	1226.77	1336.48	297.38	1448.85		1658.41	
		Emp.	90.99	1225.55	1316.54	301.91	1440.01	4840.74	1589.49	4993.20
32.	$^{176}_{72}$Hf	Expt.	88.35	1341.31	1445.79	290.18	1540.30		1727.80	
		Emp.	88.35	1340.77	1429.12	293.44	1549.15	5303.05	1694.17	5451.42
33.	$^{178}_{72}$Hf	Expt.	93.18	1174.63	1268.54	306.62	1384.46		1533.15	
		Emp.	93.18	1175.66	1268.84	309.04	1394.48	4639.89	1548.38	4795.80
34.	$^{182}_{74}$W	Expt.	100.11	1221.40	1331.12	329.43	1442.84		1623.51	
		Emp.	100.06	1221.14	1321.21	331.67	1457.98	4816.06	1621.39	4984.63
35.	$^{184}_{74}$W	Expt.	111.22	903.31	1005.97	364.07	1133.85		1294.94	
		Emp.	111.21	902.80	1014.01	366.00	1168.28	3535.62	1347.63	3722.40
36.	$^{186}_{74}$W	Expt.	122.63	737.96	862.28	396.55	1006.73		1197.30	
		Emp.	122.33	737.58	859.91	398.20	1035.21	2866.00	1226.90	3072.64
37.	$^{180}_{76}$Os	Expt.	132.11	870.44	1022.85	408.63	1196.83		1405.55	
		Emp.	132.30	870.87	1003.17	432.28	1191.35	3392.53	1400.07	3615.79
38.	$^{182}_{76}$Os	Expt.	126.89	890.61	1039.04	400.29	1190.30		1399.47	
		Emp.	127.00	890.42	1017.42	415.90	1197.88	3471.21	1398.42	3688.67
39.	$^{184}_{76}$Os	Expt.	119.77	942.87	1080.97	383.68	1224.99		1428.15	
		Emp.	119.80	942.37	1062.17	393.95	1228.65	3688.35	1421.57	3889.29
40.	$^{186}_{76}$Os	Expt.	137.16	767.48	910.47	434.09	1070.48		1275.61	
		Emp.	137.16	767.73	904.89	444.52	1104.77	2975.15	1316.37	3208.09
41.	$^{188}_{76}$Os	Expt.	155.02	633.02	789.98	477.94	965.65		1180.86	
		Emp.	155.02	633.15	788.17	489.00	1032.74	2419.03	1253.23	2687.61
42.	$^{190}_{76}$Os	Expt.	186.72	557.98	756.02	547.85	955.37		1203.86	
		Emp.	186.72	558.10	744.82	559.82	1082.52	2081.71	1304.97	2419.11

43.	$^{228}_{90}$Th	Expt.	57.77	968.38	1022.54	186.84	1091.05		1174.52	
		Emp.	57.76	967.61	1025.37	191.96	1103.71	3831.11	1198.64	3928.20
44.	$^{230}_{90}$Th	Expt.	53.23	781.38	825.66	174.11	883.60		955.04	
		Emp.	53.20	781.93	835.14	176.64	907.86	3091.17	994.74	3180.94
45.	$^{232}_{90}$Th	Expt.	49.37	785.25	829.60	162.12	890.10		960.24	
		Emp.	49.37	785.03	834.40	164.02	901.45	3106.48	982.50	3189.47
46.	$^{234}_{92}$U	Expt.	43.50	926.72	968.43	143.35	1023.77		1090.89	
		Emp.	43.50	926.75	970.24	144.74	1028.48	3677.51	1100.74	3750.48
47.	$^{236}_{92}$U	Expt.	45.24	957.90	1001.50	149.48	1058.80		1127.38	
		Emp.	45.24	957.02	1002.26	150.54	1063.03	3797.61	1137.99	3873.33
48.	$^{238}_{92}$U	Expt.	44.92	1060.27	1105.71	148.38	1168.00		1232.00	
		Emp.	44.91	1061.13	1106.04	149.48	1166.86	4213.81	1240.77	4289.43
49.	$^{238}_{94}$Pu	Expt.	44.07	1028.54	1069.93	145.94	1125.75			
		Emp.	44.08	1028.73	1072.81	146.71	1132.26	4084.95	1205.06	4159.02
50.	$^{240}_{94}$Pu	Expt.	42.82	900.32	1030.55	141.69	1076.22			
		Emp.	42.82	1016.90	1059.72	142.54	1117.70	4038.37	1188.19	4110.41
51.	$^{242}_{94}$Pu	Expt.	44.54	1102.00		147.30				
		Emp.	44.54	1100.74	1145.28	148.25	1206.01	4371.23	1278.90	4447.50
52.	$^{244}_{94}$Pu	Expt.	44.20	1015.00		155.00				
		Emp.	46.00	1015.24	1061.24	153.07	1123.40	4029.78	1199.24	4106.96
53.	$^{244}_{96}$Cm	Expt.	42.97	1020.76		142.35				
		Emp.	42.96	1126.13	1169.10	143.04	1227.89	4474.53	1297.99	4547.49
54.	$^{246}_{96}$Cm	Expt.	42.85	1124.26	1165.48	141.99	1219.95			
		Emp.	42.85	1017.56	1060.41	142.63	1118.43	4041.00	1188.97	4113.09
55.	$^{248}_{96}$Cm	Expt.	43.40	1131.00		143.80	1222.00			
		Emp.	43.38	1125.56	1168.94	144.42	1227.52	4472.72	1299.08	4545.61
56.	$^{250}_{98}$Cf	Expt.	42.72	1031.85	1071.37	141.88	1123.00			
		Emp.	42.72	1032.48	1075.20	142.21	1132.35	4101.74	1203.37	4172.63
57.	$^{252}_{98}$Cf	Expt.	45.72	804.80	845.70	151.74	900.30			
		Emp.	45.72	795.81	841.53	151.99	903.14	3152.49	978.69	3228.97

In this particular work, we have used an updated experimental data of energies for excited states. The important and determining parameter, the asymmetric parameter γ of the DF model, for energy calculation, has been calculated using Eqn. (3.10) and shown in Figure 5.1. We have used Eqn. (5.4) through Eqn. (5.7) to calculate the theoretical excitation energies in a unit of A, and the corresponding results are shown in Figure 5.2, and tabulated in Table 5.1. These energies have been converted to a unit of keV, utilizing Eqn. (5.11), and the results have been tabulated in Table

5.2 for the 57 nuclides of rare earth and actinide series. We have seen, from Figure 5.1, that the values of the asymmetric parameter γ is to a certain extent scattered for the mass region $150 \leq A \leq 190$ (rare earth), and almost similar values are obtained for the mass region $228 \leq A \leq 252$ (actinide series).

The Experimental data used in this study have been taken from (Firestone, 1999; Nuclear Data Sheet, 2017). We could not find a similar research works on this particular topic to compare our results with. In addition, due to this reason, we have compared our calculated results only with the available experimental ones. For the $4^{+''}$ and $5^{+'}$ we couldn't find, even, the appropriate available experimental data to compare with, and so that these empirically calculated results could be taken as the estimated values of the respective band energies.

This present study reveals, comparing the percentage difference between the experimental data and the results obtained from empirical calculations, that the percentage difference is very small for approximately all nuclei included in this study except for $^{150}_{62}$Sm, $^{152}_{64}$Gd and $^{154}_{66}$Dy. For these particular nuclei the percentage difference obtained is greater than 30%, for total angular momentum of 4 and greater, but for lower angular momentum the empirical calculations have perfectly matched the available experimental data.

The large percentage difference in these particular nuclides may be ascribed to the fact that these nuclides are not in a rotationally deformed region (Refer to Table 3.1). This comparison shows that the present empirical calculation is in an excellent agreement with the available experimental data.

CHAPTER 6. Conclusion

The B(E2) values for the ground state band of the even-even deformed nuclei in the rare earth and actinide regions have been investigated. This investigation reveals that the Davydov- Filippov (DF) model predictions are closer to the experimental values for higher transitions, thus giving support to the idea that the nuclear shape tends to become triaxial with higher angular momentum. Therefore, it is possible to say that, from the result obtained, there is a strong agreement between the experimental, extracted from experimental equation, and empirically estimated B(E2) values in the lower transitions than higher transitions in the experimental versus experimental, empirical versus experimental and empirical versus empirical for the present work and the previous works considered in this study.

The B(E2) values usually seen to increase with spin for low-lying states within a rotational excited band. For lower transitions, especially for $2^{+} \rightarrow 0^{+}$, the result obtained is in a very good agreement with the available experimental data and the reported works so far. Therefore, it is possible to infer the result obtained for the transitions could also be a go for result. In addition, if this is the case the theoretically (empirically) obtained results can be used to estimate the half-life or mean-life of rotational excited states of which neither the mean-life nor half-life has been experimentally not reported yet.

Mean-life predictions have been made for the 57 rotational nuclear excited states in the ground state band of the rare earth and actinide series. We have compared our empirical predictions of meanlives with the respective recent experimental values, if known, and have found a very good agreement. Moreover, a good agreement, at higher transitions, have been found for the rare earth

series. In general, the percentage difference increases as the transitions get higher. So, we observe that the predicted meanlives are observed to be in a very good agreement, especially at lower transitions, and that the asymmetric rotor model could be helpful in predicting the probable meanlives of rotational nuclear excited even-even ground state band.

The calculations of energy values for the ground and gamma band rotationally excited states of the even-even deformed nuclei in the rare earth and actinide regions have also been considered. We have compared our empirical calculation of energies with the respective recent experimental values, and have found an excellent agreement. This investigation shows that empirical energy calculations are very closer to the experimental values, thus giving support to the idea that the asymmetric rotor model of Davydov- Filippov (DF) is effective for rotational nuclear excited state in energy calculations.

Therefore, we observe that the calculated empirical energies are in an excellent agreement especially at lower spins for all nuclides considered in this particular study, and that the asymmetric rotor model could be helpful in calculating the rotational nuclear excited even-even ground and gamma band energy states.

Generally, we have found from our present investigations that the Davydov- Filippov (DF) model predictions for the B(E2) values, meanlives and rotational excited state energies are very close to the recent available experimental data, thus giving support to the idea that the nuclear shape tends to become triaxial and is capable of making predictions for any nucleus in the region of mass number in the rare earth and actinide nuclei considered in this study for which the first and second 2^+ energy states are known.

References

Akkoyun, S., Bayram, T., & Kara, S. O. (2015). A study on estimation of electric quadrupole transition probability in nuclei. *Journal of Nuclear Sciences*, *2*(2), 7 - 10.

Alya'a, A. (2016). The probability of electric transitions: The square of rotational energy and the moment of inertia for Cm (A=246) isotope. *Journal of Science and Arts*, *4*(37), 417 - 426.

Allmond, J. M. (2007). *Studies of triaxial rotors and band mixing in nuclei* (Doctoral dissertation). Georgia Institute of Technology, Atlanta, Georgia.

Alex, B. (2005). *Lecture notes in nuclear structure physics*. National Superconducting Cyclotron Laboratory and Department of Physics and Astronomy Michigan State University, E. Lansing, MI 48824.

Alex, S. (1997). *Theory of nucleus: Nuclear structure and nuclear interaction*. Springer-Science +Business Media Dordrecht.

Australian National University (Page last updated: 21 December 2011). Retrieved from *http://bricc.anu.edu.au/index.php.*

Beiser, A. (2003). *Concepts of modern physics* (6th ed.). New York, NY: McGraw-Hill Companies.

Bohr, A., & Mottelson, B. R. (1998). *Nuclear structure*, *1 &2*. Singapore: World Scientific Publishing.

Caprio, M. A. (2003). *Structure of collective modes in transitional and deformed nuclei* (Doctoral dissertation). Yale University, Yale.

Casten, R. F. (1990). *Nuclear structure from a simple perspective*. Brookhaven National Laboratory, Oxford, Oxford University Press.

David, J. R. (2010). *Nuclear collective motion: Models and theory*. New Jersey: World Scientific Publishing.

David, L. H., & John, A. W. (1953). Nuclear constitution and the interpretation of fission phenomena. *Phys. Rev. 89*, (5), 1102 - 1145.

Davydov, A. S., & Filippov, G. F. (1958). Rotational states in even atomic nuclei. *Nuclear Physics 8*, 237- 249.

DeMille, G. R., Kavanagh, T. M., Moore, R. B., Weaver, R. S., & White, W. (1959*).* Rotational states of even-even nuclei. *Can. J. Phys., 37*, 1036 -1043.

Firestone, R. B. (1999). *Eighth edition of the table of isotopes.* University of California, California.

Frank, J. M. (1978). *Hydrodynamic model wavefunctions in intrinsic coordinates and their application to the structure of even-even nuclei* (Doctoral dissertation). Iowa State University Ames, Iowa.

Girija, K. K. (2012). *Studies of shape changes of deformed nuclei and its effects on cluster emission* (Doctoral dissertation). University of Calicut.

Gregory, G. S. (1965). *Multiple coulomb excitation studies in even-even samarium nuclei* (Doctoral dissertation). Yale University, Yale.

Gupta, K. K., Varshney, V. P., & Gupta, D. K. (1982). Experimental evidence in support of triaxial shape of $^{150, 152, 154}$Sm nuclei. *Physical Review C, 26*(2), 685 - 696.

Hassan, H., Hadi, S., & Akpan, N. I. (2017). Investigation of energy and B(E2) transition rates for Bohr Hamiltonian with generalized Davidson potential. *Nuclear Physics A,* Accepted Manuscript.

Heyde, K. (1999). *Basic ideas and concepts in nuclear physics* (2nd ed.). Bristol: Institute of Physics Publishing.

Hodgson, P. E., Gadioli, E., & Gadioli, E. (1997). *Introductory nuclear physics*. New York: Oxford University Press.

Horacio, E. B. (1960). *Remarks on properties of even-even nuclei related to the asymmetric rotor theory of Davydov and Filippov* (Library circulation). Lawrence Radiation Laboratory Berkeley, University of California, California.

Ikot, A. N., Sobhani, H., & Hassanabadi, H. (2017). Study of energy and B(E2) transition rates for Davydov-Chaban Hamiltonian with generalized Davidson potential. *Nuclear Physics A,* Accepted Manuscript.

Irving, K. (1962). *Nuclear physics* (2nd ed.). Reading, England: Addison-Wesley Publishing Company.

James, M. A. (2007). *Studies of triaxial rotors and band mixing in nuclei* (Doctoral dissertation). Georgia Institute of Technology, Georgia.

Jean, L. B., James, R., & Michel, S. (2005). *Fundamentals in nuclear physics: From nuclear structure to cosmology*. New York, NY: Springer Science +Business Media.

John, D. W. (2004). *Theoretical nuclear and subnuclear physics* (2nd ed.). London, England: Imperial College Press.

John, M. B., & Victor, F. W. (1979). *Theoretical nuclear physics.* New York, NY: Springer-Verlag.

Kibedi, T. (Updated on 16-Dec-2014). *BrIcc - program to evaluate conversion coefficients users' manual for version 2.3b,* ANU-P/1839 v2.3.

Kibedi, T., Burrows, T. W., Trzhaskovskaya, M. B., Davidson, P. M., & Nestor, C. W. (2008). Evaluation of theoretical conversion coefficients using BrIcc, *Nucl. Instr. and Meth. A 589*, 202 - 229.

Kibedi, T., Burrows, T. W., Trzhaskovskaya, M. B., Nestor, C. W. J., & Davidson, P. M. (2007). *Internal conversion coefficients - How good are they now?* International Conference on Nuclear Data for Science and Technology, BNL-77996-2007-CP.

Krane, K. S. (1988). *Introductory nuclear physics* (Rev. ed.). New York, NY: John Wiley & Sons.

Liu, S. (2010). *Nuclear structure studies of neutron-rich nuclei produced in the spontaneous fission of ^{252}Cf: triaxiality near A = 110; spherical shapes and octupole correlations beyond ^{132}Sn* (Doctoral dissertation). Vanderbilt University, Nashville, Tennessee.

Malin, K. (2016). *Evolution of deformation and collectivity away from magic numbers* (Doctoral dissertation). University of Oslo, Oslo, Norway.

Marton, L., & Marton, C. (1963). M*ethods of experimental physics.* New York, NY: Academic Press.

Moore, R. B., & White, W. (1960). Tables of rotational energy levels of deformed even-even nuclei. *Can. J. Phys., 38*.

Nadirbekov, M. S. (2016). Reduced E2-transition probabilities in the excited collective states of triaxial even-even nuclei. *Nuclear Theory, 35*, 181-193.

Nadirbekov, M. S., & Yuldasheva, G. A. (2014). Triaxiality in excited states of lanthanide and actinide even-even nuclei. *International Journal of Modern Physics E, 23*(5), 1450034 - (1-16).

Nadyrbekov, M. S., & Bozarov, O. A. (2017). Reduced probabilities for E2 transitions between excited collective states of triaxial even-even nuclei. *Physics of Atomic Nuclei*, 46 - 59.

Nazarewicz, W. (1998). *Nuclear structure at the limits* (Doctoral dissertation). University of Tennessee Knoxville, Oak Ridge National Laboratory, Tennessee, U.S.A.

Nemirovskii, P. E. (1963). *Contemporary models of the atomic nucleus*. Pergamon Press.

Neugart, R., & Neyens, G. (2006). Nuclear moments. *Lect. Notes Phys. 700*, 135 - 189.

Nuclear Data Sheet-International Atomic Energy Agency. ("n.d") Retrieved December 2017, from *https://www-nds.iaea.org/relnsd/NdsEnsdf/QueryForm.html*.

Nouredine, Z. (2009). *Quantum mechanics: Concepts and applications* (2nd ed.). The Atrium, United Kingdom: John Wiley & Sons.

Obed, S. (2011). *Studying chirality in A ~ 100, 130 and 190 mass regions* (Doctoral dissertation). University of the Western Cape, Somerset West, South Africa.

Paddy, R. (2003). *Post graduate nuclear experimental techniques (4NET) course notes*. University of Surrey, Guildford, United Kingdom.

Parveen, K., & Harish, M. M. (2015). Study of Grodzins product ($E(2_1^+)$*B(E2)↑) in the framework of the asymmetric rotor model, *Open Phys. 2015, 13,* 305 - 309.

Pearson, J. (2008). *Nuclear physics* (Lectures notes). University of Manchester, Manchester, UK.

Pritychenko, B., Birch, M., Singh, B., & Horoi, M. (2013). Tables of E2 transition probabilities from the first 2^+ states in even-even nuclei. *Preprint submitted to Atomic Data and Nuclear Data Tables.*

Pritychenko, B., Birch, M., & Singh, B. (2017). Revisiting Grodzins systematics of B(E2) values. *Nuclear Physics A 962,* 73 - 102.

Ralph, S. W. (1962). *Lifetimes of excited nuclear levels* (Doctoral dissertation). McGill University, Montreal.

Raman, S., Nestor, C. W., & Tikkanen, P. (2001). Transition probability from the ground to the first-excited 2^+ state of even–even nuclides. *Atomic Data and Nuclear Data Tables 78,* 1 - 128.

Rudigier, M. (2013). *Nuclear structure studies of odd-odd and odd-A nuclei in the shape transition region around N = 60* (Doctoral dissertation). University of Cologne, Cologne, Germany.

Samuel, S. M. W. (2004). *Introductory nuclear physics*. Wiley-VCH Verlag Gmbl I & Co. KGaA, Weinheim.

Serkan, D. (2009*). Nuclear structure of the N=88 isotones: The decay of ^{156}Tm to ^{156}Er* (Doctoral dissertation). Georgia Institute of Technology, Georgia.

Shaohua, L. (2010). *Nuclear structure studies of neutron-rich nuclei produced in the spontaneous fission of ^{252}Cf: Triaxiality near A = 110; Spherical shapes and octupole correlations Beyond ^{132}Sn* (Doctoral dissertation). Vanderbilt University, Nashville, Tennessee.

Singh, M., Bihari, C., Singh, Y., Gupta, D., Varshney, A. K., Gupta, K. K., & Gupta, D. K. (2007). Evidence of rigid triaxiality in some Xenon nuclei, *Can. J. Phys. 85*, 899 - 910.

Singh, M., Sharma, A., Singh, Y., Varshney, A. K., Gupta, K. K., & Gupta, D. K. (2012). A simple approach of extracting deformation parameter β for asymmetric nuclei from $E2_1^+$. *Proceedings of the DAE Symp. on Nucl. Phys. 57,* India.

Singh, Y., Bihari, C., Sharma, A., Varshney, A. K., Singh, M., Varshney M., Dhiman, S. K, … Gupta, D. K. (2011). Study of triaxial deformation variable γ in even-even nuclei. *Proceedings of the DAE Symp. on Nucl. Phys. 56*, 418 – 419, India.

Singh, Y., Dhiman, S. K., Singh, M., Bihari, C., Varshney, A. K., Gupta, K. K., & Gupta, D. K. (2013). In search of empirical rule relating $E2_1$ and B(E2; $0^+ \rightarrow 2^+$) in asymmetric even-even nuclei of mass region *A* = 90 –120. *Can. J. Phys. 91*, 777 - 782.

Smith, A. G., Durell, J. L., Phillips, W. R., & Urban, W. (2012). Lifetime measurements and nuclear deformation in the $A \approx 100$ region. *Physical Review C 86,* 014321- (1 - 10).

Stephen. ("n.d") Retrieved November, 2017, from *http://www.wolframalpha.com/widets/view.jsp*

Stone, N. J. (2005). Table of nuclear magnetic dipole and electric quadrupole moments. *Atomic Data and Nuclear Data Tables 90*, 75 - 176.

Sukomal, B. (1973). *Rotational and quasirotational energy levels of deformed nuclei* (Doctoral dissertation). University of Ottawa, Ottawa, Canada.

Thomas, B. (2009). *The evolution of B(E2) values around the doubly-magic nucleus ^{132}Sn* (Doctoral dissertation). University of Munich, Munich, Germany.

Varshney, M., Singh, M., Singh, Y., Bihari, C., Varshney, A. K., Gupta, K. K., & Gupta, D. K. (2011). Seeking asymmetric rotors in mass region A~100–110. *Phys. Scr. 83* 015201 (7pp).

Varshney, M., Singh, M., Singh, Y., Bihari, C., Varshney, A. K., Gupta, K. K., & Gupta, D. K. (2009). Study of nuclear shapes in even mass region A~100. *Proceedings of the International Symposium on Nuclear Physics,* 124 – 125, India.

Varshney, V. P. (1982). (Doctoral dissertation). Aligarh Muslim University, India.

Yan, J., Vogel, O., Brentano, P. V., & Gelberg, A. (1993*).* Systematics of triaxial deformation in Xe, Ba, and Ce nuclei. *Physical Review C, 48*(3).

Yigitoglu, & Dennis, B. (2011). Bohr Hamiltonian with Davidson potential for triaxial nuclei. *Physical Review C 83,* 014303 (1- 8).

Yuri, A. B. (2005). *The quantum world of nuclear physics*. New Jersey, World Scientific Publishing.

Yuvraj, S., Dhiman, S. K., Singh, M., Bihari, C., Varshney, A. K., Gupta, K. K., & Gupta, D. K. (2013). In search of empirical rule relating E21 and B(E2; $0_1^+ \rightarrow 2_1^+ 1$) in asymmetric even-even nuclei of mass region A = 90–120, *Can. J. Phys. 91*: 777 - 782.

Zawischa, D., Speth, J., & Pal, D. (1978). Low and high energy collective states of deformed nuclei. *Nucl. Phys. A311,* 445 - 476.

List of Original Publications

1. Biniyam, N. E., & Chaubey, A. K. (2017). Calculation of Reduced Transition Probabilities B(E2) for Rotational Excited Ground Band States Even-Even Nuclei in Lanthanide and Actinide Series, *International Journal of Scientific Research*, Vol. 6, 561 – 565.

2. Biniyam, N. E., & Chaubey, A. K. (2018). Energy Calculation for Rotational Excited States Even-Even Nuclei in Lanthanide and Actinide Series, *International Journal of Innovative Science, Engineering & Technology*, Vol. 5, 113 - 120.

3. Biniyam, N. E., & Chaubey, A. K. (Under Review). Meanlives Predictions for Rotational Excited Ground Band States for Even-Even Nuclei in Rare Earth and Actinide Series, *European Physical Journal C*, ….

Appendix

Appendix A: Rotation and Angular Momentum

Angular momentum is as important in classical mechanics as in quantum mechanics (Nouredine, 2009). It is particularly useful for studying the dynamics of systems that move under the influence of spherically symmetric, or central, potentials, $V(\vec{r}) = V(r)$ for the orbital angular momenta of these systems are conserved.

One of the cornerstones of Bohr's model of the hydrogen atom (where the electron moves in the proton's Coulomb potential, a central potential) is based on the quantization of angular momentum. Additionally, angular momentum plays a critical role in the description of molecular rotations, the motion of electrons in atoms, and the motion of nucleons in nuclei. The quantum theory of angular momentum is thus a prerequisite for studying molecular, atomic, and nuclear systems.

A.1) General Formalism of Angular Momentum

Let us now introduce a more general angular momentum operator $\hat{J}$ that is defined by its three components $\hat{J}_x$, $\hat{J}_y$ and $\hat{J}_z$, which satisfy the following commutation relations (Nouredine, 2009):

$[\hat{J}_x, \hat{J}_y] = i\hbar\hat{J}_z$, $[\hat{J}_y, \hat{J}_z] = i\hbar\hat{J}_x$, $[\hat{J}_z, \hat{J}_x] = i\hbar\hat{J}_y$, or equivalently by $\hat{J} \times \hat{J} = i\hbar\hat{J}$ (A.1)

Since $\hat{J}_x$, $\hat{J}_y$ and $\hat{J}_z$ do not mutually commute, they cannot be simultaneously diagonalized; that is, they do not possess common eigenstates. The square of the angular momentum

$$\hat{J}^2 = \hat{J}_x^2 + \hat{J}_y^2 + \hat{J}_z^2, \tag{A.2}$$

is a scalar, hence it commutes with $\hat{J}_x$, $\hat{J}_y$ and $\hat{J}_z$:

$$[\hat{J}^2, \hat{J}_k] = 0, \tag{A.3}$$

where k stands for x, y, and z.

A.2) Matrix Representation of Angular Momentum

The formalism of the previous section is general and independent of any particular representation. There are many ways to represent the angular momentum operators and their eigenstates. In this section we are going to discuss the matrix representation of angular momentum where eigenkets and operators will be represented by column vectors and square matrices, respectively. This is achieved by expanding states and operators in a discrete basis. We will see later how to represent the orbital angular momentum in the position representation (Nouredine, 2009).

Since $\hat{J}^2$ and $\hat{J}_z$ commute, the set of their common eigenstates $\{|\, j, m\rangle\}$ can be chosen as a basis; this basis is discrete, orthonormal, and complete. For a given value of j, the orthonormalization condition for this base is $\langle j', m' \mid j, m \rangle = \delta_{j'j}\delta_{m'm}$, and the completeness condition is expressed by

$$\sum_{m=-j}^{+j} |\, j, m\rangle\langle\, j, m\,| \;=\; \hat{I} \tag{A.4}$$

where $\hat{I}$ is the unit matrix. The operators $\hat{J}^2$ and $\hat{J}_z$ are diagonal in the basis given by their joint eigenstates

$$\langle j', m'|\, \hat{J}^2 \,|\, j, m\rangle \;=\; \hbar^2 j(j+1)\delta_{j'j}\delta_{m'm'} \tag{A.5}$$

$$\langle j', m'|\, \hat{J}_z \,|\, j, m\rangle \;=\; \hbar m \delta_{j'j}\delta_{m'm} \tag{A.6}$$

Thus, the matrices representing $\hat{J}^2$ and $\hat{J}_z$ in the $\{|\, j, m\rangle\}$ eigenbasis are diagonal, their diagonal elements being equal to $\hbar^2 j(j+1)$ and $\hbar m$, respectively.

Now since the operators $\hat{J}_\pm$ do not commute with $\hat{J}_z$, they are represented in the $\{|\, j, m\rangle\}$ basis by matrices that are not diagonal:

$$\langle j', m'|\, \hat{J}_\pm \,|\, j, m\rangle \;=\; \hbar\sqrt{j(j+1) - m(m \pm 1)}\,\delta_{j'j}\delta_{m',m\pm} \tag{A.7}$$

We can infer the matrices of $\hat{J}_x$ and $\hat{J}_y$ from

$\hat{J}_x \,|\, j, m\rangle = \frac{1}{2}(\hat{J}_+ + \hat{J}_-) \,|\, j, m\rangle = \frac{\hbar}{2}\left[\sqrt{(j-m)(j+m+1)}\,|\, j, m+1\rangle + \sqrt{(j+m)(j-m+1)}\,|\, j, m-1\rangle\right]$ and $\hat{J}_y \,|\, j, m\rangle = \frac{1}{2i}(\hat{J}_+ - \hat{J}_-) \,|\, j, m\rangle$

$$= \frac{\hbar}{2i}\left[\sqrt{(j-m)(j+m+1)}\,|\,j,m+1\rangle - \sqrt{(j+m)(j-m+1)}\,|\,j,m-1\rangle\right]:\langle j',m'|\hat{J}_x\,|\,j,m\rangle$$

$$= \frac{\hbar}{2}\left[\sqrt{j(j+1)-m(m+1)}\,\delta_{m',\,m+1} + \sqrt{j(j+1)-m(m-1)}\,\delta_{m',\,m-1}\right]\delta_{j'j} \qquad \text{(A.8)}$$

$$\langle j',m'|\hat{J}_y|\,j,m\rangle = \frac{\hbar}{2i}\left[\sqrt{j(j+1)-m(m+1)}\,\delta_{m',m+1} - \sqrt{j(j+1)-m(m-1)}\,\delta_{m',\,m-1}\right]\delta_{j'j} \qquad \text{(A.9)}$$

A.3) Geometrical Representation of Angular Momentum

At issue here is the relationship between the angular momentum and its z-component; this relation can be represented geometrically as follows (Nouredine, 2009). For a fixed value of j, the total angular momentum $\hat{J}$ may be represented by a vector whose length, as displayed in Figure A, is given by $\hbar\sqrt{j(j+1)}$ and whose z-component is $\langle \hat{J}_z \rangle = \hbar m$. Since $\hat{J}_x$ and $\hat{J}_y$ are separately undefined, only their sum $\hat{J}_x^2 + \hat{J}_y^2 = \hat{J}^2 - \hat{J}_z^2$ z, which lies within the xy plane, is well defined.

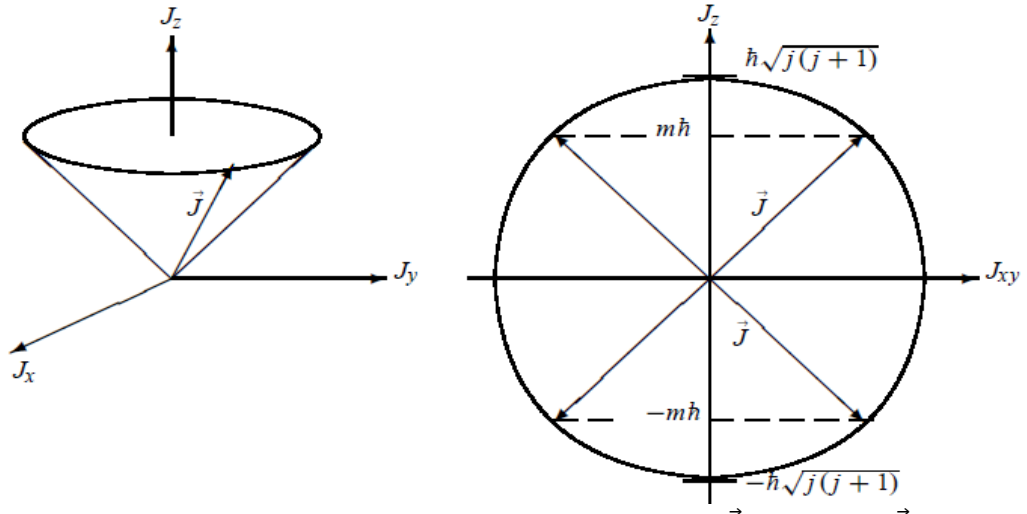

Figure A. Geometrical representation of the angular momentum $\vec{J}$: the vector $\vec{J}$ rotates along the surface of a cone about its axis; the cone's height is equal to Mħ, the projection of $\vec{J}$ on the cone's axis. The tip of $\vec{J}$ lies, within the J_z J_{xy} plane, on a circle of radius $\hbar\sqrt{J(J+1)}$.

A.4) Representation of the Rotation Operator

The rotation operator is given by (Nouredine, 2009)

$$\hat{R}(\alpha, \beta, \gamma) = \hat{R}_z(\alpha)\, \hat{R}_y(\beta)\, \hat{R}_z(\gamma) = e^{-i\alpha J_z/\hbar} e^{-i\beta J_y/\hbar} e^{-i\gamma J_z/\hbar} \tag{A.10}$$

implies that its properties are determined by the algebraic properties of the angular momentum operators $\hat{J}_x$, $\hat{J}_y$, $\hat{J}_z$. Since $\hat{R}(\alpha, \beta, \gamma)$ commutes with $\hat{J}^2$, we may look for a representation of $\hat{R}(\alpha, \beta, \gamma)$ in the basis spanned by the eigenvectors of $\hat{J}^2$ and J_z, i.e., the $|\, j, m\rangle$ states.

From (A.10), we see that $\hat{J}^2$ commutes with the rotation operator, $[\hat{J}^2, \hat{R}(\alpha, \beta, \gamma)] = 0$; thus, the total angular momentum is conserved under rotations

$$\hat{J}^2 \hat{R}(\alpha, \beta, \gamma)\, |\, j, m\rangle = \hat{R}(\alpha, \beta, \gamma)\, \hat{J}^2 |\, j, m\rangle = j(j+1)\, \hat{R}(\alpha, \beta, \gamma) |\, j, m\rangle \tag{A.11}$$

However, the z-component of the angular momentum changes under rotations, unless the axis of rotation is along the z-axis. That is, when $\hat{R}(\alpha, \beta, \gamma)$ acts on the state $|\, j, m\rangle$, we end up with a new state having the same j but with a different value of m:

$$\hat{R}(\alpha, \beta, \gamma)\, |\, j, m\rangle = \sum_{m'=-j}^{j} |\, j, m'\rangle \langle j, m' |\, \hat{R}(\alpha, \beta, \gamma)\, |\, j, m\rangle = \sum_{m'=-j}^{j} D^{(j)}_{m'm}(\alpha, \beta, \gamma)\, |\, j, m'\rangle \tag{A.12}$$

$$D^{(j)}_{m'm}(\alpha,\beta,\gamma) = \langle j, m' | \hat{R}(\alpha,\beta,\gamma) | j, m \rangle \tag{A.13}$$

These are the matrix elements of $\hat{R}(\alpha,\beta,\gamma)$ for the $|j,m\rangle$ states; $D^{(j)}_{m'm}(\alpha,\beta,\gamma)$ is the amplitude of $|j,m'\rangle$ when $|j,m\rangle$ is rotated. The rotation operator is thus represented by a (2j+1) x (2j+1) square matrix in the $\{|j,m\rangle\}$ basis. The matrix of $D^{(j)}(\alpha,\beta,\gamma)$ is known as the Wigner D-matrix and its elements $D^{(j)}_{m'm}(\alpha,\beta,\gamma)$ as the Wigner functions. This matrix representation is often referred to as the (2j+1)-dimensional irreducible representation of the rotation operator $\hat{R}(\alpha,\beta,\gamma)$.

Since $|j,m\rangle$ is an eigenstate of J_z, it is also an eigenstate of the rotation operator $e^{i\alpha J_z/\hbar}$, because $e^{i\alpha J_z/\hbar}|j,m\rangle = e^{i\alpha m/\hbar}|j,m\rangle$.

We may thus rewrite (A.13) as

$$D^{(j)}_{m'm}(\alpha,\beta,\gamma) = e^{-i\alpha(m'\alpha+m\gamma)/\hbar}\, d^{(j)}_{m'm}(\beta), \tag{A.14}$$

where

$$d^{(j)}_{m'm}(\beta) = \langle j, m' | e^{-i\beta \hat{J}_y/\hbar} | j, m \rangle \tag{A.15}$$

This shows that only the middle rotation operator, $e^{-i\beta \hat{J}_y/\hbar}$, mixes states with different values of m. Determining the matrix elements $D^{(j)}_{m'm}(\alpha,\beta,\gamma)$ therefore reduces to evaluation of the quantities $d^{(j)}_{m'm}(\beta)$.

A general expression of $d^{(j)}_{m'm}(\beta)$, called the Wigner formula, is given by the following explicit expression:

$$d^{(j)}_{m'm}(\beta) = \sum_{k} (-1)^{k+m'+m} \frac{\sqrt{(j+m)!\,(j-m)!\,(j+m')!\,(j-m')!}}{(j-m'-k)!\,(j+m-k)!\,(j-m)!\,(j+m'-m)!\,k!}$$

$$* \cos\left(\frac{\beta}{2}\right)^{2j+m-m'-2k} (\sin\frac{\beta}{2})^{m'-m+2k} \qquad (A.16)$$

The summation over k is taken such that none of the arguments of factorials in the denominator are negative.

We should note that, since the D-function $D^{(j)}_{m'm}(\alpha,\beta,\gamma)$ is a joint eigenfunction of $\hat{J}^2$ and J_z, we have

$$\hat{J}^2 D^{(j)}_{m'm}(\alpha,\beta,\gamma) = j(j+1)\hbar^2\, D^{(j)}_{m'm}(\alpha,\beta,\gamma) \qquad (A.17)$$

$$\hat{J}_z D^{(j)}_{m'm}(\alpha,\beta,\gamma) = \hbar m\, D^{(j)}_{m'm}(\alpha,\beta,\gamma) \qquad (A.18)$$

$$\hat{J}_{\pm} D^{(j)}_{m'm}(\alpha,\beta,\gamma) = \hbar\sqrt{(j \pm m)(j \mp m + 1)}\, D^{(j)}_{m'm\pm1}(\alpha,\beta,\gamma) \qquad (A.19)$$

A.5) Properties of the D-functions

We now list some of the most useful properties of the rotation matrices. The complex conjugate of the D-functions can be expressed (Nouredine, 2009) as

$$[D^{(j)}_{m'm}(\alpha,\beta,\gamma)]^* = \langle j, m' \left| \hat{R}(\alpha,\beta,\gamma) \right| j, m \rangle^* = \langle j, m \left| \hat{R}^{\dagger}(\alpha,\beta,\gamma) \right| j, m' \rangle$$

$$= \langle j, m \mid \hat{R}^{-1}(\alpha,\beta,\gamma) \mid j, m' \rangle = D^{(j)}_{mm'}(-\gamma,-\beta,-\alpha) \qquad \text{(A.20)}$$

We can easily show that

$$[D^{(j)}_{m'm}(\alpha,\beta,\gamma)]^* = (-1)^{m'-m} D^{(j)}_{-m'-m}(\alpha,\beta,\gamma) = D^{(j)}_{mm'}(-\gamma,-\beta,-\alpha) \qquad \text{(A.21)}$$

The D-functions satisfy the following unitary relations:

$$\sum_m [D^{(j)}_{km}(\alpha,\beta,\gamma)]^* D^{(j)}_{k'm}(\alpha,\beta,\gamma) = \delta_{k,\ k'} \qquad \text{(A.22)}$$

$$\sum_m [D^{(j)}_{mk}(\alpha,\beta,\gamma)]^* D^{(j)}_{mk'}(\alpha,\beta,\gamma) = \delta_{k,\ k'} \qquad \text{(A.23)}$$

since

$$\sum_m [D^{(j)}_{mk}(\alpha,\beta,\gamma)]^* D^{(j)}_{mk'}(\alpha,\beta,\gamma) = \sum_m \langle j, k \left| \hat{R}^{-1}(\alpha,\beta,\gamma) \right| j, m \rangle \langle j, m | R(\alpha,\beta,\gamma) | j, k' \rangle$$

$$= \langle j, k \left| \hat{R}^{-1}(\alpha,\beta,\gamma)\, \hat{R}(\alpha,\beta,\gamma) \right| j, k' \rangle = \langle j, k \mid j, k' \rangle = \delta_{k,\ k'} \qquad \text{(A.24)}$$

From (A.15) we can show that the d-functions satisfy the following relations:

$$d^{(j)}_{m'm}(\pi) = (-1)^{j-m} \delta_{m'-m,}\ d^{(j)}_{m'm}(0) = \delta_{m',\ m} \qquad \text{(A.25)}$$

Since $d^{j}_{m'm}$ are elements of a unitary real matrix, the matrix $d^{(j)}(\beta)$ must be orthogonal. We may thus write

$$d^{(j)}_{m'm}(\beta) = (d^{(j)}_{m'm}(\beta))^{-1} = d^{(j)}_{m\,m'}(-\beta) \tag{A.26}$$

and

$$d^{(j)}_{m'm} = (-1)^{m'-m}\, d^{(j)}_{m\,m'}(\beta) = (-1)^{m'-m}\, d^{(j)}_{-m'-m}(\beta) \tag{A.27}$$

The unitary matrices $D^{(j)}$ form a (2j + 1) dimensional irreducible representation of the SO(3) group.

A.6) Rotation Matrices and the Spherical Harmonics

In the case where the angular momentum operator $\hat{J}$ is purely orbital (i.e., the values of j are integer, j = l), there exists a connection between the D-functions and the spherical harmonics $Y_{lm}(\theta, \varphi)$. The operator $\hat{R}(\alpha, \beta, \gamma)$ when applied to a vector $|\vec{r}\rangle$ pointing in the direction (θ, φ) would generate a vector $|\vec{r'}\rangle$ along a new direction (θ', φ') (Nouredine, 2009).:

$$|\vec{r'}\rangle = \hat{R}(\alpha, \beta, \gamma)|\vec{r}\rangle \tag{A.28}$$

An expansion in terms of $|\, l, m'\rangle$ and a multiplication by $\langle\, l, m\,|$ leads to

$$\langle l, m \mid \vec{r'} \rangle = \sum_{m'} \langle l, m \mid \hat{R}(\alpha, \beta, \gamma) \mid l, m' \rangle \langle l, m' \mid \vec{r} \rangle \qquad (A.29)$$

or to

$$Y^*_{lm}(\theta', \varphi') = \sum_{m'} D^{(l)}_{m\,m'}(\alpha, \beta, \gamma)\, Y^*_{lm'}(\theta, \varphi) \qquad (A.30)$$

since

$$\langle l, m \mid \vec{r'} \rangle = Y^*_{lm}(\theta', \varphi') \text{ and } \langle l, m' \mid \vec{r} \rangle = Y^*_{lm'}(\theta, \varphi) \qquad (A.31)$$

In the case where the vector $\vec{r}$ is along the z-axis, we have $\theta = 0$; hence $m' = 0$. The $Y^*_{l0}(0, \varphi)$ is given by

$$Y^*_{lm'}(0, \varphi) = \sqrt{\frac{2l+1}{4\pi}}\, \delta_{m',0} \qquad (A.32)$$

We can thus reduce (A.30) to

$$Y^*_{lm}(\beta, \alpha) = D^{(l)}_{m\,0}(\alpha, \beta, \gamma) Y^*_{l0}(0, \varphi) = \sqrt{\frac{2l+1}{4\pi}}\, D^{(l)}_{m\,0}(\alpha, \beta, \gamma), \qquad (A.33)$$

Or to

$$D^{(l)}_{m\,0}(\alpha, \beta, \gamma) = \sqrt{\frac{4\pi}{2l+1}}\, Y^*_{lm}(\beta, \alpha) \qquad (A.34)$$

This means that a rotation through the Euler angles (α, β, γ) of the vector $\vec{r}$, when it is along the z-axis, produces a vector $\vec{r}\,'$ whose azimuthal and polar angles are given by β and α, respectively. Similarly, we can show that

$$D^{(l)}_{0m}(\gamma, \beta, \alpha) = \sqrt{\frac{4\pi}{2l+1}}\, Y_{lm}(\beta, \alpha) \tag{A.35}$$

and

$$D^{(l)}_{00}(0, \theta, 0) = P_l(\cos\theta) \tag{A.36}$$

where $P_l(\cos\theta)$ is the Legendre polynomial.

We are now well equipped to derive the theorem for the addition of spherical harmonics. Let (θ, φ) be the polar coordinates of the vector $\vec{r}$ with respect to the space-fixed x, y, z system and let (θ', φ') be its polar coordinates with respect to the rotated system x', y', z'; taking the complex conjugate of (A.30) we obtain

$$Y_{lm}(\theta', \varphi') = \sum_{m'} [D^{(l)}_{m\,m'}(\alpha, \beta, \gamma)]^*\, Y^*_{lm'}(\theta, \varphi) \tag{A.37}$$

For the case m = 0, since $Y^*_{l0}(\theta', \varphi') = \sqrt{\frac{2l+1}{4\pi}}\, P_l(\cos\theta')$ (A.38)

and since from (A.35), $[D^{(l)}_{0m'}(\alpha, \beta, \gamma)]^* = \sqrt{\frac{4\pi}{2l+1}}\, Y^*_{lm'}(\beta, \gamma)$ (A.39)

we can reduce (A.37) to

$$\sqrt{\frac{2l+1}{4\pi}}\, P_l(\cos\theta') = \sum_{m'} \sqrt{\frac{4\pi}{2l+1}}\, Y^*_{lm'}(\beta,\gamma) Y_{lm'}(\theta,\varphi) \qquad (A.40)$$

or to

$$P_l(\cos\theta') = \frac{4\pi}{2l+1} \sum_{m'} Y^*_{lm'}(\beta,\gamma) Y_{lm'}(\theta,\varphi) \qquad (A.41)$$

A.7) Transformation between Bases: Clebsch–Gordan Coefficients

Let us now return to the addition of $\hat{\vec{J}}_1$ and $\hat{\vec{J}}_2$. This problem consists in essence of obtaining the eigenvalues of $\hat{\vec{J}}^2$ and $\hat{J}_z$ and of expressing the states $|\, j, m \rangle$ in terms of $|\, j_1, j_2; m_1, m_2 \rangle$. We should mention that $|\, j, m \rangle$ is the state in which $\hat{\vec{J}}^2$ and $\hat{J}_z$ have fixed values, j (j + 1) and m, but in general not a state in which the values of $\hat{\vec{J}}_{1z}$ and $\hat{\vec{J}}_{2z}$ are fixed; as for $|\, j_1, j_2; m_1, m_2 \rangle$, it is the state in which $\hat{\vec{J}}_1^{\,2}$, $\hat{\vec{J}}_2^{\,2}$, $\hat{\vec{J}}_{1z}$, and $\hat{\vec{J}}_{2z}$ have fixed values (Nouredine, 2009).

The $\{|\, j_1, j_2;\ m_1, m_2\ \rangle\}$ and $\{|\, j,\ m\ \rangle\}$ bases can be connected by means of a transformation as follows. Inserting the identity operator as a sum over the complete basis $|\, j_1, j_2;\ m_1, m_2\ \rangle$, we can write

$$|\, j, m\ \rangle = \Big(\sum_{m_1=-j_1}^{j_1} \sum_{m_2=-j_2}^{j_2} |\, j_1, j_2;\ m_1, m_2\ \rangle\langle\ j_1, j_2;\ m_1, m_2\ |\Big)\, |\, j, m\ \rangle$$

$$= \sum_{m_1 m_2} \langle\ j_1, j_2;\ m_1, m_2\ |\, j, m\ \rangle\, |\, j_1, j_2;\ m_1, m_2\ \rangle \qquad (A.42)$$

where we have used the normalization condition

$$\sum_{m_1=-j_1}^{j_1} \sum_{m_2=-j_2}^{j_2} |\, j_1, j_2;\ m_1, m_2\ \rangle\langle\ j_1, j_2;\ m_1, m_2| = 1 \qquad (A.43)$$

since the bases $\{|\, j_1, j_2;\ m_1, m_2\ \rangle\}$ and $\{|\, j,\ m\ \rangle\}$ are both normalized, this transformation must be unitary. The coefficients $\langle\ j_1, j_2;\ m_1, m_2\ |\, j,\ m\ \rangle$, which depend only on the quantities j_1, j_2, m_1, m_2, and m, are the matrix elements of the unitary transformation which connects the $\{|\, j,\ m\ \rangle\}$ and $\{|\, j_1, j_2;\ m_1, m_2\ \rangle\}$ bases. These coefficients are called the Clebsch–Gordan coefficients.

The problem of angular momentum addition reduces then to finding the Clebsch–Gordan coefficients $\langle\ j_1, j_2;\ m_1, m_2\ |\, j,\ m\ \rangle$. These coefficients are taken to be real by convention; hence

$$\langle\ j_1, j_2;\ m_1, m_2\ |\, j,\ m\ \rangle = \langle\ j, m\ |\, j_1, j_2;\ m_1, m_2\rangle \qquad (A.44)$$

Using normalization condition (A.43) and the orthonormal basis $\langle j', m' \mid j, m \rangle = \delta_{j'j}\,\delta_{m'm}$ we can infer the orthonormalization relation for the Clebsch - Gordan coefficients:

$$\sum_{m_1 m_2} \langle j', m' \mid j_1, j_2;\ m_1, m_2 \rangle \langle j_1, j_2;\ m_1, m_2 \mid j, m \rangle = \delta_{j',\ j}\,\delta_{m',\ m} \qquad (A.45)$$

and since the Clebsch–Gordan coefficients are real, this relation can be rewritten as

$$\sum_{m_1 m_2} \langle j_1, j_2;\ m_1, m_2 \mid j', m' \rangle \langle\ j_1, j_2;\ m_1, m_2 \mid j, m \rangle = \delta_{j',\ j}\,\delta_{m',\ m} \qquad (A.46)$$

which leads to

$$\sum_{m_1 m_2} \langle j_1, j_2;\ m_1, m_2 \mid j, m \rangle^2 = 1 \qquad (A.47)$$

Likewise, we have

$$\sum_{j} \sum_{m=-j}^{j} \langle j_1, j_2;\ m'_1, m'_2 \mid j, m \rangle \langle\ j_1, j_2;\ m_1, m_2 \mid j, m \rangle = \delta_{m'_1,\ m_1}\,\delta_{m'_2,\ m_2} \qquad (A.48)$$

and, in particular,

$$\sum_{j} \sum_{m} \langle j_1, j_2;\ m_1, m_2 \mid j, m \rangle^2 = 1 \qquad (A.49)$$

A.8) Calculation of the Clebsch–Gordan Coefficients

First, we should point out that the Clebsch–Gordan coefficients corresponding to the two limiting cases where $j_1 = m_1, m_2 = j_2; j = j_1 + j_2, m = j_1 + j_2$ and $m_1 = -j_1 = , m_2 = -j_2,\ j = j_1 + j_2, m = -(j_1 + j_2)$ are equal to one (Nouredine, 2009):

$$\langle j_1, j_2;\ j_1, j_2 \,|(j_1 + j_2), (j_1 + j_2)\rangle = 1,$$
$$\langle j_1, j_2;\ -j_1, -j_2 \,|(j_1 + j_2), -(j_1 + j_2)\rangle = 1 \qquad \text{(A.50)}$$

These results can be inferred from (A.42), since$|(j_1 + j_2), (j_1 + j_2)\rangle$, and $|(j_1 + j_2), -(j_1 + j_2)\rangle$ have one element each:

$$|(j_1 + j_2), (j_1 + j_2)\rangle = \langle j_1, j_2;\ j_1, j_2 \,|(j_1 + j_2), (j_1 + j_2)\rangle |\, j_1, j_2;\ j_1, j_2\rangle \qquad \text{(A.51)}$$

$$|(j_1 + j_2), -(j_1 + j_2)\rangle = \langle j_1, j_2; -j_1, -j_2 \,|(j_1 + j_2), -(j_1 + j_2)\rangle |\, j_1, j_2; -j_1, -j_2\rangle \qquad \text{(A.52)}$$

where $|(j_1 + j_2), (j_1 + j_2)\rangle, |(j_1 + j_2), -(j_1 + j_2)\rangle, |\, j_1, j_2;\ j_1, j_2\rangle$ and $|\, j_1, j_2;\ -j_1, -j_2\rangle$ are all normalized.

The calculations of the other coefficients are generally more involved than the two limiting cases mentioned above. For this, we need to derive the recursion relations between the matrix elements of the unitary transformation between the $\{|\, j, m\rangle\}$ and $\{|\, j_1, j_2;\ m_1, m_2\rangle\}$ bases, since, when j_1, j_2 and j are fixed, the various Clebsch–Gordan coefficients are related to one another by means of

recursion relations. To find the recursion relations, we need to evaluate the matrix elements $\langle j_1, j_2;\ m_1, m_2 | \hat{j}_\pm | j, m \rangle$ in two different ways. First, allow $\hat{j}_\pm$ to act to the right, i.e., on $| j, m \rangle$:

$$\langle j_1, j_2;\ m_1, m_2 | \hat{j}_\pm | j, m \rangle = \hbar\sqrt{(j \mp m)(j \pm m + 1)}\langle j_1, j_2;\ m_1, m_2 | j, m \pm 1 \rangle \qquad \text{(A.53)}$$

Second, make $\hat{j}_\pm = \hat{j}_{1\pm} + \hat{j}_{2\pm}$ act to the left, i.e., on $\langle j_1, j_2;\ m_1, m_2 |$:

$$\langle j_1, j_2;\ m_1, m_2 | \hat{j}_\pm | j, m \rangle = \hbar\sqrt{(j_1 \pm m_1)(j_1 \mp m_1 + 1)}\ \langle j_1, j_2;\ m_1 \mp 1, m_2 | j, m \rangle$$

$$+ \hbar\sqrt{(j_2 \pm m_2)(j_2 \mp m_2 + 1)}\ \langle j_1, j_2;\ m_1, m_2 \mp 1 | j, m \rangle \qquad \text{(A.54)}$$

Equating (A.53) and (A.54) we obtain the desired recursion relations for the Clebsch–Gordan coefficients:

$$\sqrt{(j \mp m)(j \pm m + 1)}\langle j_1, j_2;\ m_1, m_2 | j, m \pm 1 \rangle = \sqrt{(j_1 \pm m_1)(j_1 \mp m_1 + 1)}\langle j_1, j_2;\ m_1 \mp$$

$$1, m_2 | j, m \rangle + \sqrt{(j_2 \pm m_2)(j_2 \mp m_2 + 1)}\ \langle j_1, j_2;\ m_1, m_2 \mp 1 | j, m \rangle \qquad \text{(A.55)}$$

These relations, together with the orthonormalization relation (A.47), determine all Clebsch–Gordan coefficients for any given values of j_1, j_2 and j. To see this, let us substitute $m_1 = j_1$ and m = j into the lower part of (A.55). Since m_2 can be equal only to $m_2 = j - j_1 - 1$, we obtain

$$\sqrt{2j}\langle j_1, j_2;\ j_1, (j - j_1 - 1) | j, j - 1 \rangle = \sqrt{(j_2 - j + j_1 + 1)(j_2 + j - j_1)}^*\langle j_1, j_2;\ j_1, (j - j_1) | j, j \rangle \qquad \text{(A.56)}$$

Thus, knowing $\langle j_1, j_2;\ j_1, (j\ -\ j_1)\,|\,j, j\rangle$, we can determine $\langle j_1, j_2;\ j_1, (j\ -\ j_1 - 1)|\,j, j-1\rangle$.

In addition, substituting$m_1 = j_1$, m = j - 1 and $m_2 = j - j_1$ into the upper part of (A.55), we end up with

$$\sqrt{2j}\langle j_1, j_2;\ j_1, (j\ -\ j_1)|\,j, j\rangle = \sqrt{2j_1}\langle j_1, j_2; (j_1 - 1), (j\ -\ j_1)|\,j, j-1\rangle +$$

$$\sqrt{(j_2 + j - j_1 + 1)(j_2 - j + j_1 + 1)}\ \langle j_1, j_2;\ j_1, (j - j_1 - 1)\,|\,j, j-1\rangle \qquad \text{(A.57)}$$

Thus knowing $\langle j_1, j_2;\ j_1, (j\ -\ j_1)|\,j, j\rangle$and $\langle j_1, j_2; j_1, (j\ -\ j_1 - 1)|\,j, j-1\rangle$, we can determine $\langle j_1, j_2; (j_1 - 1), (j\ -\ j_1)|\,j, j-1\rangle$. Repeated application of the recursion relation (A.55) will determine all the other Clebsch–Gordan coefficients, provided we know only one of them: $\langle j_1, j_2;\ j_1, (j\ -\ j_1)|\,j, j\rangle$. As for the absolute value of this coefficient, it can be determined from the normalization condition (A.46). Thus, the recursion relation (A.55), in conjunction with the normalization condition (A.46), determines all the Clebsch–Gordan coefficients except for a sign. But how does one determine this sign?

The convention, known as the phase convention, is to consider $\langle j_1, j_2;\ j_1, (j\ -\ j_1)|\,j, j\rangle$ to be real and positive. This phase convention implies that

$$\langle j_1, j_2;\ m_1, m_2|\,j, m\rangle = (-1)^{j-j_1-j_2}\langle j_2, j_1;\ m_2, m_1|\,j, m\rangle \qquad \text{(A.58)}$$

Hence,

$$\langle j_1, j_2;\ m_1, m_2 | j, m \rangle = (-1)^{j-j_1-j_2} \langle j_1, j_2;\ -m_1, -m_2 | j, -m \rangle = \langle j_2, j_1;\ -m_2, -m_1 | j, -m \rangle \qquad \text{(A.59)}$$

Note that, since all the Clebsch–Gordan coefficients are obtained from a single coefficient $\langle j_1, j_2;\ j_1, (j - j_1) | j, j \rangle$, and since this coefficient is real, all other Clebsch–Gordan coefficients must also be real numbers.

Following the same method that led to (A.55) from $\langle j_1, j_2;\ m_1, m_2 | J_{\pm} | j, m \rangle$, we can show that a calculation of $\langle j_1, j_2;\ m_1, m_2 | J_{\pm} | j, m \mp 1 \rangle$ leads to the following recursion relation:

$$\sqrt{(j \mp m + 1)(j \pm m)} \langle j_1, j_2;\ m_1, m_2 | j, m \rangle = \sqrt{(j_1 \pm m_1)(j_1 \mp m_1 + 1)} \langle j_1, j_2;\ m_1 \mp 1, m_2 | j, m \mp 1 \rangle + \sqrt{(j_2 \pm m_2 + 1)(j_2 \mp m_2 + 1)} \langle j_1, j_2;\ m_1, m_2 \mp 1 | j, m \mp 1 \rangle \qquad \text{(A.60)}$$

We can use the recursion relations (A.55) and (A.60) to obtain the values of the various Clebsch–Gordan coefficients. For instance, if we insert $m_1 = j_1$, $m_2 = j_2 - 1$, $j = j_1 + j_2$, and $m = j_1 + j_2$ into the lower sign of (A.55), we obtain

$$\langle j_1, j_2; j_1, (j_2 - 1) | (j_1 + j_2), (j_1 + j_2 - 1) \rangle = \sqrt{\frac{j_2}{j_1 + j_2}} \qquad \text{(A.61)}$$

Similarly, a substitution of $m_1 = j_1 - 1$, $m_2 = j_2$, $j = j_1 + j_2$, and $m = j_1 + j_2$ into the lower sign of (A.55) leads to

$$\langle j_1, j_2; (j_1 - 1), j_2 | (j_1 + j_2), (j_1 + j_2 - 1) \rangle = \sqrt{\frac{j_1}{j_1 + j_2}} \tag{A.62}$$

We can also show that

$$\langle j, 1;\ m, 0 \mid j, m \rangle = \frac{m}{\sqrt{j(j+1)}}, \qquad \langle j, 0;\ m, 0 \mid j, m \rangle = 1 \tag{A.63}$$

Appendix B: The Solution of Eqn. (5.4)

The roots of this equation have been computed using Wolfram Mathematica (online software). Mathematica is the creation of Stephen Wolfram, a theoretical physicist who has made important contributions to mathematics and computer science. Wolfram describes Mathematica as "the world's only fully integrated environment for technical computing." At the heart of Mathematica is a computer algebra system, that is, a system for doing algebraic manipulations symbolically (and therefore exactly). However, Mathematica also incorporates floating point (or finite precision) computation, arbitrary precision arithmetic, graphics, and text processing. It is also a programming environment.

Mathematica has many capabilities, such as the fact that one can write programs made up of Mathematica commands. The simplest way to use Mathematica, though, is as an interactive computing environment (essentially, a very fancy graphing calculator). You enter a command and the Mathematica kernel (the part of the software that actually does the computation) executes it and returns the result.

The three spin 4 energy levels are the roots of the third degree equation

$\varepsilon^3 - \frac{90}{\mathrm{Sin}^2(3\gamma)}\varepsilon^2 + \frac{48}{\mathrm{Sin}^4(3\gamma)}[27+26\mathrm{Sin}^2(3\gamma)]\varepsilon - \frac{640}{\mathrm{Sin}^4(3\gamma)}[27+7\mathrm{Sin}^2(3\gamma)] = 0$, this equation can be given in a simpler form as

$$\varepsilon^3 - 90\csc^2(3\gamma) + 48\varepsilon\,(26\mathrm{Sin}^2(3\gamma) + 27)\,\csc^4(3\gamma) - 640\,(7\mathrm{Sin}^2(3\gamma) + 27)\,\csc^4(3\gamma) = 0$$

The solution of this equation is given using the Mathematica software as follows:

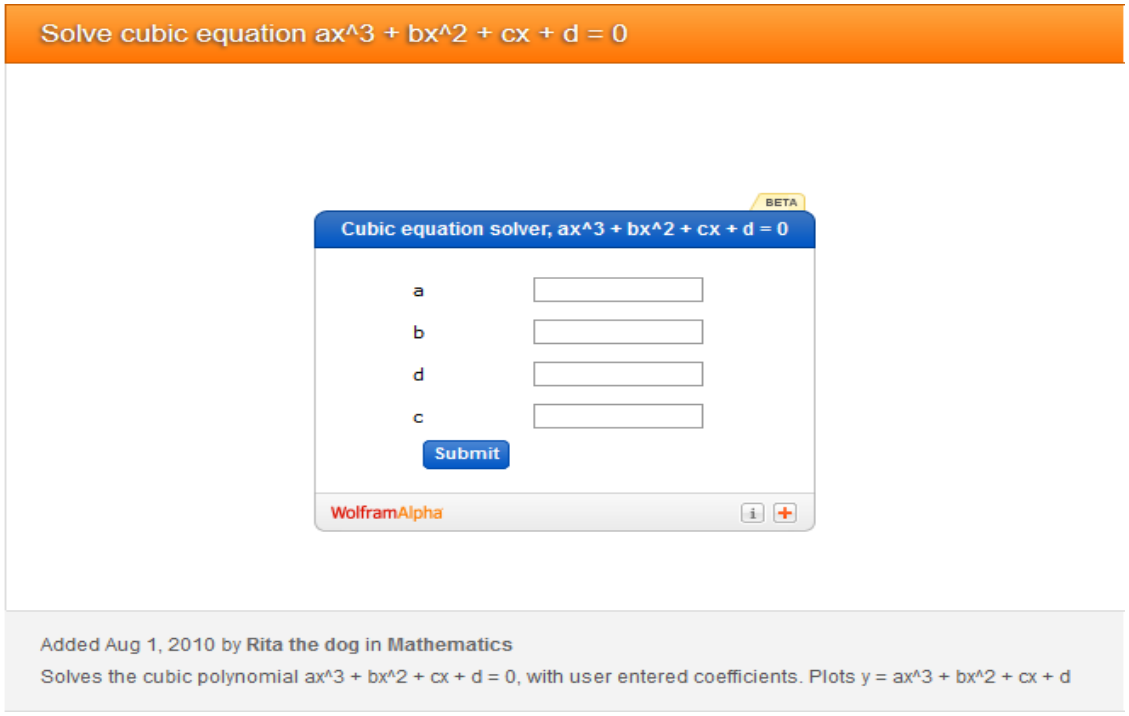

a)

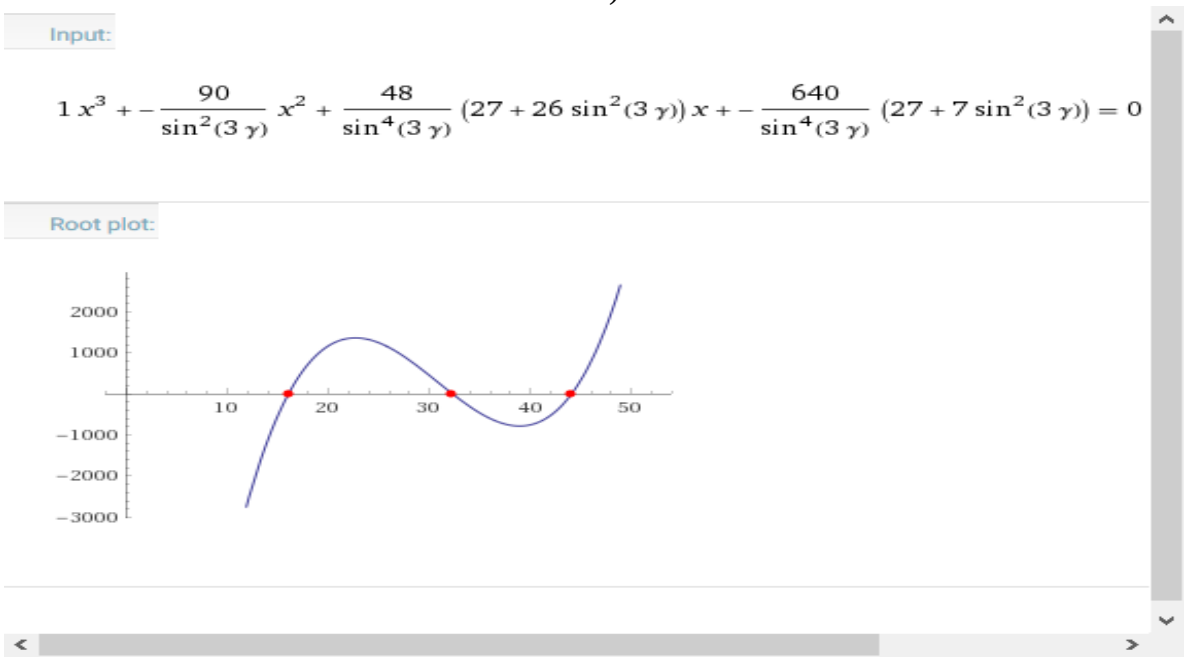

b)

Figure B. Cubic equation solving procedures using wolfram alpha (Mathematica software): a) User entered coefficients form, and b) Root plot.

Appendix C: Internal Conversion Coefficient Calculator

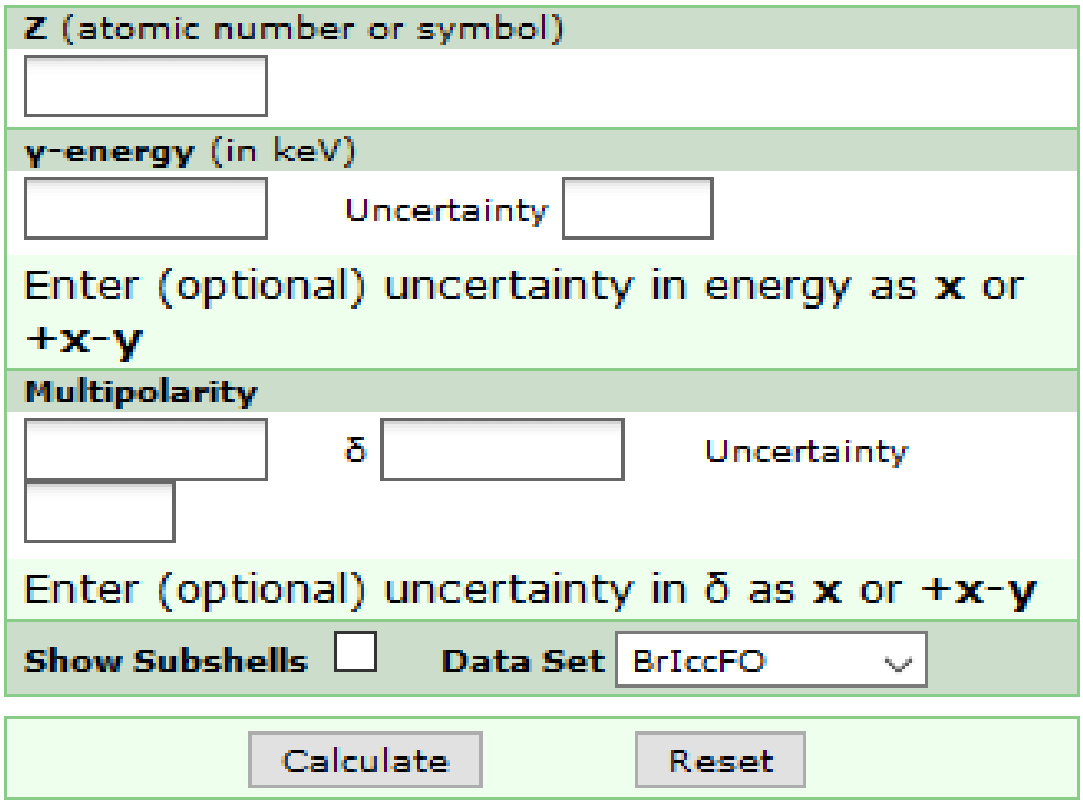

Figure C. BrIcc v2.3S conversion coefficient calculator, input parameters feeding form.

Appendix D: Evaluated Nuclear Structure Data File (ENSDF) Database

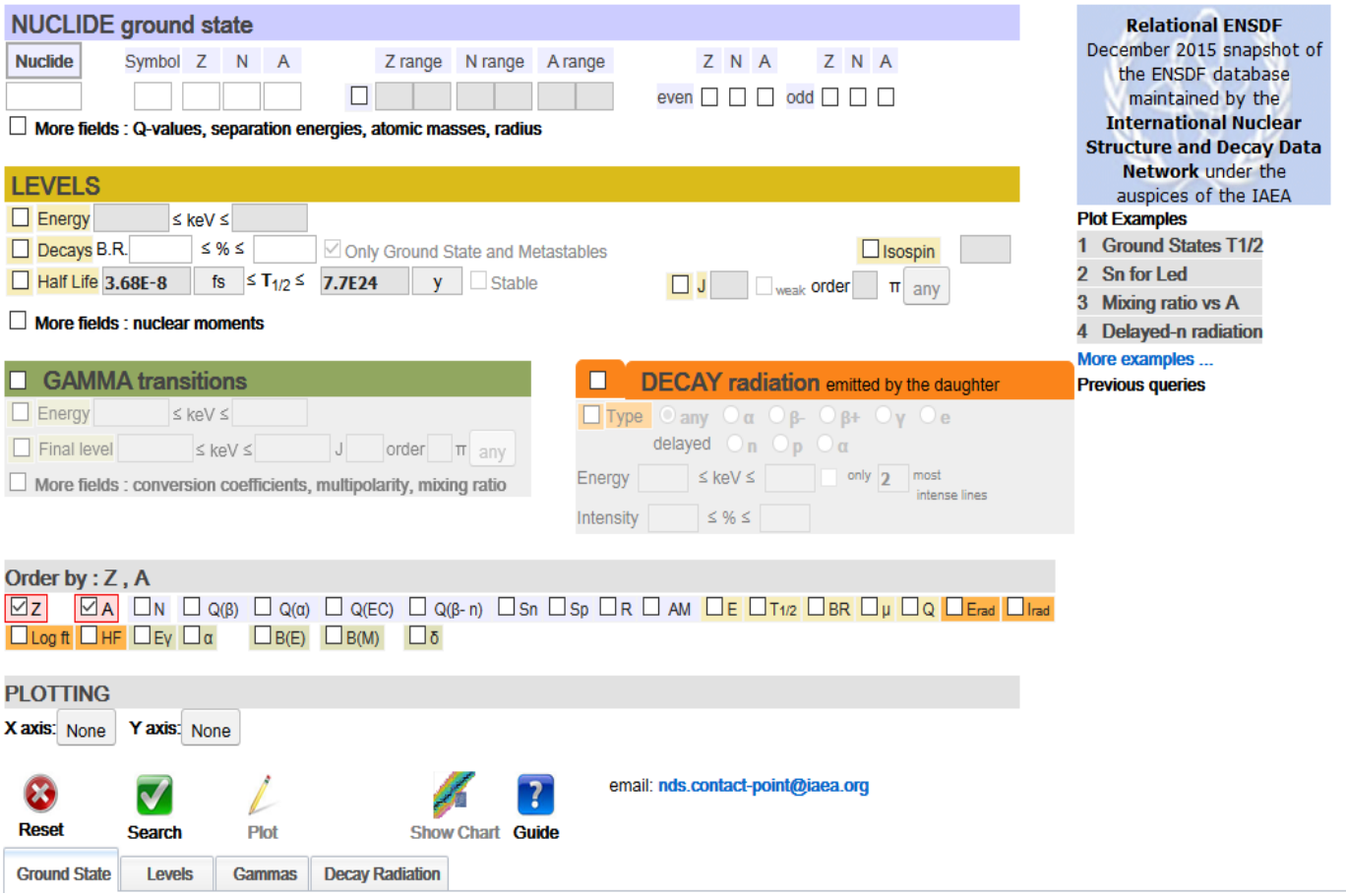

Figure D. Relational ENSDF database maintained by the International Nuclear Structure and Decay Data Network under the auspices of the IAEA.